UNIVERSITY OF SOUTHAMPTON

Fabrication and characterization of dye sensitized solar cells (DSSCs) for wearable energy harvesting applications

By

Jingqi Liu

A thesis submitted in partial fulfilment for the

degree of Doctor of Philosophy

in the

Faculty of Engineering and Physical Sciences

School of Electronics and Computer Science

July, 2019

This page intentionally left blank

Abstract

By Jingqi Liu

This thesis presents the novel use of printing and coating techniques to fabricate liquid and solid-state dye sensitised solar cell (DSSC) on textiles for wearable energy harvesting applications. E-textiles have attracted increasing research interest, and a persistent challenge remains the supply of electrical power. Solar energy is one of the most abundant renewable energy sources, which has an efficient solution to power the wearable electronics by commercially available photovoltaic devices such as solar watch or solar backpack. DSSC have emerged into the PV market demonstrating efficiencies of 11.9%, and offering a relatively low cost of manufacturing, compared to conventional silicon based solar cells. However, the conventional DSSC consists of two rigid glass substrates, which is incompatible with e-textile applications.

In order to fabricate the DSSC on a textile substrate, a set of temperature varying functional material formulations have been investigated. This research presents a systematic investigation into the formulation of titanium dioxide suitable for low temperature process. Low temperature processed DSSCs were fabricated onto FTO glass substrates at 150 ^{o}C and achieved a maximum PCE of 4.3%. The materials and process were used to replace both the FTO coated glass substrates with a flexible interface coated polyester cotton textile and an ITO coated PET substrate all fabricated at 150 ^{o}C. This DSSC approach achieved a maximum PCE of 4.04%. However, at this stage the flexible textile DSSCs still required the ITO coated PET film. In order to achieve a fully solution processed flexible DSSCs on purely textile substrates, solid-state DSSCs were achieved with customised solid-state electrolyte formulation. Since the TiO_2 compact layer requires 450 ^{o}C for crystallisation, a glass fibre textile is used. This required a polyimide layer as a temperature resistant interface layer. The glass fibre textile ssDSSC achieved a max PCE of 0.4%.

This page intentionally left blank

DECLARATION OF AUTHORSHIP

I, JINGQI LIU declare that the thesis entitled **Fabrication and characterization of dye sensitized solar cells (DSSCs) for wearable energy harvesting applications** and the work presented in the thesis are both my own and have been generated by me as the result of my own original research. I confirm that:

- this work was done wholly or mainly while in candidature for a research degree at this University;
- where any part of this thesis has previously been submitted for a degree or any other qualification at this University or any other institution, this has been clearly stated;
- where I have consulted the published work of others, this is always clearly attributed;
- where I have quoted from the work of others, the source is always given. Except for such quotations, this thesis is entirely my own work;
- I have acknowledged all main sources of help;
- where the thesis is based on work done by myself jointly with others, I have made clear exactly what was done by others and what I have contributed myself;

Signature:

This page left as blank

Table of Contents

List of Figures

List of Tables

This page intentionally left blank

List of Acronyms

DSSC	Dye-sensitized solar cell
ssDSSC	Solid-state dye-sensitized solar cell
TCO	Transparent conductive oxides
CNTs	Carbon nanotubes
FTO	Fluorine tin oxide
ITO	Indium tin oxide
Standard Fabric	Standard 65/35 polyester cotton fabric
AgNW	Silver nanowire
HOMO	Highest occupied molecular orbital
MWCNT	Multi-walled carbon nantube
IF fabric	Interface coated standard polyester cotton fabric
CB	Conduction band
LUMO	Lowest unoccupied molecular orbital
Ag	Silver
Au	Gold
OSC	Organic semiconductor
PEDOT/PSS	Poly (3,4-ethylenedioxythiophene) – Poly (styrenesulfonate)
PET	Polyethylene terephthalate
PEN	Polyethylene naphthalate
PU Fabric	Polyurethane coated stretchable fabric
SnO_2	tin oxide
Nb_2O_5	Niobium pentoxide
TFT	Thin film transistor
P3HT	Poly(3-hexylthiophene)
CuSCN	copper thiocyanate
CuI	copper iodide
PCE	Power conversion efficiency

This page intentionally left blank

List of Symbols

η	Overall power to energy conversion efficiency
V_{oc}	Open circuit voltage
J_{sc}	Current density
P_{in}	Incident power
P_{max}	Maximum power
V_{max}	Maximum voltage
I_{max}	Maximum current
λ	The light wavelength
AM 1.5G	Air mass 1.5 Global
Φ	Elevation angle between the sun and the Zenith
k	Boltzmann constant
T	Temperature
q	Unit charger

This page intentionally left blank

Acknowledgements

Firstly, I would like to express my sincerest gratitude to my supervisor Professor Steve Beeby to give me this opportunity to join this research group. I could not give enough thanks for his excellent guidance, suggestions and immense knowledge in this research field during my PhD study. His guidance helped me in all the time in my research area, and I could not go to this stage without his help.

Secondly, I would also like to express my sincerest thanks to Dr. Sasikumar Arumugam who helps me to develop my background knowledge and share experience with me. I am also grateful to Dr. Yi Li, for his help with my report, and giving me much valuable advice in my research area. Thanks for their patience, motivations, and encouragements.

I would like to take this opportunity to thank every member in my research group. Thank you for their help, and the valuable suggestions and stimulation discussions with me.

Last but not the least, I would like to give my grateful thanks to my parents who are living in China. I will never forget their endless support and unceasing encouragement in my student life abroad. I really appreciate it from the bottom of my heart.

I also place on record, my sense of gratitude to one and all, whom directly or indirectly, have helped me in my study.

This page intentionally left blank

Chapter 1

1 Introduction

1.1 Introduction

Textiles are the most common raw materials used in our daily lives which are regarded as our "second skin"[1, 2]. They also represent an attractive platform for supporting electronic integration and enable functional additives[1]. Textiles are made of woven fibres, including yarn, yarn products and anything related to fibres. Electronic textile (e-textile) consist of traditional fabrics with integrated electronic devices and sensors [3]. E-textiles based wearable technology has been demonstrated for various applications in recent years, for example, intelligent biomedical garments for monitoring, diagnosing and treatment of medical conditions[4, 5], wireless cardiac signal monitoring in sports[5, 6] and military clothing integrating fabric antennas to support networks and communications[7, 8]. Wearable applications requiring energy harvesting are essentially concerned with the area of smart fabrics, providing the power to the wearable electronics, sensors or systems. They can also be applied to outdoor sun-exposed applications such as tents or boat sails[9]. However, in every e-textiles application the issue of supplying power remains a significant challenge. E-textiles are typically battery powered using conventional rigid batteries that alter the characteristics (e.g. feel and drape) of the fabric. Batteries also require periodic replacement and are therefore inconvenient to use and dispose of. One alternative approach to batteries is to investigate energy harvesting technologies on textiles. Energy harvesting involves the conversion of ambient energy (e.g. kinetic, thermal or light) into electrical energy and this can provide a long-term, easy to use power supply that can potentially be embedded within the textile (i.e. the fabric is functionalized such that it becomes the energy harvester)[10] to meet the individual needs. Harvesting light energy through textile based solar cells is expected to be a promising approach. Therefore, textile-based photovoltaic devices will play a critical role in the wearable energy harvesting. Generally, the conventional solar cell manufacturing techniques cannot be applied to textiles, because conventional solar cells are silicon based and require a smooth, flat and rigid surface. Also, the manufacturing procedures are quite complicated with high

production costs. Dye-sensitized solar cells have emerged in the solar cell research field as a new generation of devices with several advantages such as the low cost of material and relatively high efficiency. It is also compatible with solution processing, which is more suitable for application on the textile substrate using printing techniques. Currently, screen printing and spray coating are the most widely used printing techniques for depositing functional materials films onto fabrics in a single-step deposition which will not damage the substrate or the previous functional layer. Therefore, this thesis presents work on evaluating the characteristics of the DSSC and the printing rheological specifications of the functional materials to create a flexible DSSC on textiles.

Fabrics also place constraints on the technologies that can be used (e.g. limiting process temperatures) and the surface roughness presents a challenging substrate on which functional film must be deposited. There are many existing examples of solar cells on fabrics that use conventional rigid silicon (glass) or plastic solar cells, as standalone PV devices, which are attached onto the fabric as a functional patch[11]. This approach alters the feel of the textile dramatically making the fabric relatively inflexible and non-breathable, and the fabric itself has no added functionality.

1.2 Background

It is predicted that the world's energy consumption is going to increase by 65% from 2010 to 2040 [12]. In addition, the majority of the world's electricity is generated from traditional energy sources, so the depletion of fossil fuels, coal, global warming, environmental pollution, and oil price increases has led the governments and researchers paying particular attention to developing and exploiting renewable energy sources as an alternative[13]. To solve these problems, many researchers are focusing on the development of renewable energies and new technologies for generating electricity[14]. There are various types of renewable energy resources including hydropower, thermal power, wind power, geothermal energy, and solar power[15]. Unlike fossil fuels, these types of energies are effectively unlimited. Solar energy is one of the most powerful and ubiquitous energy sources[16] since it converts solar energy directly into electrical power using solar cells[17] and has limited impact on the environment[18].

Although solar cells technology has developed rapidly in recent decades and the efficiency of silicon based solar cells has reached 15% to 20%[19], and the III-V semiconductor concentrator solar has the world record efficiency of 44.7% [20]. But the high cost of the core material and the complicated manufacturing process has made these silicon based solar cells limited to use on a large scale production[21]. In order to solve these problems, it is imperative to develop and research new solar cell materials and manufacturing technologies. Compared to the silicon based solar cells, flexible organic and dye-sensitized solar cells are already being commercialised and have more advantages such as low cost of the manufacturing process[22]. Currently, dye-sensitized solar cells (DSSCs) are being invited by Michael Grätzel, and are a promising alternative method for harvesting solar energy [23]. The efficiency of DSSC is not as high as for silicon based solar cell, however the cost of manufacturing is much lower, and this DSSC technology could be used for harvesting both indoor and outdoor light [24].

The DSSC has become a promising alternative method for solar cells due to its low-cost materials; and simple manufacturing process[25]. In contrast to silicon based solar cells, DSSCs are photo-electrochemical solar cells, which have attracted intensive research work over the few decades [26]. The DSSC typically has a sandwich structure; the active layer is a mesoporous semiconductor oxide film which is usually nano-crystalline TiO_2 coated on a transparent conductive oxide glass sheet, and covered by a monolayer of dye molecules, which forms the photo anode [27]. The visible light is absorbed by the dye molecule, and the excited electrons in the dye molecule are injected into the conduction band of the TiO_2 nano-crystalline layer [28]. The electrolyte, which contains a redox mediator, is in contact with the dye-sensitized TiO_2 nanoparticles, and transport the holes to the counter electrode which is a platinum coated transparent conductive oxide (TCO) glass sheet [29].

Some previous research has demonstrated DSSCs on flexible substrates such as plastic (ITO-PEN) substrates to extend the applications of DSSCs and also to further reduce the material cost [25]. In its planar form, they could be used for large scale production using low cost printing techniques[30] which have advantages over other types such as 3D structured photovoltaic fibre based DSSCs [31].

1.3 Objectives

The aim of this research is to fabricate DSSCs on fabric substrates in order to achieve a lightweight, flexible energy harvesting textiles for smart applications. The DSSC devices were initially fabricated using FTO glass substrates to investigate the characterization of DSSCs and to explore the formulation of a low temperature processed photoactive layer fabricated from a TiO_2 paste/ink suitable for different printing techniques such as screen printing and spray coating. This screen printed and spray coated TiO_2 paste/ink was used on FTO glass, plastic and textile substrate to study the morphology of the TiO_2 film and the rheological specifications of different printing techniques used for TiO_2 deposition.

The DSSC devices were investigated with liquid and gel based electrolytes forming solid-state DSSC with different substrates using the low temperature processed TiO_2 ink. The research plan targeted the following objectives:

(1) Evaluate different flexible substrates with a final objective of the standard 65% polyester 35% cotton fabric, and glass fibre textile as the DSSC bottom electrode.

(2) Investigate and formulate low temperature processed TiO_2 paste and ink to for application on fabric using different printing techniques, and achieve the rheological specifications for the different printing techniques used.

(3) Fabricate and analyse screen printed and spray coated low temperature processed TiO_2 film on FTO glass, polyimide film (Kapton) and standard 65% polyester 35% cotton fabric.

(4) Fabricate and analyse fully flexible liquid electrolyte based DSSC on interface (Fabink-IF-UV4) coated standard 65/35 polyester cotton fabric (IF fabric) with encapsulation.

(5) Fabricate and analyse fully flexible liquid electrolyte based DSSC on glass fibre textile with encapsulation.

(6) Fabricate and analyse solid-state DSSC on glass fibre textile with encapsulation and perform bending tests to characterise the flexible DSSC.

1.4 Statement of novelty

There are 6 main novel aspects in this research which are summarized below:

(1) Investigation the formulation of low temperature processed TiO_2 paste/ink for use on flexible substrates.

(2) Investigation of the rheological specification of low temperature processed TiO_2 paste/ink and characterization of DSSC on Kapton and fabric with interface substrate.

(3) Fully flexible fabric based DSSC based on liquid electrolyte with a maximum PCE value of 4.04%.

(4) Solid-state dye-sensitized solar cell (ssDSSC) using AgNW coated PEDOT: PSS as the top electrode with a maximum PCE value of 2.8%.

(5) Investigation of different conductive layer in DSSC.

(6) Investigation of the methods to reduce the surface roughness of the textile.

The novelty of this research is briefly explained in Figure 1.1 based on two research paths (liquid electrolyte DSSC and solid-state DSSC) towards the final research target. The conventional DSSC structure (Fig1.1, stage 1.1) contains a thin layer of TiO_2, dye molecules and platinum metal sandwiched between two FTO glass substrates introducing the liquid electrolyte which is presented in Chapter 4. Glass/FTO/TiO_2/Dye/Liquid electrolyte (I^-/I_3^-)/Platinum/FTO/Glass was first assembled as a reference device with an efficiency of 9.1%. The low temperature processed TiO_2 materials for different printing techniques were investigated using this structure; while the formulation of the TiO_2 and the specific rheological requirements for screen printing and spray coating were also investigated at this stage. A maximum PCE value of 4.3 % was achieved with low temperature processed TiO_2 paste on FTO glass substrate. To achieve a fully flexible DSSC, the DSSC device was firstly printed onto Kapton (non-conductive substrate) as the intermediate stage towards the final target fabric substrate since it is smoother than the fabric. The device is then printed on the interface coated fabric to study the rheological specification of printing the formulated low temperature processed TiO_2 paste. Using the FTO glass substrate as the top electrode (Fig1.1, stage 1.2) with an efficiency of 7.03% on Kapton, and 2.78% on the fabric interface substrate which is presented in Chapter 5. Different conductive layer Ag and AgNW was compared in this chapter as well. Subsequently, the top FTO glass electrode was replaced with a graphite coated ITO/PET plastic substrate (Fig1.1, stage 1.3) with an efficiency of 3.24 % achieved on interface coated fabric and 4.04% on the glass fibre textile substrate which is presented in Chapter 6.

To realise a wearable textile solar cell, the liquid electrolyte is not suitable to print on the textile substrate and also the leakage and evaporation of the liquid electrolyte will affect the long-term stability of the DSSC device. Therefore, the liquid electrolyte was replaced by a solid electrolyte (spiro-OMeTAD), and AgNW coated PEDOT:PSS was used as the counter electrode instead of the platinum coated FTO glass substrates.

The solid-state dye-sensitized solar cells (ssDSSCs) on FTO bottom glass substrates is usually combined with opaque top metal electrodes deposited by thermal evaporation. This architecture basically restricts illumination to only through the bottom transparent electrode. Recently, significant research has been focussed on solution-processed silver nano wires (AgNWs) coated PEDOT:PSS that can be applied as a flexible semi-transparent top electrode in ssDSSCs. With this semi-transparent top electrode, ssDSSCs can be screen printed or spray coated on plastic or textile substrates allowing for easier processing and depositing of all functional layers. The structure of ssDSSC (Fig1.1, stage 2.1) was Glass/FTO/TiO_2/Solid electrolyte (spiro-OMeTAD)/PEDOT:PSS/AgNW. A reference ssDSSC device was built first to investigate the characterization of the functional material with an efficiency of 2.8 % achieved on a single FTO glass substrate which is presented in Chapter 7.

Next, the conductive FTO was changed to silver (Ag), while the structure (Fig1.1, stage 2.2) used was Glass/Ag/TiO_2/Dye/Solid electrolyte (spiro-OMeTAD)/PEDOT:PSS/AgNW. There are two main reasons of a high temperature (usually 450°C) is needed for ssDSSCs processing. Firstly, to remove organic binders which contributed to increasing the viscosity of the nanoparticle TiO_2 colloidal pastes for printing purposes, and secondly to create an electromechanical bond between the nanoparticles in the TiO_2 layer for efficient collection of the excited electrons, and also to enable the TiO_2 compact layer to form the crystalline structure.

In this study, a glass fibre textile, which can be processed at temperatures beyond 450°C, has been used to fabricate high temperature processed DSSC. In order to improve the performance of the ssDSSC, an additional polyimide layer was screen printed onto the glass fibre textile to reduce the surface roughness (fig. 1.1, stage 2.3) is presented in Chapter 8, which enabled the deposition of a homogenous TiO_2 film. However, polyester cotton wearable textile substrates can only be treated only up to 150°C, and this research has also focused on realizing the methods to fabricate the TiO_2 compact layer at lower temperatures.

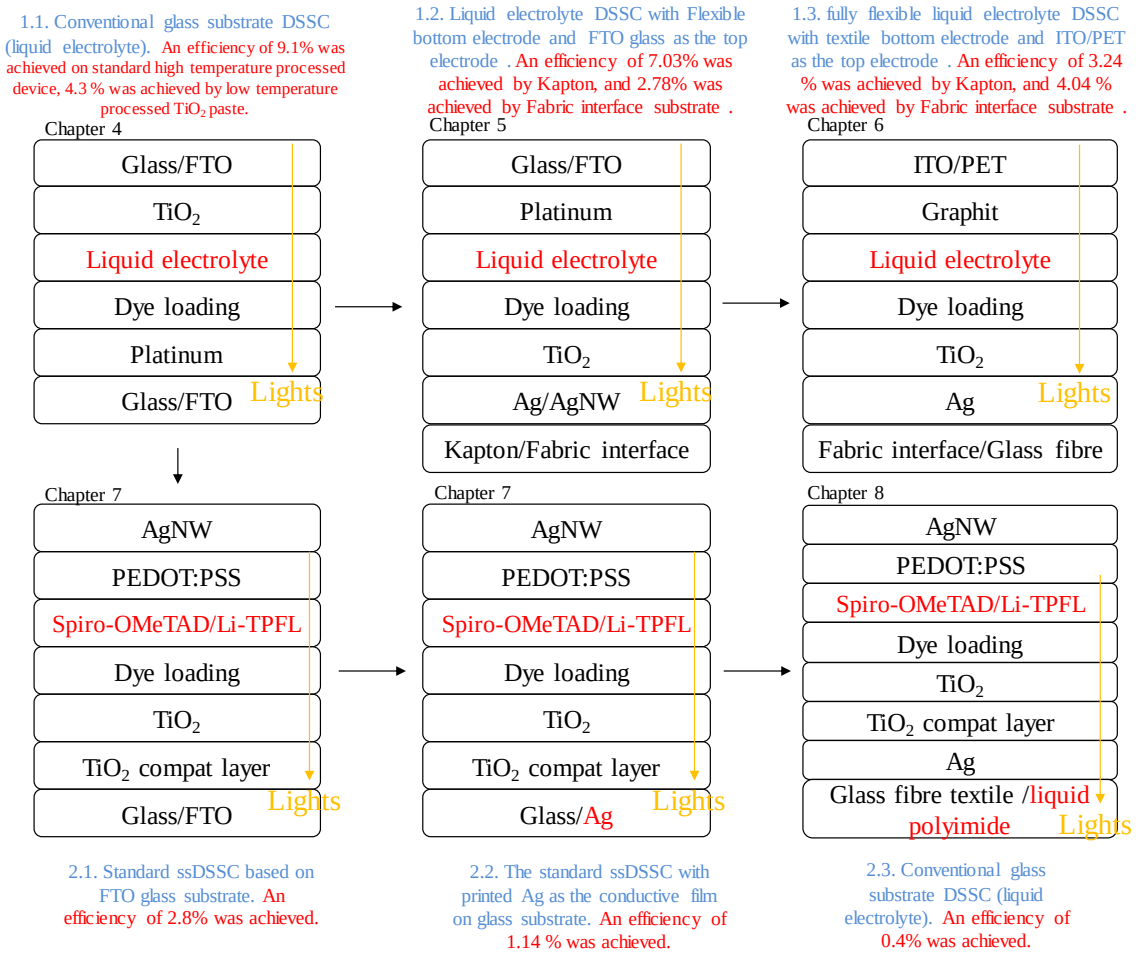

Figure 1.1. Research pathway for the development of textile based DSSCs.

1.5 Publications arising from this research

Conference Posters:

1) J. Liu, Y. Li, S. Arumugam and S.P. Beeby, 'Screen Printed Dye Sensitized Solar Cells (DSSCs) on Woven Polyester Cotton Fabric for Wearable Energy Harvesting Applications' 1st International conference on Advanced Energy Materials (AEM), 388 Stag Hill, Guildford, *University of Surrey*, GU2 7XH , *12th – 14th Sep. 2016.*

2) Y. Li, J. Liu, S. Arumugam and S.P. Beeby, 'Investigation of Low Temperature Processed Titanium Dioxide (TiO_2) Films for Printed Dye Sensitized Solar Cells (DSSCs) for Large Area Flexible Applications' 1st International conference on Advanced Energy Materials (AEM), *University of Surrey, 12th – 14th Sep. 2016.*

3) Y.Li, S.Arumugam, J.Liu, R.Torah and S.Beeby, Fully spray coated solar cells on woven polyester cotton fabric for wearable energy harvesting applications, Department of Electronics and Computer Science, University of Southampton. Energy harvesting conference, London UK,19th March 2015.

4) J.Liu, S.Arumugam, Y.Li, and S.Beeby, Solid-state dye-sensitized solar cell on textile for wearable energy harvesting applications, Department of Electronics and Computer Science, University of Southampton. 5th NanoToday conference, 69-275 Waikoloa Beach Drive,Hawaii USA, 6 December, 2017.

Conference papers:

1) J. Liu, Y. Li, S. Arumugam and S.P. Beeby, 'Screen Printed Dye Sensitized Solar Cells (DSSCs) on Woven Polyester Cotton Fabric for Wearable Energy Harvesting Applications' *Materials Today Proceedings, vol. 5, pp.13753-13758, 2016, doi:10.1016/j.matpr.2018.02.015*.

2) J. Liu, Y. Li, S. Arumugam and S.P. Beeby, 'Investigation of Low Temperature Processed Titanium Dioxide (TiO_2) Films for Printed Dye Sensitized Solar Cells (DSSCs) for Large Area Flexible Applications' *Materials Today Proceedings, vol. 5, pp.13846-13854, 2016, doi:10.1016/j.matpr.2018.02.026*.

3) S.Arumugam, J.Liu, Y.Li, and S.Beeby. Optimised process of fully spray-coated organic solar cells on woven polyester cotton fabrics, *Materials today : proceedings, vol. 5, pp. 13846-13854proceedings, vol. 5, pp. 13745-13752*, 2016, *doi.org/10.1016/j.matpr.2018.02.014*.

4) M.Li, R.Torah, J.Liu, A.Komolafe, J.Tudor, S.Beeby 'The thickness and material optimization of flexible electronic packaging for functional electronic textile', *2018 symposium on Design, Test, Integration & Packaging of MEMS and MOEMS (DTIP), 10.1109/DTIP.2018.8394186*.

Journal papers:

1) J. Liu, Y. Li, S. Arumugam and S.P. Beeby, Flexible Printed Monolithic-Structured Solid-State Dye Sensitized Solar Cells on Woven Glass Fibre Textile for E-Textile Applications' *Scientific Reports, 2019,* *doi.org/10.1038/s41598-018-37590-8.*

2) J. Liu, Y. Li, S. Arumugam and S.P. Beeby, 'Processing of Printed Dye-sensitized Solar Cell on Woven Textiles', *IEEE Journal of Photovoltaics, Volume:9, 2019,* *doi.org/10/1109/JPHOTOV.2019.2899432*.

3) M.Li, R.Torah, J.Liu, A.Komolafe, J.Tudor, S.Beeby, Finite element analysis (FEA) modelling and experiment verification to optimize flexible electronic packing for e-texitles, Microsystem Technologies, 2018 (accepted).

1.6 Structure of this thesis

Chapter 1 introduces the underlying motivation of this research and outlines the areas of focus. An introduction to the research work is also presented, emphasising the critical features of textile based DSSC and the novelty achieved in realising printed DSSC and ssDSSC on different substrates.

Chapter 2 mainly describes the structure, operational process, and mechanism of the conventional DSSC and ssDSSC in detail, including the solar device testing conditions and calculations. Some semiconductor theory is also included.

Chapter 3 presents an intensive review of the existing research methods contributing to the fabrication of DSSC on the textile substrate. Approaches to formulating the low temperature of liquid electrolyte DSSC on FTO glass and ITO/PEN substrate were first introduced by the TiO_2 colloidal sol-gel method or additional $TiCl_4$ treatment method. Methods for fabricating semi-flexible DSSC with textile as the bottom electrode and FTO such as the graphene oxide coated conductive cotton fabric, multi-walled carbon nanotube (MWCNT) coated polyester fabric based DSSC are discussed. The fully flexible DSSC with 3D fibre architecture, weaving or attaching method, and a combination of textile substrate and ITO/PEN substrate are analysed. Finally, low temperature processed ssDSSC and its evolution type perovskite solar cell are discussed.

Chapter 4 summarises the investigation of the low temperature processed TiO_2 paste formulations for both screen printing and spray coating on glass substrates with the conventional DSSC structure. The main part of this chapter summarizes the formulation of the low temperature processed TiO_2 ink with different annealing temperatures and solvents.

Chapter 5 explores the fabrication process and methods for the screen printed DSSC on fabric and Kapton substrates based on the liquid electrolyte of DSSC using FTO glass substrates as the top electrode. This chapter includes the theory and design of four types of screen printed and spray coated DSSC on polyimide (Kapton) and polyurethane (interface) coated polyester cotton fabric substrates with different conductive films. The treatment and the coatings of the substrate is described with different conductive films to evaluate the different substrates and processes. Kapton is used as a high temperature non-conductive plastic substrate to be investigated the performance of DSSC on a con-conductive high temperature plastic also as the intermediate stage towards the textile substrate. The next section presents the results and measurements in order to evaluate and analyse the characterization of the DSSC. Finally, an overall discussion and conclusion are presented. Chapters 6, 7 and 8 follow the same chapter structure as in Chapter 5 in sections of theory, design, architecture, fabrication and results discussion for the fully flexible liquid electrolyte DSSC, ssDSSC on glass substrate, and the textile based ssDSSC.

Chapter 9 summarises the research work completed to achieve the objectives and novelties. In addition, this last section highlights the possible research direction for future work towards improving the final target of the research, a highly efficient and flexible textile based solar cell on single fabric substrate at low temperature via solution process.

Chapter 2

2 Literature review: Literature review: Dye-sensitized solar cells (DSSCs) theory and characterization

2.1 Introduction

Many photovoltaic technologies exist in the current PV market suitable for converting sunlight into the electricity. Currently, monocrystalline and polycrystalline silicon wafer based solar cells occupy 90% of the PV market with efficiencies of over 20 % possible, and the bulk Si solar cell has approached the thermodynamic limit of 26.6% [32]. Monocrystalline Si solar cell has been driven to push the efficiency around 30% Shockley-Queisser limit, PV community is striving to reduce the cost of the device. Polycrystalline Si solar cells contain small-sized grains have improved the efficiency to 21.9% by controlling the recombination at grain boundaries and optimizing the passivated interfaces and deposition process. The multi-junction thin-film amorphous Silicon solar cell has reached an efficiency of 13.6% with low-cost fabrication process [33, 34]. However, the high cost of the silicon wafer and associated processes has restricted the applications of silicon based solar cell. In order to bring down the cost of the silicon based solar cell, the 2nd generation solar cells was explored based upon thin-films using cadmium telluride (CdTe) and copper indium diselenide (CIGS) compound semiconductors. In the laboratory CIGS and CdTe solar cell has reached 21.7% [35] and 21.5% [36] respectively. Although the thin-film solar cell has been demonstrated a promising way to harvest sunlight it still relies on complex manufacturing procedures and uses toxic materials. The 3rd generation of photovoltaic devices include organic solar cell (OSC), dye-sensitized solar cell (DSSC), and the most recent demonstrated perovskite solar cell (PSC). The low cost of the functional material, solution processed roll-to-roll manufacturing and also the relevant high PCE make it competitive in the current photovoltaic research field.

Among the 3rd generation photovoltaic solar cell devices, dye-sensitized solar cell has emerged as a reliable photovoltaic device with low cost, fully solution based processes suitable for flexible substrate. The first nanocrystalline DSSC, also known as the Grätzel cell, was reported

in 1991 with a solar energy conversion efficiency 7.1% [37, 38], which led to considerable research work on improving the efficiency of DSSC over the last two decades. In 1993, Grätzel et al. reported 9.6% efficiency of the DSSCs, and in 1997, an efficiency of 10% was achieved at the national Renewable Energy Laboratory (NREL) [39]. Yella et al. had demonstrated an efficiency of 12.3% by using zinc porphyrin dye (YD2-o-C8) and cobalt-based redox electrolyte in 2011[40]. Then, an efficiency of DSSC has been improved to 13% based on sensitizing with molecularly engineered porphyrin dye[41]. A higher efficiency of 14.3% was achieved by fabricating with Au/GNP as the counter electrode, and $Co^{3+/2+}$ as the redox couple, and LEG4 + ADEKA-1 as the photo-sensitizer was reported by Kakiage et al in 2015[42]. To date, DSSC efficiency has achieved to 15% by using perovskite sensitizer which is reported by Burschka et al.[43]. Although the efficiency of DSSCs are not as high as conventional silicon based solar cells, which can achieve up to 24.5 % [44], it is a lower cost alternative.

A conventional DSSC is typically comprises a photo anode, photo-sensitizer, electrolyte, and the counter electrode[31]. The photo anode is typically a FTO or ITO coated TCO glass substrate, with a mesoporous nano-crystalline semiconductor film deposited on it[45]. Several semiconductor film materials have been investigated for use in this layer such as Titanium Dioxide (TiO_2), Zinc oxide (ZnO) [46], Tin oxide (SnO_2) [37] and Niobium pentoxide (Nb_2O_5) [47]. In this research, TiO_2 will used as the photoactive material in the photo anode. The sun light in the visible region (around a wavelength of 400nm ~800nm)[48] can be absorbed by the photo-sensitizer under AM1.5G condition (or one sun condition)[49]. It is usually a monolayer of dye molecules deposited on the semiconductor film[29] and the standard photo-sensitizer which was developed in the early stage of DSSC research is a Ruthinium based complex (Ru-II) such as N3, N719 and black dyes (N749)[50]. The electrolyte is like a mediator contact between the dyes and the counter electrodes[51] which enables the charge transportation between the counter electrode and the dyes[52] to form a continuous loop. The counter electrode of the DSSC acts as the electron collector to collect the electrons[53] from the external load, and transport to the electrolyte [54].

The DSSC is measured under 1 sun condition in this thesis, and there are some parameters being used to evaluate the performance of the DSSC, such as the incident photon to current efficiency (IPCE) [50], overall light to electrical efficiency (η), maximum output power (P_{max}), open circuit voltage (V_{oc}), short circuit current (I_{sc}), fill factor (FF) and the current density (J_{sc}) [48, 49]. The values of these parameters depend on the structure and materials used in the DSSC. These values can be found or calculated based on the IV properties of the cell.

2.2 Solar cell background

A solar cell is a type of energy harvester that collects solar power from sunlight and converts it into electrical power. The conventional photovoltaic device is based on silicon, and photovoltaic energy conversion consists mainly of two steps. Firstly, once the sunlight enters the cell, an electron – hole pair will be generated by the absorption of the sunlight. The generated electron and hole pair will subsequently separate due to the structure of the photovoltaic device, with the electrons moving to the negative terminal and the holes moving to the positive terminal. The electrons and holes will travel through the external circuit and thus electrical power is generated.

2.2.1 Principle of solar cells and semiconductors

Every solid has its own energy band structure, and materials can be categorized as metal, semiconductor or insulator by different band gaps. The energy bands of a metal, semiconductor and insulator are shown in figure 2.1. Mostly, the electrons are filled in the valence band below the Fermi energy level in static state, while the conduction band (above the Fermi level) is usually empty. Electrons are free to move into the empty conduction band with an electric field. In a metal, the electrons can easily pass into the conduction band since the conduction band and valence band overlap. If the metal is in a low oxidation state (electron rich) and the ligand possesses low-lying empty orbitals, then a metal-to-ligand charge transfer compounds having n-acceptor ligands. Upon the absorption of light, electrons in the metal orbitals are excited to the ligand excited orbitals. In semiconductors, electrons in the valence band need to gain greater energy than the band gap energy level to pass between the conduction band and the valence band to enter into the empty conduction band. There is a large gap between the conduction and valence band in an insulator which means even higher levels of energy is needed to allow the electron to jump into the conduction band from the valence band.

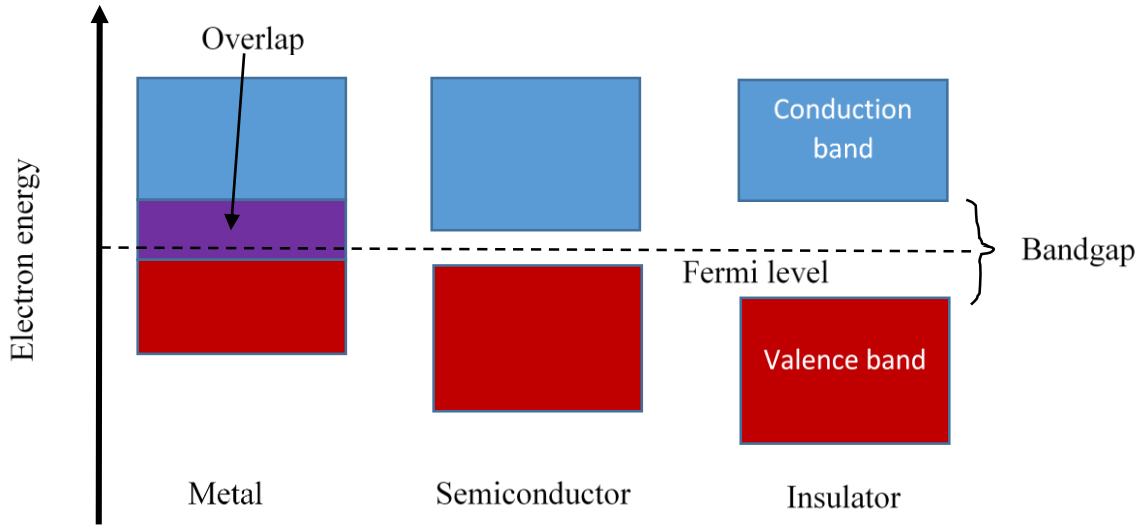

Figure 2.1. Bandgap diagram of metal, semiconductor and insulator[55].

In molecular materials, the energy level can be referred to as the energy level of the semiconductor materials as shown in figure 2.2. The electrons in a semiconductor are usually characterized by the Fermi level (E_f), and this is considered to be located in the middle of the band gap under thermodynamic equilibrium state. Therefore, the band gap is a major factor that determines the electrical conductivity of a solid. The electron affinity is the energy gained when an electron is moved from the vacuum level to the conduction band edge. The energy required to promote an electron from the valence band of the semiconductor to the vacuum level is the ionization potential, which will determine the ability of a compound to be oxidized. These factors are used to analyse and improve the performance of the semiconductor devices[56].

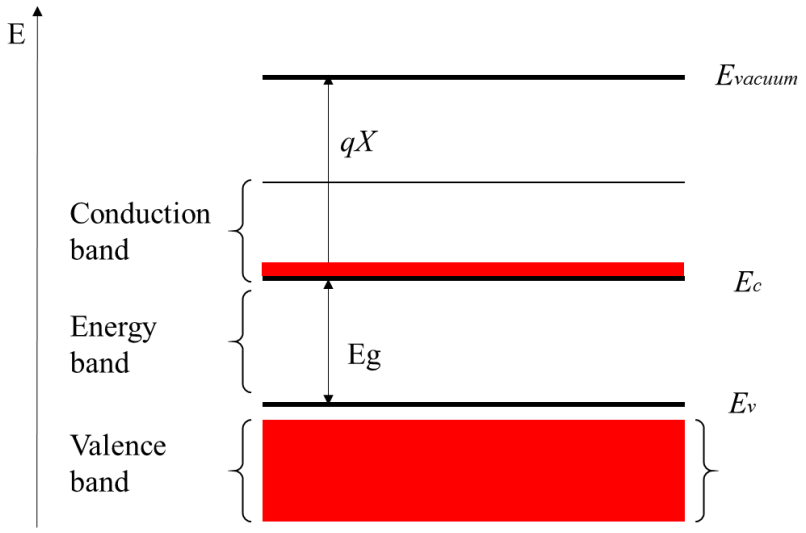

Figure 2.2. Energy band diagram of a semiconductor, E_v is the edge of valence band, and E_c is the edge of conduction band, E_{vacuum} is the vacuum level, electron affinity χ, and the energy band gap E_g[56].

A p-n junction is one of the key technologies in solid-state electronics. It is the boundary of p type and n type semiconductor materials. The p-n junction is formed by joining n-type and p-type semiconductor materials together. After joining the n-type semiconductor and p-type semiconductor materials together, a large density gradient exists between both sides of the p-n junction (refer to figure 2.3). Electrons near the p-n junction interface of the n region tend to diffuse into the other side of the p-n junction, which leaves a positively charged ion in the n region and combines with the holes in the p region. Meanwhile, the holes from the p-type semiconductors begin to diffuse into the n-type semiconductor material, leaving a negatively charged ion in the p region that combines with the electrons in the n region. The electrons in the p region that migrated from the n region are now acting as negative ions, and the holes in the n region are positive ions. A depletion layer is then formed by the movement of the carriers near the p-n interface region, and an electric field is created by this depletion layer. In order to maintain a neutral charge condition around the p-n junction, the total carrier charge of each side must be equivalent to the opposite side in a p-n junction.

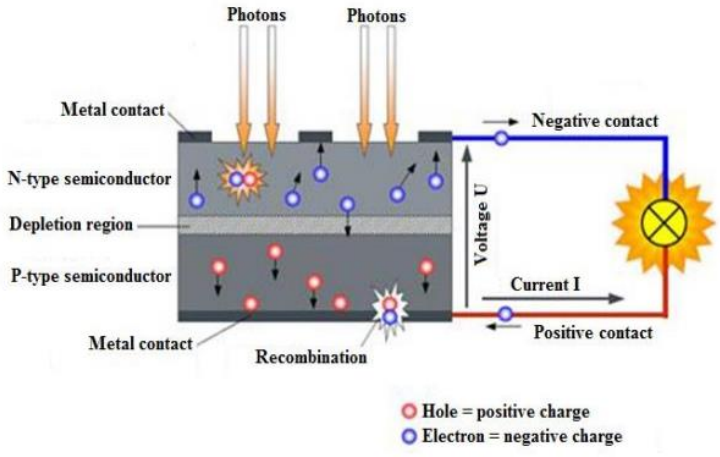

Figure 2.3. P-n junction and semiconductor working principle [57].

A solar cell uses semiconductor technology to absorb sunlight and converts it to electricity based on the effect of the p-n (or p-i-n) junction. Briefly, photons absorbed sufficient energy will cause electrons in the valence band to jump into the conduction band, which then generated electrons and hole pairs. Subsequently, the generated electrons and hole pairs within the p-n junction depletion region travel to the opposite side by the electric field effect in the depletion region, and then the electrons and holes pass through the external circuit to produce the power.

2.2.2 Sun energy and calculations for solar cell

The sunlight is emitted from the sun and can be classified into several regions by the wavelength. The wavelength is from the shorter wave length γ-rays, x-rays, ultraviolet, visible, and infrared to the long radio wavelengths [58]. The electro-magnetic spectrum is shown in Figure 2.4. The rays with a shorter wavelength have higher energy. For the semiconductor used in the photovoltaic devices such as silicon, the electrons in the valence bands need to gain enough energy to move across the band gap (1.14eV) to the conduction band. Visible light, with the wavelength from 380nm to 750nm, has sufficient energy[58] to enable the electrons to move across the band gap. It is not only the visible light, the light outside the visible spectral range also excite electrons across the bandgap when the photon energy is greater than the band gap. The energy of light depends on the wavelength, which is $E = h\upsilon$, where E is the energy, υ is the frequency and h is Planck's constant ($h = 6.626 \times 10^{-34}$ J.s) [58]. The frequency $\upsilon = c/\lambda$ [59], where λ is the wavelength of the light and c is the speed of the light which is 3×10^8 m/s [59]. Therefore, the energy of the light can be calculated by $E = hc/\lambda$ [59].

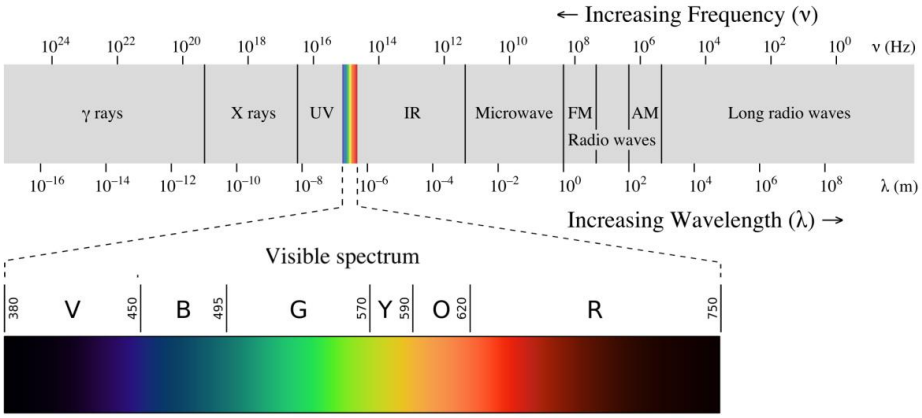

Figure 2.4. Electromagnetic radiation spectrum [58].

The current–voltage characteristics of a solar cell is shown in figure 2.5(a) in the dark and under illumination permit an evaluation of most of its photovoltaic performances as well as its electric behaviour [60]. In the dark, a typical diode-type I-V response with limited current flows in the reverse bias direction (V<0) can be recorded. As the cell is illuminated, the I-V curve is ideally shifted down at all potentials because of the additional photocurrent, and power is generated in the devices. Note that the photovoltaic effect only occurs in forward bias (V>0), where the cell generates power when the product of the current and the voltage is negative. V_{oc} is the voltage across the solar cell when the cell current is zero. J_{sc} is the cell current density when there is no applied bias to the cell. I_{max} and V_{max} are the values of the current density and voltage that provide the maximum power P_{max} delivered by the PV cell. Fill factor (FF) is a parameter obtained from the illuminated cell I-V curve and is defined as the ratio of the maximum output power to the product of short circuit current and open circuit voltage (Equation (1)).

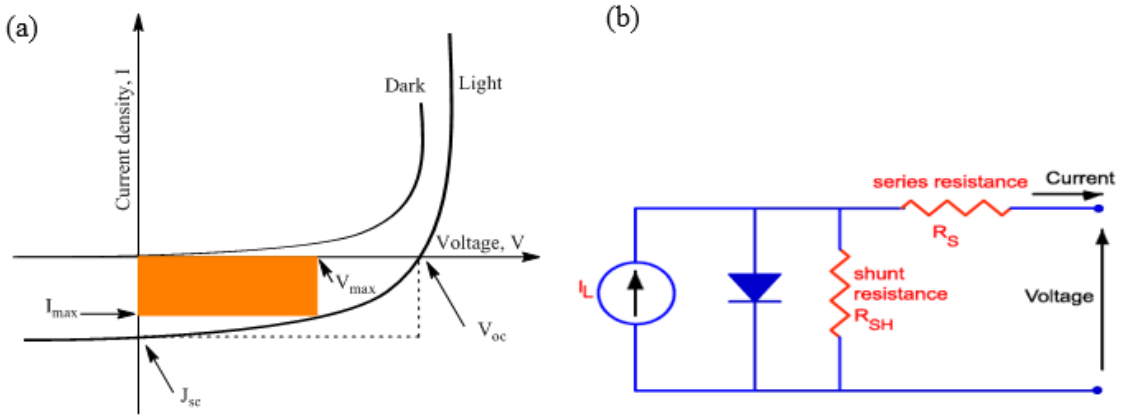

Figure 2.5. (a) I-V characteristics of an organic solar cell under dark, and illuminated conditions and (b) circuit diagram of shunt (R_P) and series resistance (R_S) [61].

$$FF = \frac{I_{max} \times V_{max}}{I_{sc} \times V_{oc}} = \frac{P_{max}}{I_{sc} \times V_{oc}} \quad (1)$$

$$\eta_{max} = \frac{P_{max}}{P_{in}} = \frac{I_{sc} \times V_{oc} \times FF}{P_{in}} \quad (2)$$

FF is directly affected by the series and shunt resistance values of the cells, as shown in figure 2.5(b). Increasing the shunt resistance (R_P) and decreasing the series resistance (R_S) would lead to larger FF and could push the device output power (P_{max}) towards its theoretical maximum. According to equation 10, power conversion efficiency (PCE), η is defined as the ratio of the maximum electrical power generated to the incident light intensity (as shown in Equation (2)). Because of the light intensity dependence on the photovoltaic response, the efficiency should be measured under standard test conditions. The conditions normally used are AM1.5 (air mass 1.5) corresponding to solar irradiation with a zenith angle of 48.2° which gives a pathway of the sunlight across the atmosphere that is as long as 1.5 times its thickness with the light intensity of 1000 W/m^2 and characteristic solar spectral distribution [62].

2.3 Structure of DSSC

DSSCs have emerged as a promising renewable alternative to the traditional solid-state solar cell due to its distinctive cell structure[63]. The structure of a conventional DSSC is shown in figure 2.6. The DSSCs generally consist of four primary parts [64].

A photo anode is on top of the cell and the incident light goes through the cell from this side. It is made of a TCO glass substrate coated with FTO or ITO [29], and a semiconductor oxide film which is normally TiO_2 coated on a glass substrate. The morphology of TiO_2 is mesoporous nanoparticles [65]. Screen printing and the spray coating methods could be used to fabricate TiO_2 film on the substrate. The ideal thickness for the TiO_2 is from 5 μm to 30μm with pore size diameter of 15 nm to 20 nm [29].

The next functional material is the photo-sensitizer, which plays an important role in DSSC. The theoretical value of the panchromatic photo-sensitizer is 920 nm [50], which is able to absorb light up to a wavelength of 920 nm at the higher wavelength range of infrared [50]. The most commonly used photo-sensitizer is the Ruthenium (Ru) based metal complex (Ru II) sensitizer, tris (2, 2'-bipyridyl-4, 4'-carboxylate) ruthenium (II) [66]. It contains an anchor group, carboxylate, to enable the dye molecules to shift towards the TiO_2 surface [26]. Therefore, a monolayer of dye molecules is adsorbed firmly on the surface of the TiO_2 nanoparticles after soaking the photo anode into the dye solution. The light is harvested by these two elements [67].

The electrolyte is added between the dyes and the counter electrode. It contains the redox mediator [41], and transports the negative charges (electrons) to the dye molecules and the positive charges (holes) to the counter electrode to form a continuous charge carrying loop [29]. The organic solvent iodide/tri-iodide (I^-/I_3^-) is the most commonly used liquid electrolyte [68].

The back side of the DSSCs is the counter electrode, which is a platinized FTO coated TCO glass substrate. It collects the external electrons and passes them to the oxidized electrolyte through the platinum [69]. The platinum used in the counter electrode has two main functions. One acts as a catalyst to enable the electrons from the external circuit to move to the oxidized electrolyte efficiently [70]. Thus, the reduction reaction will take place at the counter electrode. The other function is that the platinum will partially block the incident light going out of the cell. Meanwhile, the oxidized dyes are restored in the electrolyte [71].

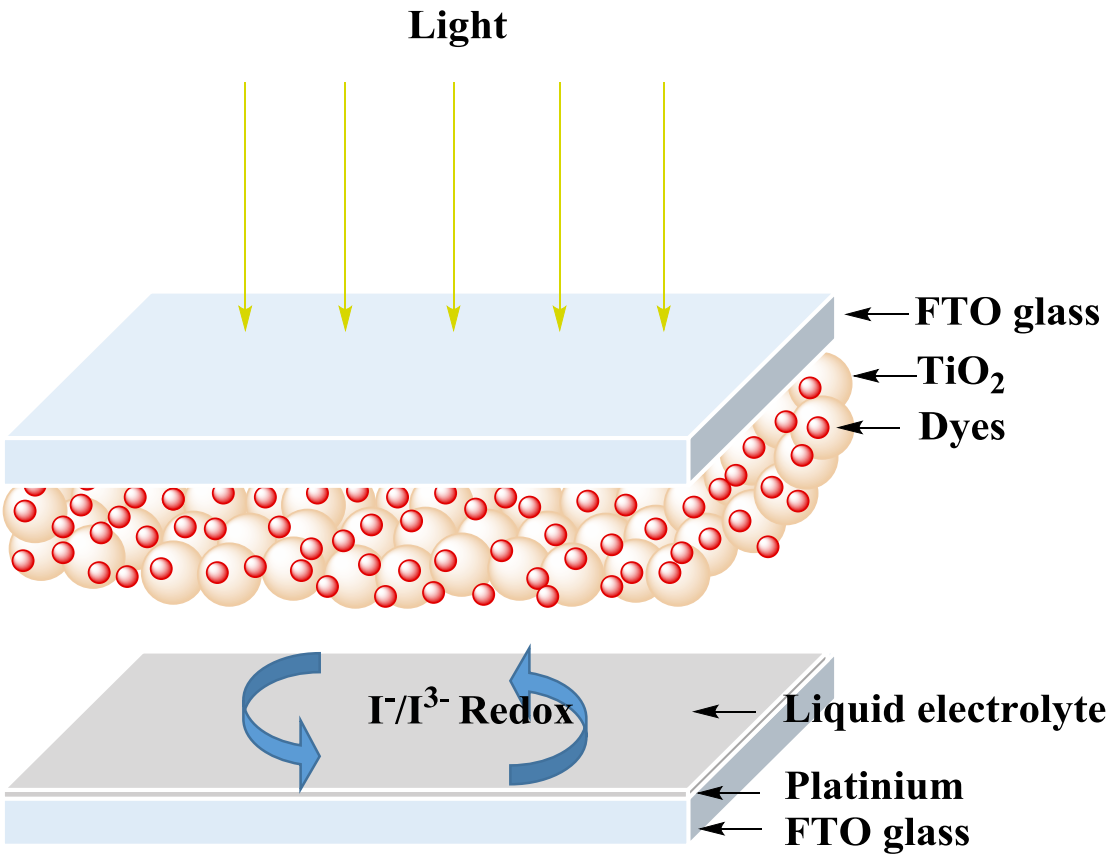

Figure 2.6.Structure of a conventional DSSC [64].

2.4 Operation of DSSC

The operation diagram of a DSSC is presented in figure 2.7. DSSC is a heterojunction solar cell and consists of 5 layers. The operation process could simply be considered as the photosynthesis process in a leaf, as the chloroplasts absorb the sunlight and convert carbon dioxide (CO_2) into oxygen (O_2) and carbohydrates[17]. In DSSC, the chloroplasts are replaced with the dyes, when the incident light comes into the cell through the transparent photo anode and passes to the counter cathode[30]. The dye molecules absorb the light and gain enough energy to excite its electrons from the ground state to the excited state. Consequently, the excited dye molecules graft the electrons to the conduction band of the porous TiO_2 nanoparticles, and finally become oxidized. Subsequently, the injected electrons in the conduction band of TiO_2 are transported through the titanium dioxide film, and then reach the conductive glass substrate which is connected to an external circuit. The electrons travel through the external circuit and arrive at the counter electrode[66]. Meanwhile, the oxidized dye molecules gain electrons from the electrolyte and are restored to their initial state[72].

Since the electrolyte reduced the dye molecules by donating electrons to the oxidized dye molecules, it becomes oxidized. The electrolyte regenerates at the counter electrode by accepting the electrons from the external circuit and this completes one cycle[54].

The whole process in a DSSC can be referred to the content of figure 2.7 and is summarized in the following steps:

1) The incident photons excite the electrons in the dye molecule and move from ground (S) state to excited state (S*) [13].
2) Electrons from the excited state are injected into the conduction band of the TiO_2 [37].
3) The injected electrons are transported through the mesoporous TiO_2 film and followed the external circuit to reach the counter electrode [50].
4) Dye molecules are reduced by accepting electrons from the electrolyte [50].
5) The electrolyte regenerates at the counter electrode [50].

The processes listed above are the forward processes to enable the normal operation for a DSSC. There are still some undesirable processes which are charge recombination processes that take place in the cell. These undesirable processes move the electrons backwards which are the main detrimental effect on the DSSC performance causing energy losses during charge transportation [19]. There are three undesirable processes happening in one transport cycle, which are listed below:

1) The electrons from the excited state go back to the ground state [22].
2) Recombination of the electrons which are injected into the conduction band of the TiO_2 film with the oxidized dye molecules [73].
3) Recombination of the electrons which are injected into the conduction band of the TiO_2 film with the electrolyte [74].

In order to reduce the undesirable processes in DSSC, the electron injection process should be finished in a quantum yield[50]. The highest occupied molecular orbital (HOMO) energy level[48] should be higher than the redox couple energy level, and the lowest occupied molecular orbital (LOMO) energy level should be much higher than the energy level of the TiO_2 conduction band[48].

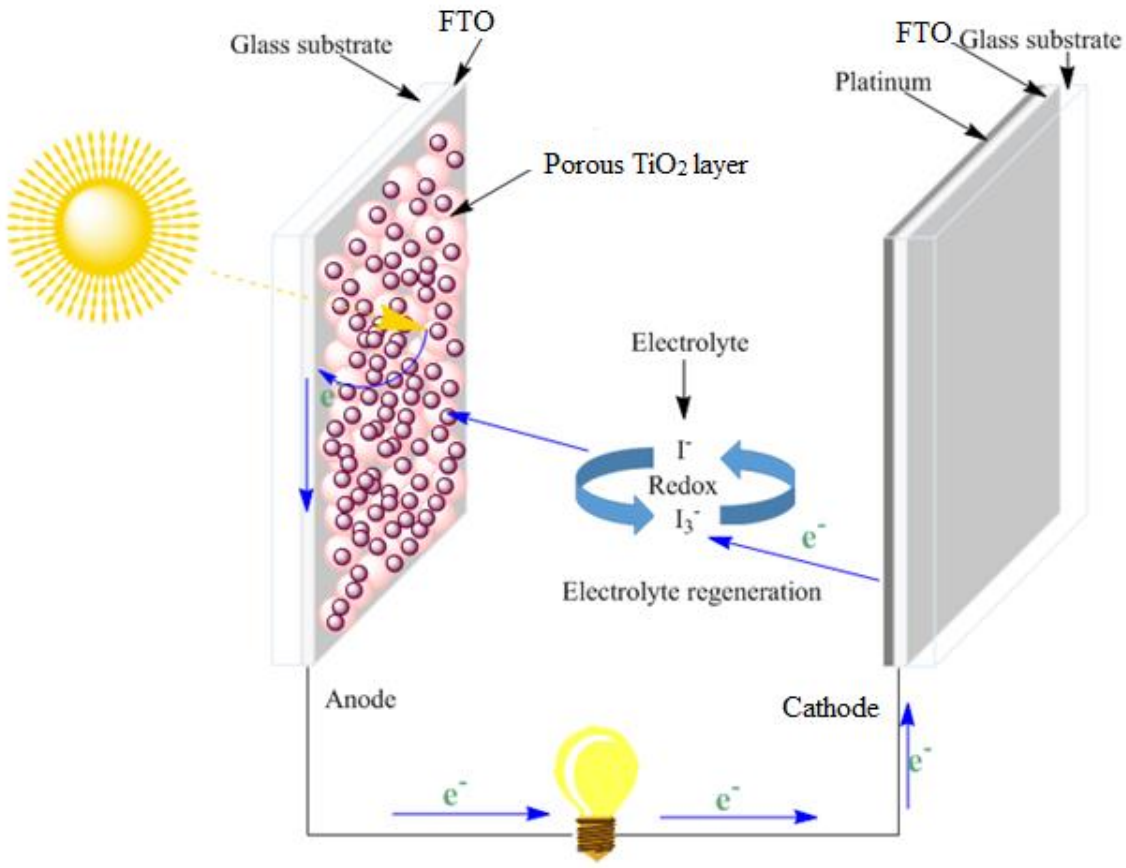

Figure 2.7. Typical structure and working principle of DSSCs [37].

2.5 Mechanism of DSSC

Figure 2.8 shows the mechanism process of the DSSC. The reactions in the whole process are listed in Table 2.1， where S stands for dye molecules, and $E_{h\vartheta}$ [48] is the quantum energy. The mechanism of a conventional DSSC is summarised in 8 paths.

In the initial state, dye molecules are at HOMO energy level. When the light is absorbed, the electrons in the dye molecule are excited from the HOMO (S) to the LUMO energy level (path 1). The reaction equation of this process is shown in equation (1) in table 2.1. The HOMO and LUMO energy levels (S^*) of the dyes are located around -5.5 eV and -3.5 eV respectively [48].

Next, the electrons will be injected into the conduction band of the TiO_2 film quickly (path 2, equation 2), and the dyes become oxidized from S^* to S^+. The timescale for this process is around 1 ps [50], which is much faster than the decay time of dyes. The energy level of the

conduction band of TiO_2 is located at around -4.1 eV [48] which is lower than the LUMO level of the dye molecules, so that the electron can be injected from the dye molecules into the conduction band of TiO_2 [50].

There is also an excited state decay of the dye molecules that needs to be considered (path 3, equation 3). This process occurs in around 1 ns [50]. This is an undesirable process which compares with the electron injection. In order to make the cell efficiently, the rate of the dye decay should be lower than the electron injection into the conduction band.

Subsequently, the oxidized dye molecules are regenerated by the electrolyte (path 4, equation 4), and it takes about a nanosecond [50] which is very efficient compared to the charge recombination process. The HOMO energy level redox I^-/I_3^- is around -4.9 eV [48], which is higher than the HOMO energy level of the dye molecules; that enables the electrons to transfer from the electrolyte to the dyes [28].

After the electrons injection process, it normally takes 1 ms [50] for the electrons to pass through the TiO_2 conduction band (path 5), and arrive at the conductive substrate. When the electrons reach the counter electrode through the external circuit, they will diffuse to the electrolyte and reduce the oxidized electrolyte (path 8, equation 8) [23].

There are two charge recombination processes, which are the reverse reactions of the charge transportation during one charge transportation cycle due to the different electron transfer rates [63]. One is the dye recombination (path 6, equation 6). In this process, some electrons from the conduction band of the TiO_2 reverse to the HOMO state of the dyes [50]. The other one is the electrolyte recombination (path 7, equation 7). The electrons which are injected into the conduction band of the TiO_2 move back to the redox [75].

In order to improve the performance of the DSSC, and to avoid the charge recombination in the DSSC, the rate of the dye regeneration must be faster than the dye recombination rate and electron recombination rate [76]. The rate of the electron injection must be higher than the excited dye decay to the ground state, and the rate of the electrolyte regeneration at the counter side must also be fast enough [76].

The potential and energy level of DSSC are indicated in figure 2.8. The maximum output voltage of a DSSC is the different potential between the Fermi level [76] of the TiO_2 and the redox couple. Under the standard operation, the voltage generates by DSSC is around 0.6-0.8 V [76], and the current is around 16-25 mA, and the efficiency is around 10% [77].

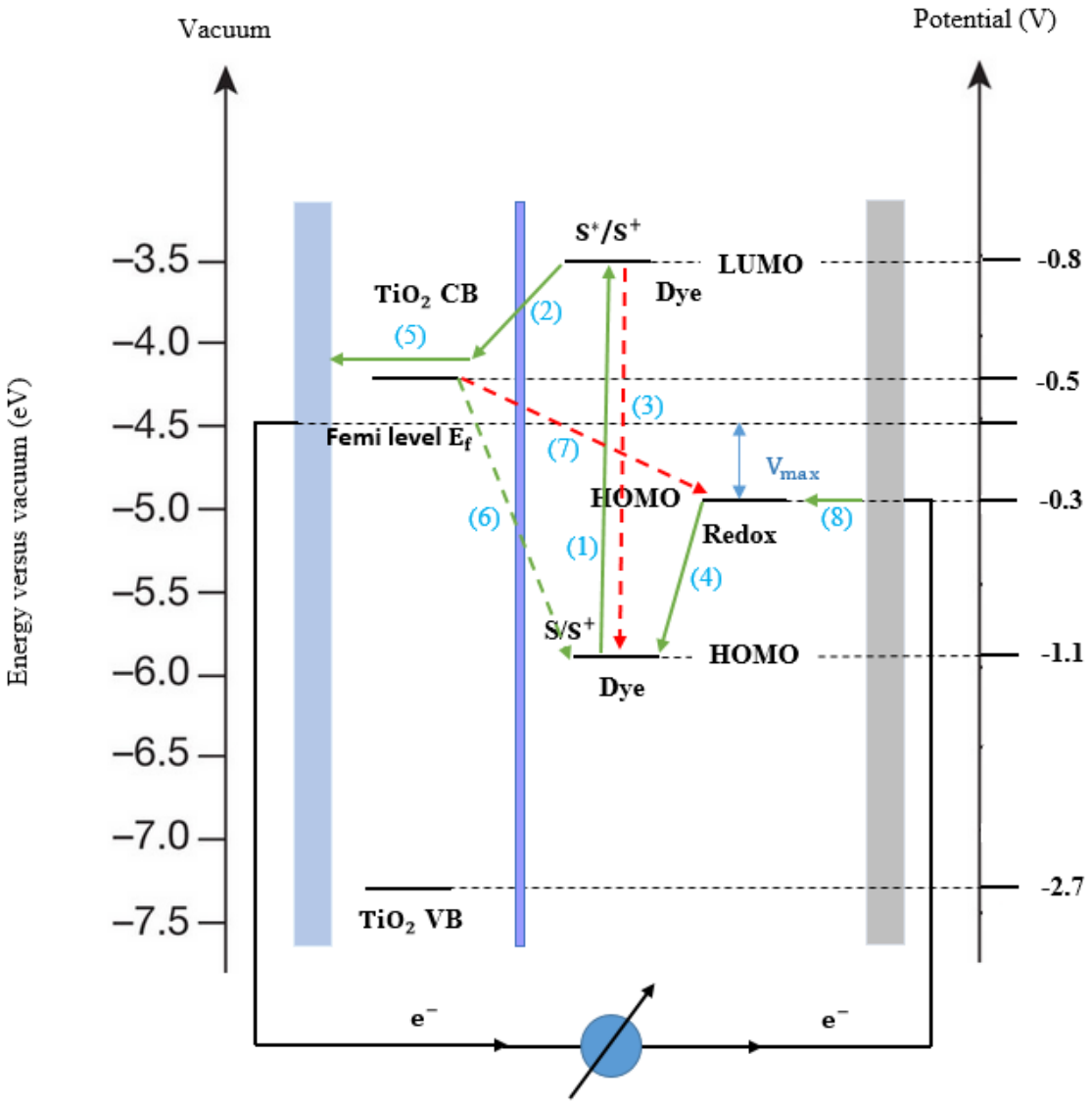

Figure 2.8. Mechanism processes of DSSC [78].

Table 2.1. Reaction equations of DSSC working process [50].

Number	Forward Reaction Equation	Description
(1)	$S + E_{h\upsilon} \longrightarrow S^{*}_{LUMO}$	Dye excitation
(2)	$S^{*}_{LUMO} + TiO_2 \longrightarrow S^{+} + e_{TiO2}^{-}$	Electron injection
(3)	$S^{*}_{LUMO} \longrightarrow S_{LUMO} + E_{h\upsilon}$	Dye decay
(4)	$S^{+} + 3I^{-} \longrightarrow I_3^{-} + S$	Dye regeneration
(6)	$e_{TiO2}^{-} + S^{+} \longrightarrow S^{*}_{LUMO} + TiO_2$	Dye recombination
(7)	$e_{TiO2}^{-} + I_3^{-} \longrightarrow 3I^{-} + TiO_2$	Electrolyte recombination
(8)	$e_{pt} + I_3^{-} \longrightarrow 3I^{-}$	Electrolyte reduction

2.6 Solid-state dye-sensitized solar cells (ssDSSCs) mechanism

The conventional DSSC is usually based on the electrolyte which contains I^-/I_3^- [79]. Although the conventional liquid based DSSC has shown good results, however, the leakage and evaporation of the liquid electrolyte is still a challenge for conventional liquid based DSSC [80].

The evaporation of the liquid electrolyte in DSSC will affect the long-term stability of the cell, and it will evaporate even after the cell is fully assembled [81]. The liquid electrolyte may also react with the water vapour and the oxygen in the air, which will degrade the cell in performance[27]. The leakage of the electrolyte is still another significant problem of the conventional DSSC. It will not only reduce the efficiency, but will also cause problems with short circuit of the cell. When the cell is assembled, the working electrode and the counter electrode are joined together, which makes the liquid electrolyte come into the contact area of the cell and consequently causes the cell to short circuit [71].

Therefore, in order to solve these two problems, the solid-state electrolyte has been investigated and developed as the hole transporting material to replace the ionic liquid electrolyte. This kind of DSSC is called the solid-state Dye-Sensitized Solar Cell (ssDSSC), and the solid-state electrolyte is also known as the Hole Transporting Material (HTM) [82]. The structure of the ssDSSC is similar to that of the conventional liquid electrolyte based DSSC. There are three main types of solidstate electrolyte:

(1) organic HTMs such as spirobiflurorenen (spiro-OMeTAD) which is the most commonly used solid-state electrolyte [83].
(2) inorganic HTMs such as copper(I) thiocyanate (CuSCN) and copper(I) iodide (CuI) [84].
(3) polymer electrolyte such as P3HT (Poly-3-hexylthiophene-2,5-diyl) [45].

The ssDSSC developed in this research is based on spiro-OMeTAD based ssDSSC as shown in figure 2.9. The spiro-OMeTAD has been demonstrated the most efficient hole transporting material (HTM) used in ssDSSC in the literature [85]. The liquid electrolyte is replaced with the spiro -OMeTAD [86]. Since the insufficient pore filling of the HTM into the mesoporous

TiO_2 film is one of the main limitations on the ssDSSC performance. The pore filling starts with the deposition of the HTM solution onto the mesoporous TiO_2 layer, it forms a wet over layer and gradually diffuses into the mesoporous TiO_2 film, the evaporation of the solvent in the HTM leads to a high concentration of the HTM solution and the HTM may not be dispersed homogenously or entirely into the TiO_2 layer. Therefore, the HTM requires a high solubility to dissolve the HTM in the solvent and should also demonstrate a good ability to achieve a sufficient pore filling [87]. There are two important features of spiro -OMeTAD for the demonstrated reliable performance of ssDSSC, one is its stability and the other is its solubility. The spiro -OMeTAD (2,2',7, 7'-tetrakis(N,N-di-p-methosyphenyl-amine)9,9'-spirobifluorene) [88] is an amorphous organic HTM, which belongs to the molecular glass group [82]. The stability of spiro-OMeTAD is determined by its molecular structure, which is shown in figure 2.10, and the structure depends on the glass-transition temperature, which could change the state of spiro-OMeTAD. The glass-transition temperature has been improved to 120 ^oC [71] for spiro-OMeTAD, which improves the stability of spiro-OMeTAD [82]. The spiro-OMeTAD is also soluble in most of the solvents such as chlorobenzene, tetrahydrofuran and acetone [82].

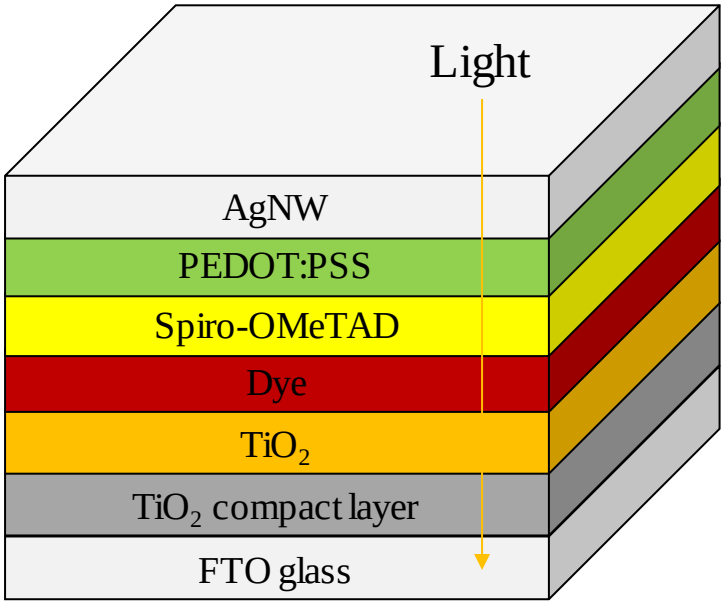

Figure 2.9.Structure of a Sipro-OMeTAD based solid-state dye sensitized solar cell [86].

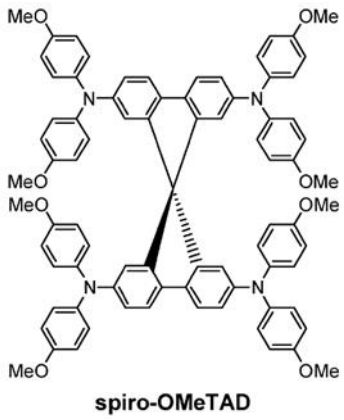

Figure 2.10.Structure of a Spiro-OMeTAD [86].

The ssDSSCs have solved the leakage problem in liquid based conventional DSSC. However, the efficiency of ssDSSCs are not as good as liquid electrolyte based DSSC[89]. The main cause for the lower efficiency of ssDSSC compared to the liquid based DSSC is the pore filling problem[90]. The permeability of solid-state electrolytes is not as good as that of liquid electrolytes. When the cells are assembled together, the liquid electrolyte will permeate through the mesoporous TiO_2 completely, however, most solid-state electrolytes does not come into contact with the TiO_2 fully[91]. In order to make an efficient DSSC, all the dye molecules should be fully in contact with both the mesoporous TiO_2 film layer and the electrolyte, and the path for transferring the HTM electrons to the dyes should also be unobstructed [92]. A thinner layer of TiO_2 film is required to allow more solid electrolyte to diffuse, but it may not absorb enough light which also affects the efficiency of the ssDDSC [92]. The highest reported PCE for spiro-OMeTAD was achieved with a 5μm thickness of the TiO_2 film [84].

2.7 Conclusions

In this chapter, the fundamentals physics of semiconductors, energy band gap and p-n junctions are introduced to fully understand the working principle of the dye-sensitized solar cell. The mechanism of DSSC and ssDSSC including the operation and the energy level were described. The solar cell efficiency calculation is also studied in this chapter which is used to calculate the device efficiency in the following chapters.

In this thesis, a highly flexible DSSC with both flexible photo anode and the counter electrode is going to be fabricated on textile based on the 2D planar device structure. There are two kinds of flexible DSSCs is developed on textile substrate based on liquid and solid-state electrolyte. The solid-state electrolyte is used to prevent the leakage, and also suitable to fabricate the device on single textile substrate by using printing techniques. AgNW coated PEDOT:PSS based solid-state DSSC is fabricated first before transferring the device fabrication process onto textile. The proposed structure is shown in figure 2.9, where the platinum FTO glass counter electrode is replaced with a AgNW coated transparent conductive polymer (PEDOT:PSS). AgNW is synthesized from silver, is extremely flexible and compatible with roll-to-roll printing on flexible substrates. Poly (3, 4-ethylenedioxythiophene) polystryrene sulfonate (PEDOT:PSS) is a conductive polymer, the conductivity is higher than ITO when silver nanowire is coated on top. The main advantage of this counter electrode is that PEDOT:PSS is a high mobility hole transport material, and AgNW is semi-transparent which allows light transmission. When the device is moved onto the textile based DSSC, the sunlight will pass through the AgNW to the cell. A solid-state electrolyte Spiro-OMeTAD is sandwiched between the photo anode and the counter electrode. Therefore, a solid-state DSSC structure is used in this DSSC with a flexible AgNW coated conductive polymer PEDOT:PSS, which could be easily improved further on both high (450^{o}C) and low temperature (150^{o}C) textile materials.

Chapter 3

3 Literature review: wearable and flexible DSSCs and ssDSSCs

3.1 Introduction

To date, conventional DSSCs have been in the leading position in the DSSC research field. The lower production cost and easier fabrication process compared to silicon based solar cells has attracted intensive research interest in DSSCs [93]. However, a conventional DSSC is usually structured by a working electrode, a dye, a liquid electrolyte that contains I^-/I_3^- redox, and a counter electrode [94]. Both working and counter electrodes are made of rigid FTO coated glass which costs one third of the total cost of a DSSC [95], and the counter electrode is coated with platinum which is a high cost material. Nowadays, the conventional DSSCs are challenged with their heavy weight, rigidity, and expensive counter electrode material [95]. These disadvantages will limit the further development of DSSCs in the future.

Recently, the demand for lightweight, flexible and wearable DSSC devices has increased rapidly in our modern society [96]. In DSSC research, the textile based DSSCs have attracted intensive interest. Besides its lightweight, flexible, and wearable features, other features such as printable, stretchable and low cost material replacement are also worth investigating [97].

Three types of flexible textile based DSSCs introduced in this chapter. One is the DSSCs with fibre architecture [98], and the other two are DSSCs with a planar architecture. The FTO glass substrates in the counter electrode are replaced with fabric to realise the wearable DSSCs on fabric substrate [99].

3.2 Investigation of low temperature processed TiO_2 film on FTO glass substrate and conductive plastic substrate

The dye-sensitized solar cell has attracted more research interest from the pioneering work of O'Regan and Grätzel in 1991 [38]. The material and processes of DSSC have been a significant focus of current research on DSSC [100] in terms of investigating the fundamentals of each functional layer. The conventional structure is usually based on a TCO glass substrate, and the typical electron transport material is a viscous TiO_2 paste with organic binders to improve the film viscosity and adhesion to the glass substrate. However, the conventional DSSC needs to be annealled at a high temperature ($\geq 450\ ^oC$) to remove the organic binder in the mesoporous TiO_2 film and to increase the electron mobility. The high processing temperature of conventional DSSC limits the application on flexible substrate such as polymer and textiles. The low temperature processing of mesoporous TiO_2 film is key in the DSSC device conversion from glass to plastic substrate. Therefore, the investigation of low temperature processed TiO_2 film has become a focus of significant research interest in order to enable the application on flexible substrates. There are several TiO_2 film synthesizing and processing methods to deposit the functional material at low temperature processing, such as mechanical compression [101], electrospraying of TiO_2 paste [52] hydrothermal necking of titanium salts [102], ultraviolet (UV) curing [103], chemical vapor deposition [104], light scattering [105], modified TiO_2 binder free sol-gel and colloidal [65, 106] with some acid or sintered with $TiCl_4$ treatment method [107] to widen the application of DSSC on flexible substrates.

The key challenge in preparing the low temperature processed TiO_2 paste is to formulate a good TiO_2 particle interconnection to achieve a uniform and homogenous TiO_2 film with lower remaining organic context to improve the electron transportation. Some research work has tested the formulated low temperature TiO_2 film on the FTO glass substrate and moved onto the conductive plastic substrate. In this section, different low temperature processed TiO_2 film formulation and deposition methods on FTO glass and polymer substrates are studied, compared and analyzed.

3.2.1 Low temperature processed TiO_2 film on FTO glass substrate

In the current DSSC research, the challenge in formulating and developing low temperature DSSCs is the preparation of the TiO_2 electrodes at a low temperature ($\leq 150\ ^oC$). This

processing temperature enables the DSSC fabrication on some flexible substrates such as polymeric and textile substrates, which opens up the possibility for the large area production by continuous roll-to-roll processing for more applications. Several process methods have been investigated for fabricating low temperature processed TiO_2 electrodes. One type is investigating the formulation of the low temperature processed TiO_2 film, and other types focus on the deposition methods investigation.

A preferred approach to formulate low temperature processed TiO_2 film is synthesizing the TiO_2 colloidal or sol-gel. The formulation developed usually uses a binder free system to maximize the electron transport in the TiO_2 film, but this system gives a lower viscosity and results in a non-uniform morphology of the TiO_2 film. Park et al. [108] reported a method by adding a small amount of ammonia solution into an acetic acid TiO_2 colloid solution. The addition of electrolytes led to an increase of the ion concentration of CH_3COO^- and NH_4. The ions in the slurry increase the interconnection of the TiO_2 nanoparticles, which enhances the flocculation and viscosity. A maximum electrical energy conversion efficiency of 2.83% was achieved on the ITO/glass substrate using this method after heat treatment to 150 ^oC.

Additional improvements were made by Yune et al. [109] with an energy conversion efficiency as high as 5.44 % after the thermal treatment of 150 ^oC. An organic-binder free titania paste was synthesized by chemical modification of an acidic TiO_2 sol with ammonia. The viscosity of the acidic TiO_2 suspension is controlled by varying the concentration of the ammonia. This paper found that acetates from the TiO_2 precursor preparation were retained within the electrode structure after thermal treatment at 150 ^oC. This paper investigated the influence of the ammonia concentration on the viscosity and nanoparticles binding in the TiO_2 colloidal suspension. On the basis of Park's research, Yune uses an equal amount of acid and titanium alkoxide which is mixed together to prepare the TiO_2 colloidal suspension. This significantly reduces the organic binders that remain in the TiO_2 paste. A binder-free TiO_2 film was formulated by adding a different weight ratio of ammonia solution. A homogenous TiO_2 film was achieved on the FTO glass substrate by casting. The mechanism of the TiO_2 nanoparticles' interconnection in the thermal treatment is studied in this paper as shown in figure 3.1. The TiO_2 nanoparticles are interconnected by necking [107], and the hydroxyls on the TiO_2 surface are dehydrated at 150 ^oC thermal treatment [110]. In addition, the stability of TiO_2 paste developed by this method lasts for over 9 months. Although a stable and homogenous thick film of the TiO_2 electrode can last for 9 months, the organics within the TiO_2 film are not

entirely eliminated after 24 hour thermal treatment at 150 ^{o}C. A higher annealing temperature ($\geq$ 450 ^{o}C) is still needed to remove all the organics within the film.

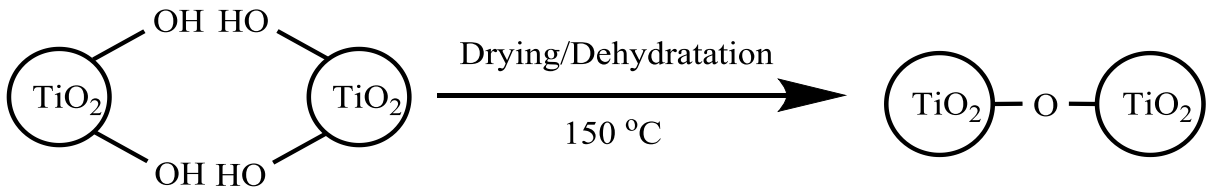

Figure 3.1. A mechanism for TiO_2 particles interconnection via a dehydratation process within the film annealing at 150 ^{o}C.

Further research work have investigated improving the TiO_2 electrode by $TiCl_4$ treatment. The TiO_2 film was immersed in a solution of $TiCl_4$ to facilitate the interconnection of the TiO_2 nanoparticles [111]. A new method of fabricating a low temperature TiO_2 electrode was demonstrated by the chemical bath deposition [105]. A light scattering layer was deposited on a nanostructured mesoporous TiO_2 layer in the device structure. The TiO_2 nanoparticles were formed on the top surface of the photoanode by $TiCl_4$ hydrolysis processing at 70 ^{o}C. The scattering layer was produced by this controlled chemical bath deposition process in a $TiCl_4$ solution. Four different concentrations of $TiCl_4$ were investigated in the chemical bath from 100 mM to the 400 mM to control the size and agglomeration of the TiO_2 nanoparticles via hydrolysis process. The concentration of $TiCl_4$ under 300 mM has the largest particles on the top surface of photoanodes and exhibited the highest PCE of 8.54% compared to 7.10% for the prime solar cell.

Zhang et al [112] have improved this $TiCl_4$ treatment approach by mixing the anatase TiO_2 powder with a blend of P25 and 200 nm particle sizes and fabricated the device on the ITO/polyethylene teraphtalate (PET) substrate using FTO glass substrate as the top electrode. The TiO_2 electrode was fabricated by the chemical sintering method using hydrothermal cement. The low temperature TiO_2 paste was deposited on the ITO/polyethylene teraphtalate (PET) substrate by doctor-blading and annealing at 120 ^{o}C. A maximum PCE value of 4.0 % was achieved on half the ITO/polyethylene teraphtalate (PET) substrate and half FTO glass substrate.

An improvement was made by Miyasaka et al. with a maximum PCE value of 5.8 %. The TiO_2 nanoparticles are a mixture of rutile and anatase with an average nano particle size of 30 – 150 nm. An aqueous colloidal sol was used as the TiO_2 nanoparticle inter-connection agent. This agent contains brookite-type TiO_2 with size 10 -35 nm and mixed the solvent of 25 %

hydrochloric acid (pH 4) and 75% ethanol. This binder-free TiO_2 paste was deposited on the ITO/PEN substrate using the Doctor Blading method, and dried at 110-125 ^oC. The platinum coated FTO substrate was assembled after the TiO_2 electrode sintering process. This aqueous colloidal TiO_2 sol was used as the cement agent to increase the inter connection of the TiO_2 nano-particles which still contains acid inside the TiO_2 paste.

The low temperature processed TiO_2 film plays a critical role in the flexible DSSC device. The most common method to prepare the TiO_2 film is using a TiO_2 sol-gel colloidal, this sol-gel method is usually using an acid based suspension or by a further $TiCl_4$ treatment. The main barriers with achieving an efficient DSSC on low temperature flexible substrate are having both good quality TiO_2 mesporous film and high electron conductivity. In order to achieve good quality TiO_2 film, the organic binder needs to be present in the TiO_2 paste formulation. These organic binders will not be eliminated under low temperature processing, which will decline the electron transport inside the TiO_2 film. Therefore, some research focuses on the organic binder free TiO_2 film with some specialized deposition and compression of the TiO_2 film to enable the DSSC application on the flexible substrate.

3.2.2 Low temperature processed TiO_2 film on conductive plastic substrate

In the recent investigation of TiO_2 binder-free systems, Weerasinghe et al. [113, 114] have focused on the rheological performance of ethanoic or mixed ethanoic water P25 paste prepared for flexible DSSC on polymeric substrate. The TiO_2 slurry was modified either by adding an acidic or base material to increase the TiO_2 paste viscosity thus to achieve a good quality TiO_2 film. These studies show that this chemical modification results in improving both the nanoparticle interconnection and the adhesion to the polymer substrate. An improved power to energy conversion efficiency of 5% was reported under the processing temperature of 150 ^oC.

A low temperature fabrication method of the mesoporous TiO_2 layer on the conductive plastic substrate was reported by Miyasaka et al. [115] by using the electrophoretical deposition method combined with other post-treatments as shown in figure 3.2. The electrophoretic deposition was done by elevating the DC electric field. The TiO_2 nano particles are highly positively charged when dispersed in organic polar solvents (ζ potential of + 260 mV in t-butanol). Three post-treatments were carried out to evaluate the TiO_2 particles' inter bonding: the microwave irradiation with 2450 MHz, chemical vapour deposition of titanium

tetraisopropoxide on the TiO_2 particle layer, and the TiO_2 aqueous sol employment. These three post-treatments all demonstrate a good interconnection of the TiO_2 nano-particles, but the TiO_2 containing aqueous sol was reported to be the most efficient in this study. After the post-treatment, the TiO_2 electrode was annealed at 150 ^oC in air for 5 minutes and dried at 110 ^oC for 20 minutes before sintering.

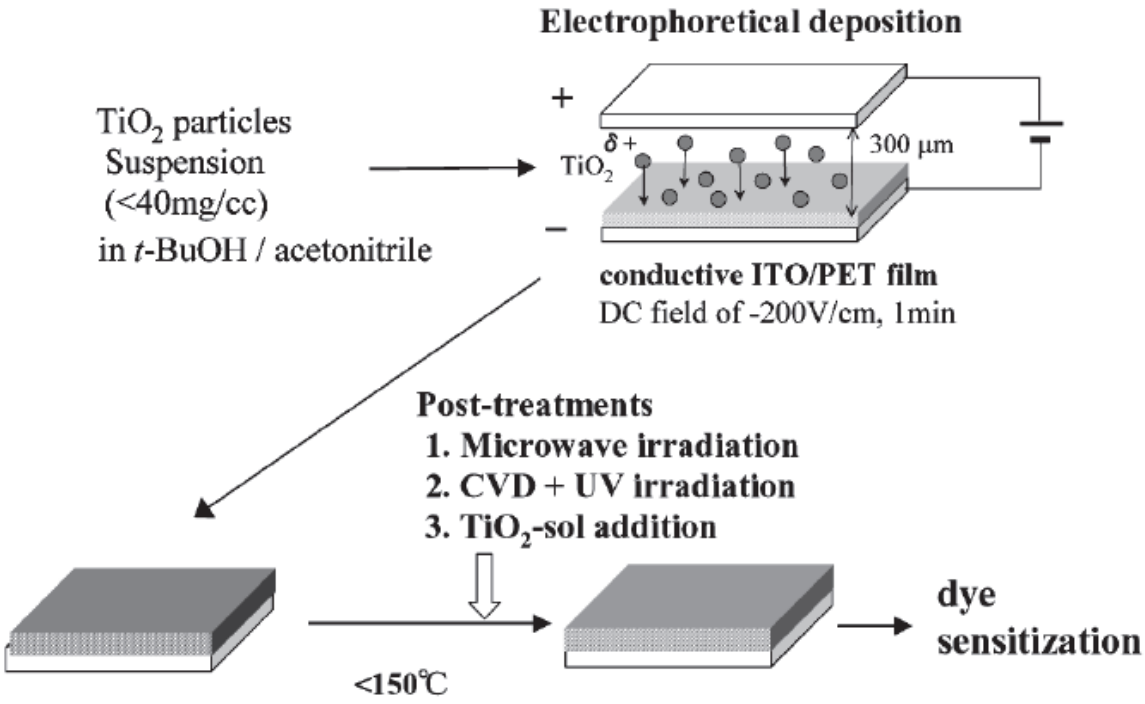

Figure 3.2. Fabrication process of low temperature processed TiO_2 electrode by electrophoretical method [115].

The cold isostatic pressing (CIP) technique applies equal pressure in all directions of the nanoparticles, which allows a complex shapes to be pressed[101]. Therefore, high quality and uniform TiO_2 thin films can be achieved using this approach. The TiO_2 paste used in this method is ethanol based P-25 titania suspensions. The doctor blading was used to deposit TiO_2 film on the ITO/PEN substrate. The fabrication of the TiO_2 electrode is shown in figure 3.3. After the TiO_2 film was dried in the air, the TiO_2 electrode was put in a polyethylene envelope to be sealed by vacuum. Different pressures were tested between the ranges 35 to 200 MPa. The DSSC devices were assembled by attaching the platinum coated ITO/PEN substrate top electrode to this dye coated TiO_2 electrode. The compressed TiO_2 electrode using the CIP technique has significantly improved the interconnection of the TiO_2 nanoparticles with a maximum PCE value of 6.3% achieved by a thickness of 17.3 μm. However, this study

observed that the compression caused some damage to the conductive ITO layer which also reduced adhesion to the plastic substrate.

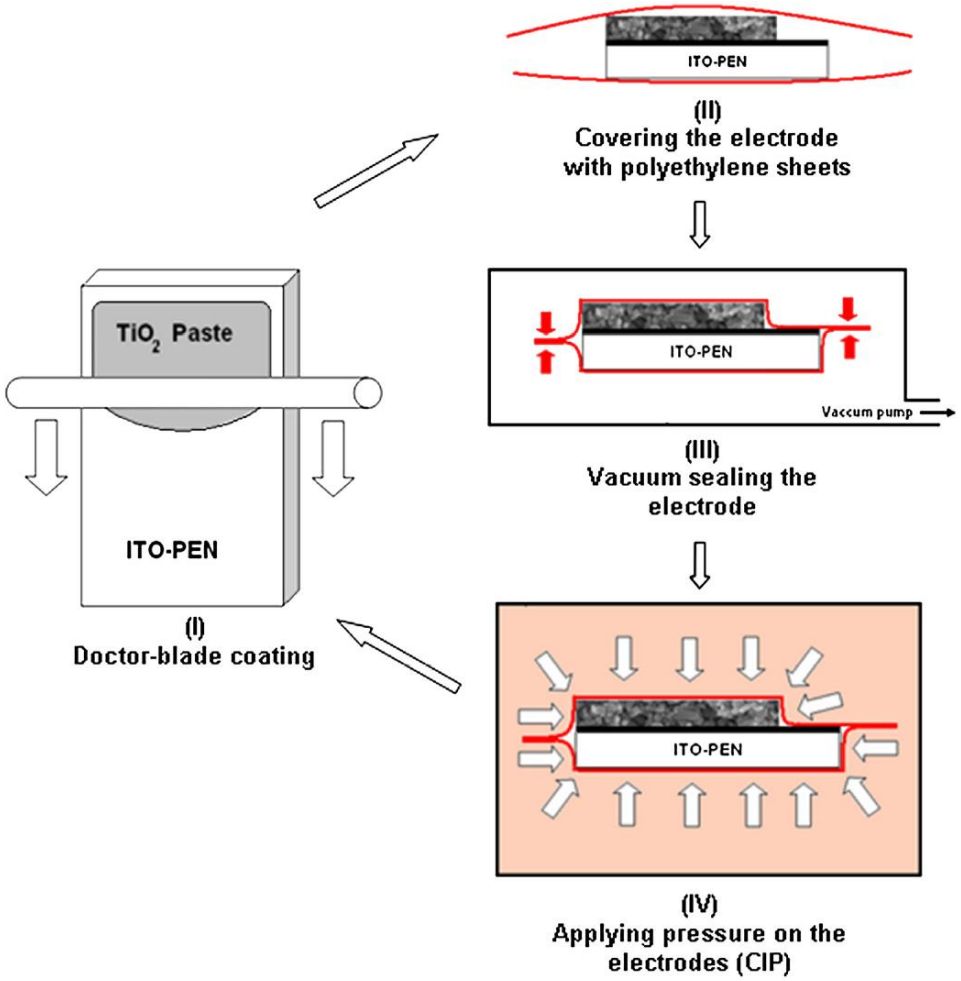

Figure 3.3. Fabrication process of TiO_2 electrode on ITO/PEN substrate by cold isostatic pressing (CIP) technique [101].

Another approach reported by Yamaguchi et al. combined the pressing method with the water and ethanol based low temperature TiO_2 paste. The TiO_2 paste comprised of a mixture of 10 wt% nanocrystalline TiO_2 and water. Two types of anatase-TiO_2 particles 20 and 100 nm were prepared by autoclave treatment followed by the hydrolysis of $Ti(OCH(CH3)2)_4$. After the autoclave treatment, ethanol was added to the TiO_2 suspension. After being mixed, the solvent was removed from the suspension. Then, the water was again added to the TiO_2 suspension. Finally, ethanol replaced the water in the TiO_2 suspension, resulting in a TiO_2 paste that only contains TiO_2 particles and water with no added organic binders. The obtained TiO_2 paste was coated onto the ITO/PEN substrate using the doctor blading method and pressed for 1 minutes

at room temperature after drying. A maximum efficiency of 7.6% was achieved on the ITO-coated polyethylene naphthalate (ITO-PEN) substrate.

The research methods reported above have exhibited the possibility of fabricating the DSSC on the flexible substrates. However, besides the complicated fabrication method, the low-temperature binder-free TiO_2 film are usually acid based which will damage the flexible substrate. Therefore, the new formulation of low temperature processed non-acid based TiO_2 paste for flexible substrate needs to be investigated in future research to improve the TiO_2 film quality and adhesion to the flexible substrate.

3.3 Textile and FTO glass based liquid DSSC

Extensive research has been focused on the electronic textile (E-textile) due to its various applications, such as sportswear, healthcare and environmental monitoring system, and military uniform [116-119]. These wide-ranging applications of E-textile have stimulated large demands on the wearable energy sources to provide wireless power to the sensors on the textile [120].

The DSSC device has been successfully achieved on the conductive plastic substrate, so some research has moved the DSSC device closer to the use of a textile substrate as the counter electrode. The expensive platinum coated FTO glass counter electrode has been replaced by the cheap textile substrates and also lead the research on achieving a fully textile based DSSC.

3.3.1 Graphene coated conductive cotton fabric based DSSC

Recent research has developed a graphene-coated cotton fabric counter electrode to replace the conventional platinum-coated FTO glass substrates [121]. It is flexible, light-weight and cost effectiveness of cotton fabric compared to other materials could make its application broader [99]. The structure and fabrication process is shown in figure 3.4. The photo anode is a sheet of holed FTO glass coated with titania nanotubes (TNT) and TiO_2 paste, using a ionomer resin as a spacer [121]. The counter electrode is a Graphene-coated cotton fabric attached to a PET sheet [121]. The gel electrolyte is used in between the photo anode and the counter electrode to synthesise the device [121].

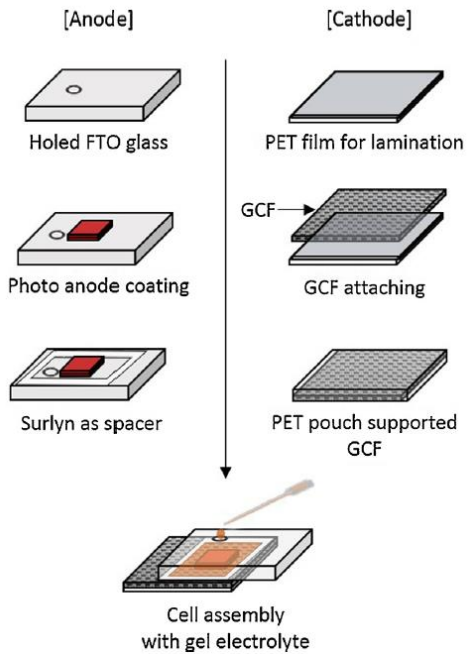

Figure 3.4. The structure and fabrication process for graphene coated cotton fabric based DSSC [121].

The material and fabrication process of this graphene-coated cotton fabric DSSC are quite similar to that of the conventional DSSCs. The FTO glass substrate is first coated with P25 [121]. Then the photo anode is prepared by depositing titania nanotubes (TNT) and TiO_2 paste on to a holed FTO glass substrate, and then put into $TiCl_4$ solution and heated at 70^oC for half an hour. Next, the photo anode is annealed at 500^oC for half an hour to remove the organic binder in the TiO_2 paste. The TNT and TiO_2 pasted coated electrode are loading by dye solution for 15 hours, after the dye molecules are adsorbed properly on the TiO_2. Finally, the electrodes are washed with ethanol and water, and dried by the nitrogen [121].

The counter electrodes are prepared by coating the graphene oxide nanosheets on the cotton fabric, and then attached to the PET pouch. The first step is to make the graphene oxide nanosheet. The graphene oxide nanosheet is comprised of a mixture of 5g graphite powder, 200 ml H_2SO_4, and 25g $KMnO_4$ [121]. The graphite powder was first mixed with 200 ml H_2SO_4 for 30 minutes under 10^oC and the $KMnO_4$ was added to the compounds subsequently. Then, the graphite is stirred for 4 hours at room temperature [121]. After, 250 ml of deionized (DI) water is injected to the graphite at 10^oC, 5 ml of H_2O_2 (30%) is added to the mixture and it is stirred for another half an hour. After 2 hours, the final graphene oxide nanosheet is created by adding another 250 ml DI water and the supernatant which appears on the mixture should be rinsed with HCl and DI water [121]. The next step is to coat the graphene oxide nanosheets on

the cotton fabric. Firstly, the fabric is immersed into the graphene oxide solution with a concentration of 1% at 80 ^{o}C for half an hour. Afterwards, the cotton fabric substrates are sintered at 80^{o}C again for 20 minutes. The fabric is fumigated by the hydronic acid vapours so the deposited graphite oxide is converted to the reduced graphite oxide. The chemically reduced graphite oxide on the fabric surface could be reduced by washing with the deionized water until the pH value is neutral. The electrodes are reheated at 100 ^{o}C for half an hour to evaporate the liquid on the graphene [121].

An efficiency of 2.52% is achieved by using this graphene coated cotton fabric based DSSC [121], compared to the platinum-coated counter electrode, which reached 7.2% [121]. However, the fabrication process is quite complicated, and it is quite difficult to get a good quality coating of graphene on the cotton fabric.

Printed DSSC on textile is a promising approach as the printing methods are a straightforward fabrication process and the material could be simply printed layer by layer, and no additive solvents are needed to complete the fabrication process. It would be easier to fabricate on a flexible substrate such as Kapton [99].

3.3.2 Multi-walled carbon nanotube coated polyester fabric based DSSC

Multi-walled carbon nanotube (MWCNT) coated polyester fabric has also been used as the counter electrode of a DSSC. This textile based DSSC demonstrated a high PCE of 5.69% [95]. The structure of the MWCNT coated polyester fabric DSSC is shown in figure 3.5 (a) and compared with conventional DSSC in figure 3.5 (b). The working electrode is FTO glass coated with TiO_2 film immersed in the dye solution for staining. The counter electrode is made of polyester fabric coated with enzyme-dispersed MWCNT (E-MWCNT). The polymer gel electrolyte is sandwiched between the working and counter electrode [95].

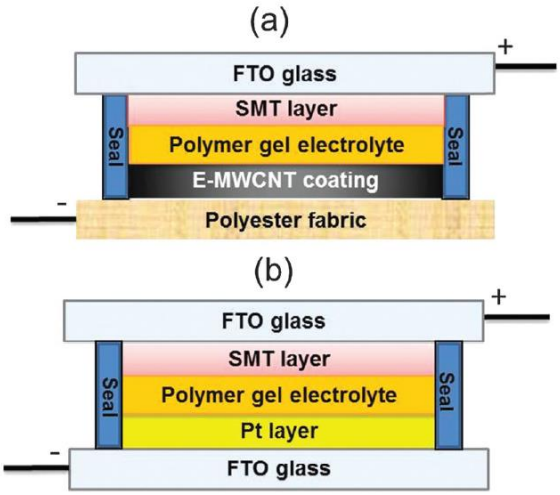

Figure 3.5. (a) Structure of multi-walled carbon nanotube coated polyester fabric based DSSC (b) Structure of Conventional DSSC [95].

There are three main parts in the fabrication process of MWCNT coated polyester fabric based DSSC:

(1) Fabrication of photo anode
(2) Fabrication of counter electrode
(3) Cell assembling

The fabrication of photo anode is similar with the conventional DSSC. The TiO_2 paste is screen printed onto the FTO glass substrate by scalpel blade [95] with a thickness of 0.03 mm and an active area of 20 mm^2. The photo anode was heated at the temperature of 70^oC for half an hour, 325^oC for 5 minutes, 375^oC for 5 minutes, 450^oC for 15 minutes, and 500^oC for 15 minutes respectively. Afterwards, the photo anode was loaded into $TiCl_4$ solution for half an hour at 70^oC, and subsequently heated again for half an hour at 500^oC. Then, the photo anodes were loaded to D719 dye solution for 10 hours when the electrodes cooled to 100^oC. Finally, the photo anode was completed by rinsing with ethanol [95].

The diagram of the fabrication process of E-MWCNT fabric electrode is shown in figure 3.6. In order to make enzymes adsorb on the MWCNT surface without changing any electronic characteristics, pure dispersed MWCNTs of 0.4 g was added to 50 ml of aqueous enzyme solution with continuous stirring at room temperature for 12 hours (path a in figure 3.6). Next, a Polytetrafluoroethylene polymer membrane filter with a pore size of 0.5 µm was used to filter the E-MWCNT solution (path b in figure 3.6), and the remaining enzyme residuum were washed with water. Then, an E-MWCNT paste was made by dispersing the filtered E-MWCNT in a mortar (path c in figure 3.6), and left over night at room temperature before use. The E-

MWCNT paste was coated on polyester fabric by air drying at a temperature of 50 ^{o}C. The paste was enclosed by a simple tape and was dried in the oven for half an hour (path d in figure 3.6). The unused fabric was cut off and made into an area of 15 × 15 mm^2 [95].

The last step is to assemble the cell by sandwiching a gel electrolyte between the photo anode and the E-MWCNT coated polyester fabric counter electrode [95]. The final E-MWCNT coated polyester fabric is shown in figure 3.7.

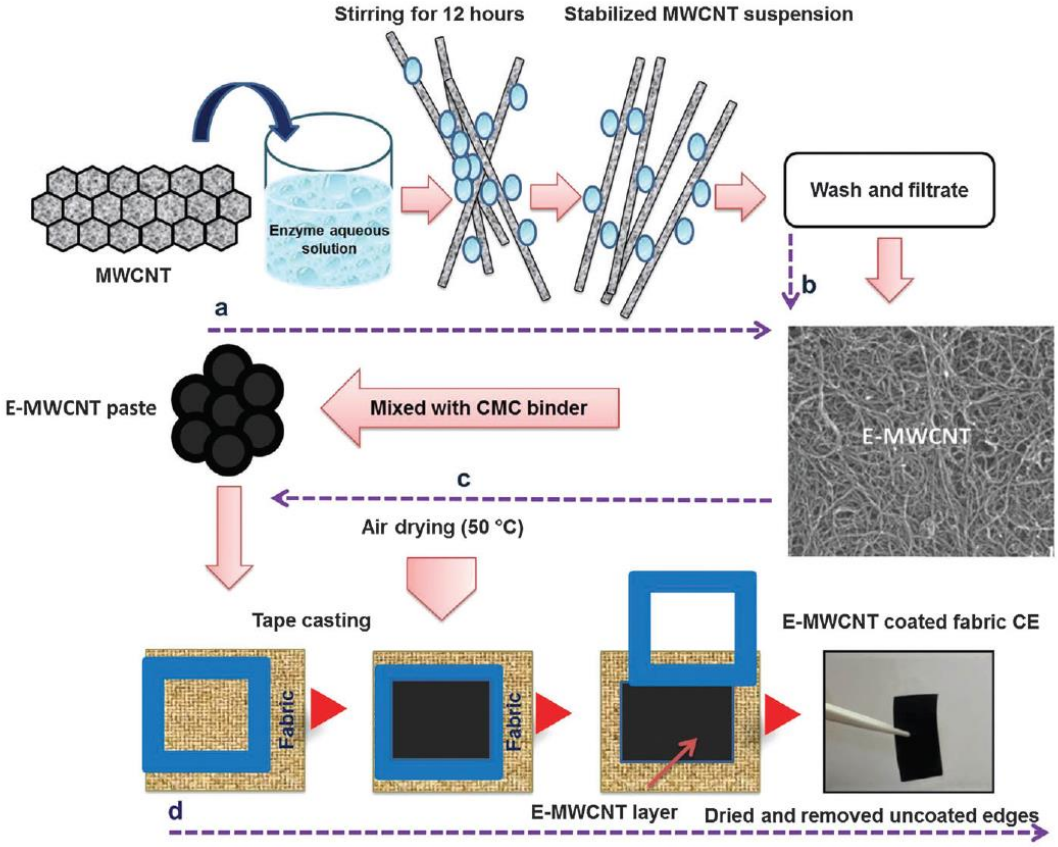

Figure 3.6. Fabrication process of multi-walled carbon nanotube coated polyester fabric based DSSC [95].

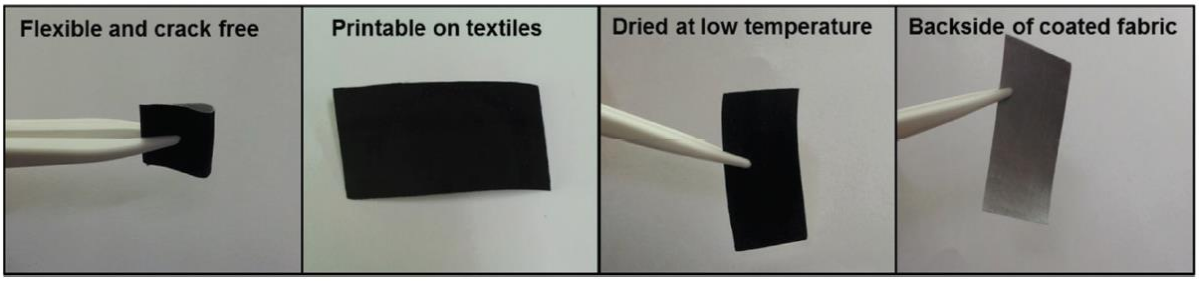

Figure 3.7. The final feature of E-MWCNT coated polyester fabric counter electrode for DSSC [95].

The results of this proposed E-MWCNT coated polyester fabric based DSSC is shown in table 3.1 in a comparison with the conventional ones. The efficiency of 5.59% is achieved [95], with an open circuit voltage of 0.688. An improvement was made by further research work with activated charcoal doped into the multi-walled carbon nanotube. A maximum PCE value of 7.29 % was achieved by this improved method [122]. The photo electrode in this case is still made of rigid FTO glass which means the flexibility of the cell still needs to be improved [95].

Table 3.1. Comparison results of platinum FTO glass counter electrode and E-MWCNT polyester fabric counter electrode [95].

Counter Electrode	**Open circuit voltage (V_{oc}), V**	**Fill factor (FF)**	**Current density (J_{sc}), mA/cm^2**	**Efficiency (η)%**
Platinum coated FTO glass	0.701	72.06	14.18	7.16
E-MWCNT polyester fabric	0.688	69.39	11.92	5.69

3.4 Fully flexible DSSC based on liquid electrolyte

The DSSC device with FTO glass and textile as the top and bottom electrode structure has moved towards a fully textile-structured solar cells. Research has been frequently discussed recently as the increasing demands of the portable wearable power supply. The current approaches to fabricate fully textile structured DSSCs are fibre or wire based 3D architecture DSSC. There are also some research on attaching and weaving the fabric electrodes to achieve a fully textile based DSSC as discussed in this section.

3.4.1 Flexible fibre type DSSC based on liquid electrolyte

The wearable DSSCs have been developed rapidly in recent years with more advantages than the conventional ones. In this section, a yarn based DSSC with a fibre architecture [123] is introduced. It has a 3D architecture, the main idea for this kind of wearable DSSC is to design

a special yarn which consists of individual multi-walled carbon nanotubes (MWNTs) coated with the TiO_2 film, and weaving them together to make a 3 dimensional photo electrode as the photo anode of the DSSC, as shown in figure 3.8 [94]. The yarn is made of several carbon nanotube fibers coated with the dye sensitized TiO_2 film.

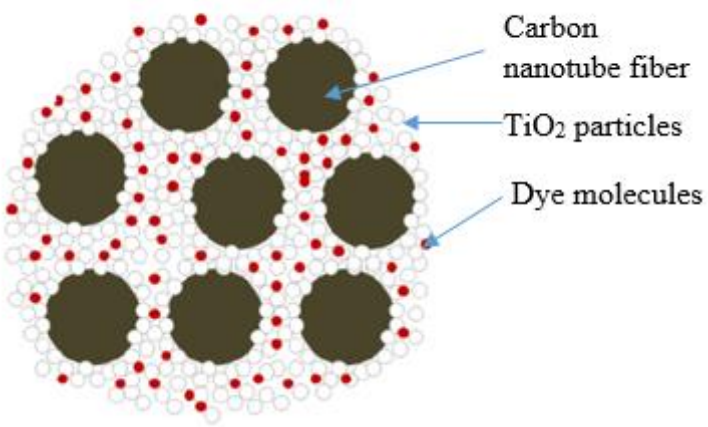

Figure 3.8. Photo anode of yarn based DSSC [94].

The structure of this yarn based DSSC is shown in figure 3.8, and is quite similar to the standard DSSC. The cell consists of a photo electrode, a counter electrode, and the I^-/I^{3-} electrolyte in between. Unlike the rigid conventional DSSCs, both photo electrode and counter electrode are made of yarn which consists of carbon nanotube fibers [124]. The photo anode is coated with dye sensitized TiO_2 film which absorbs the light, and the electrons travel through the external circuit and come to the counter electrode which is platinum coated carbon nanotube fibre [95]. The liquid electrolyte which contains I^-/I_3^- is used in this DSSC.

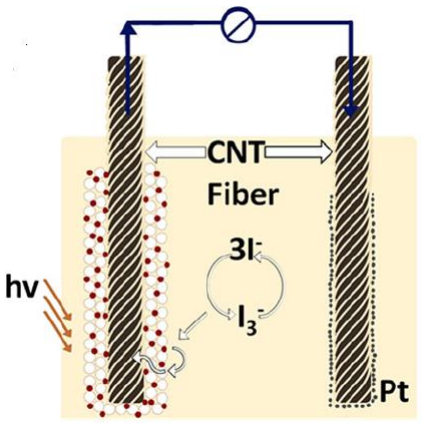

Figure 3.9. Structure of yarn based DSSC [94].

The results of the yarn based DSSCs with different yarn thickness is shown in table 3.2. The device with a higher yarn thickness shows a higher efficiency of 3.4% [94]. However, the main problem for this type of DSSC is the unstable performance of the cell, and the higher thickness will degrade its flexibility. The fabrication process is quite complicated and it is not easy to control each layer of the cell.

Yarn thickness	Open circuit voltage, V_{oc} (V)	Short circuit current, I_{sc} (mA/cm^2)	Fill factor, FF	Efficiency (η)%
High case (220nm)	0.54	19.8	0.319	3.4
Low case (200nm)	0.54	18.0	0.319	3.1

Table 3.2. Results of this fibre typed DSSC with different thicknesses of yarns [125].

Another approach to make the fully flexible textile based DSSC is the wire-shaped DSSC. A reported method of spinning graphene into flexible fibres using a low-cost and effective solution process has achieved a maximum efficiency of 8.45 % as shown in figure 3.10 [99]. The titanium nanotube grow perpendicular to the Ti wire as the working electrode, and the platinum was coated on the graphene based fibre by electrodepostion working as the counter electrode. These two electrodes were twisted together for the sintering process [99].

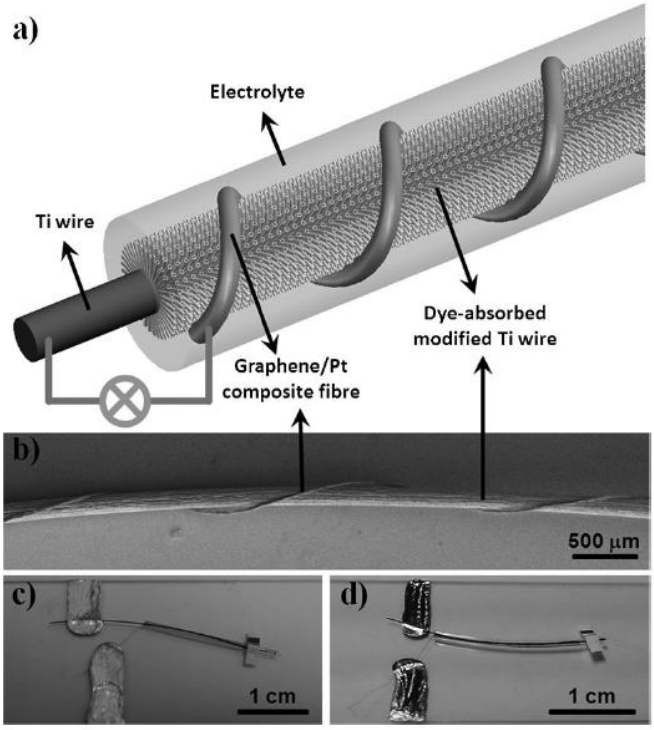

Figure 3.10. (a) Schematic of wire-shaped DSSC structure, (b) SEM, (c) and (d) photograph of the sealed device in capillary glass tube and a flexible fluorinated ethylene propylene tube [99].

The fibre-type DSSC has demonstrated a relevant higher efficiency, but the complicated fabrication of the completed cell makes the performance of the cell unstable. Besides the high friction during the weaving process, the shaped area of each fibre after weaving also degrades the performance of the device compared to the 2D planar structured DSSC device.

3.4.2 Flexible textile DSSC based sewing, attaching and weaving method

A high efficiency wearable and stretchable textile based DSSC was reported by using traditional sewing the DSSC electrodes on common textiles such as cotton, felt, and silk [126]. A maximum PCE value of 5.8 % was achieved by this approach with a binder curvature radius of 4 mm over one thousand binding cycles. There are three main steps in fabricating this textile based DSSC: weaving the photoanode textile electrode, counter textile electrode, and attaching these two electrodes together using the traditional sewing method. A stainless steel ribbon with periodic holes of 70 µm, and Ti wires of 100 µm were woven as the wefts and warp direction respectively for the photoanode electrode as shown in figure 3.11 (b). A glass fibre yarn and Ti wires were woven as the wefts and warp direction respectively for counter electrode. Subsequently, TiO_2 film and platinum were deposited onto the photoanode and counter electrode respectively. These two electrodes were sewn together on a cloth and then sintered. The device fabricated by the sewing method shows high flexibility and passes through 1000 bending cycles of 90^o at 10 cm radius, and maintained 80% of the original performance. The photovoltaic device performance was reduced to 70% after bending to a 1 cm radius, and further reduced to 30 % after bending to 4 mm radius of curvature [126].

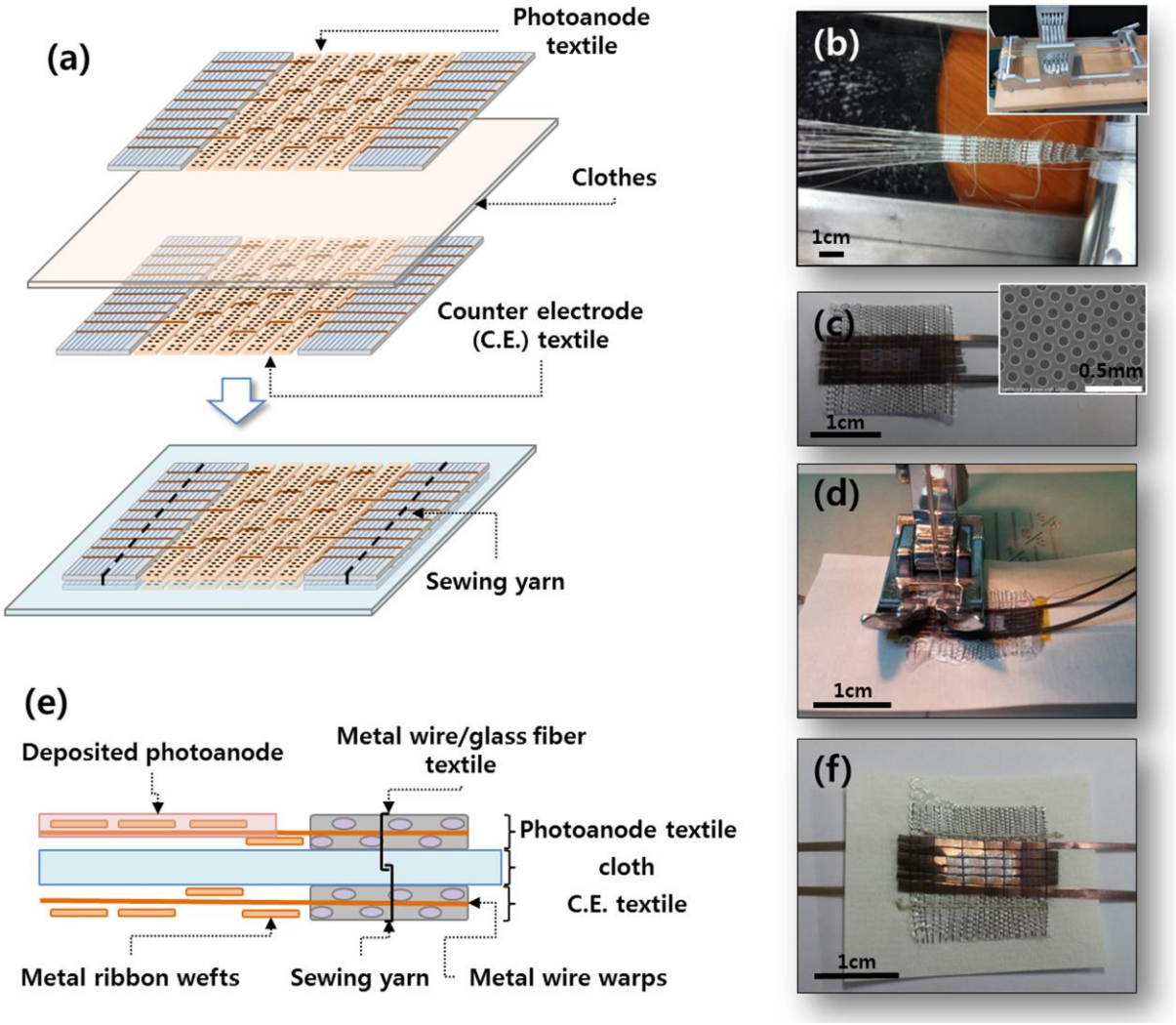

Figure 3.11. (a) Fabrication process of textile based DSSC by sewing two electrodes onto cloth, photograph of (b) woven photoanode electrode, (c) woven counter electrode, (d) sewing process for attaching two electrodes, (e) schematic of cross-sectional view of the device, (f) photograph of the textile based DSSC on Hanji [126].

Besides the flexibility, the devices also suffer from the evaporation of the liquid electrolyte on the exposed surface of the cells due to the lack of sealing during the measurement. Also, the poor diffusion within the electrolyte in Hanji substrate leads to the short circuit of the device. This paper shows the complexity of the fabrication process, which is still considered as a lab scale process. The traditional weaving method for the textile electrode also exhibits high friction. Further research needs to investigate the use of a solid electrolyte instead of a liquid electrolyte via the printing process to overcome the above mentioned barrier to ensure the cell's long lasting performance.

Another approach investigated by this research group involved incorporating the DSSC into the textile during the weaving process instead of sewing the two electrodes onto a cloth. Textile warp is used as a spacer to maintain the DSSC structure and to also avoid a short circuit. The dye-loaded TiO_2 coated metal ribbon is used as the photoanodes, while the Pt coated nanoparticle–loaded carbon yarn was used as the counter electrode. These two electrodes were woven into the textile instead of attaching it, as shown in Figure 3.12 (a). A maximum PCE value of 2.63% was achieved in this report. Nylon warp is used as the spacer to support the device and also to prevent a short circuit as shown in Figure 3.12 (b). The device was then underwent bending radius of 1 cm because of the high stiffness of the metal ribbon and carbon yarn [127].

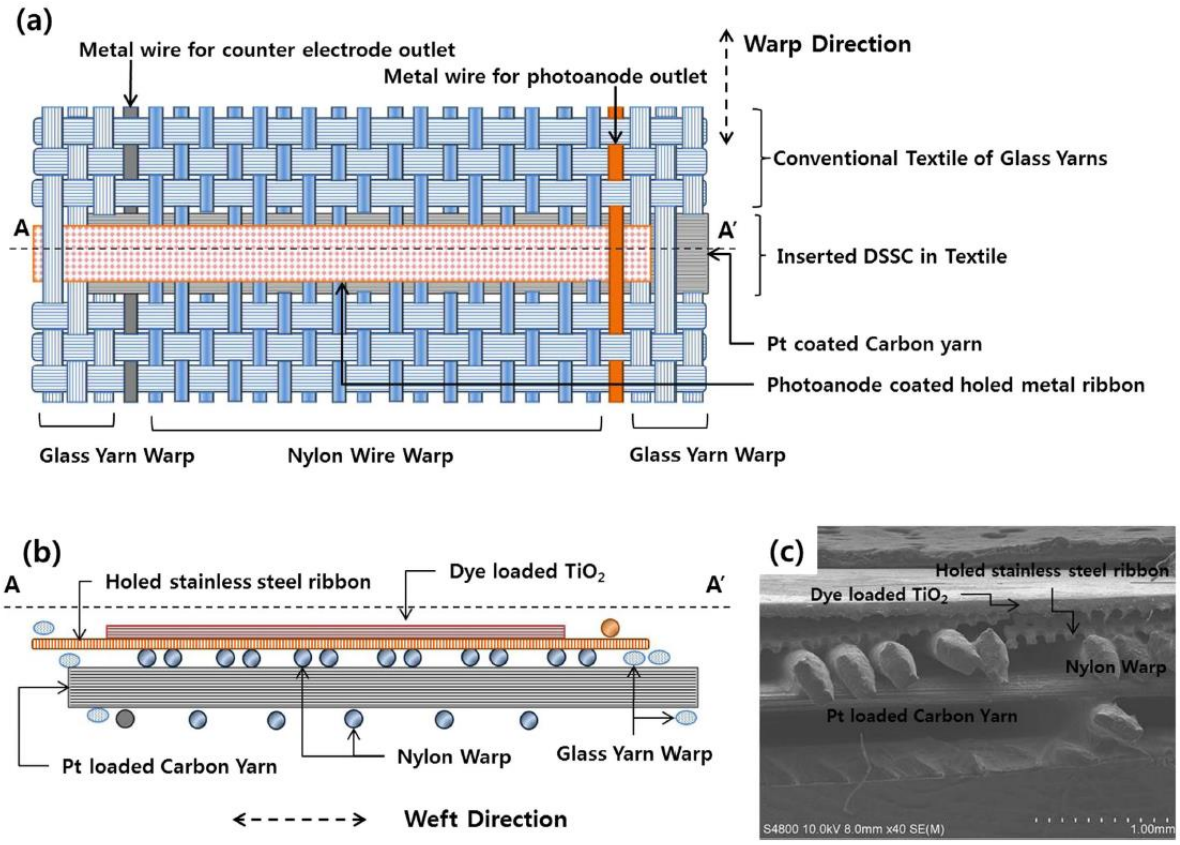

Figure 3.12. (a) Planar view of structure of the inserted dye-sensitized solar cells (DSSCs), (b) Cross-sectional view of the device structure, (c) SEM images of the cross-sectional view of the device [127].

This approach fabricated the liquid electrolyte DSSC on the metal ribbon and carbon yarns as the standalone PV cells, and then these standalone PV cells on the flexible ribbon is woven into standard woven textile, as the inserted PV cells into the textile. This approach is vulnerable to short circuiting during bending, which proves to be an impractical solution to textile solar

cells. Also, the spacer between the photoanode and counter electrode degrades the performance of the cell, so friction in the weaving process still remains an issue. Research still needs to consider the approach to add PV functionality on top of the existing woven textile.

The previous research has been improved with a monolithic-structured single layered textile based DSSC. In this method, the glass yarns were used as the spacer to prevent the short circuit and also for the liquid electrolyte injection. The Ti metal wires were used as the conducting wires in the photoande and counter electrode. It was pre-coated with platinum as used for the counter electrode. The glass yarns and Ti metal wires were woven into the textile for TiO_2 deposition and dye loading as shown in figure 3.13. The electrolyte was injected into the spacer glass yarns and the device was sealed by Kapton tape [128].

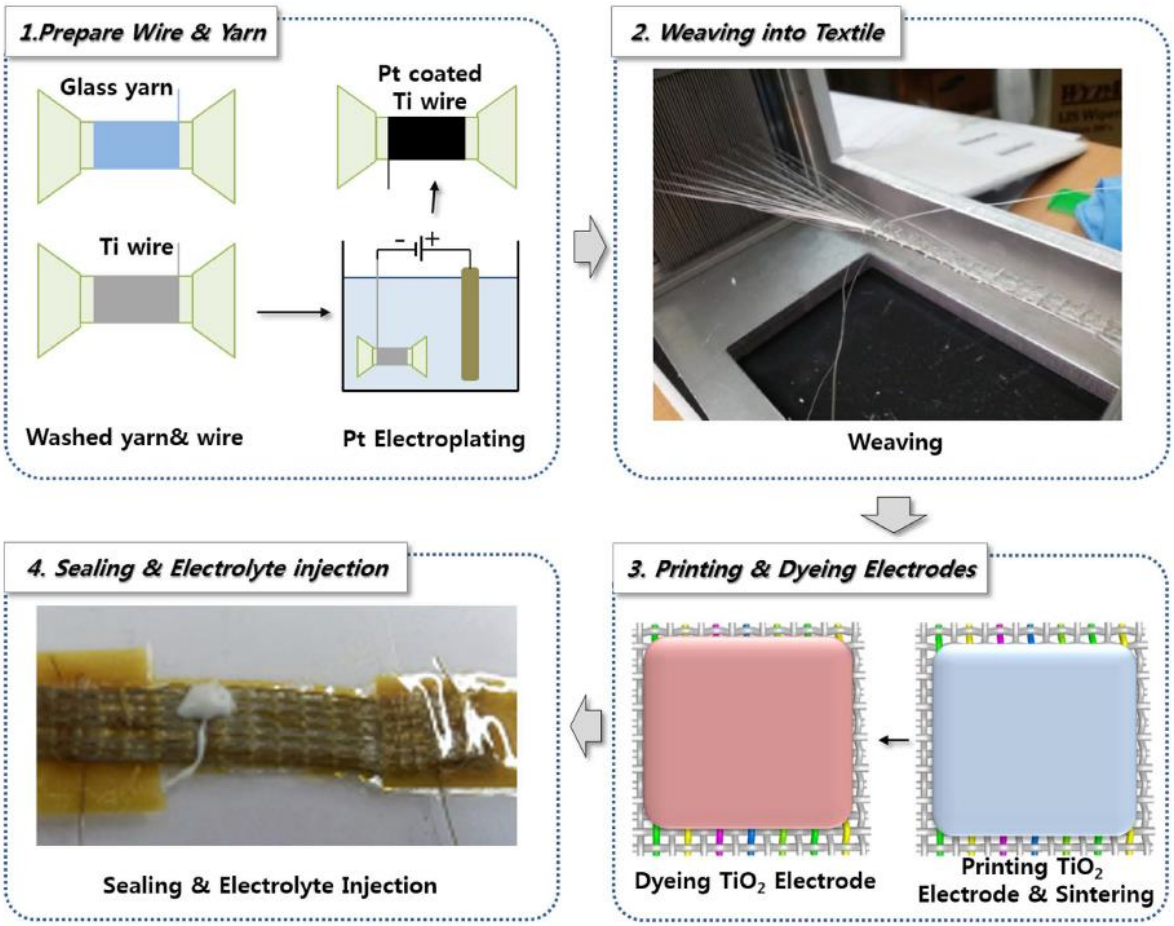

Figure 3.13. Fabrication process of monolithic single layered DSSC [128].

This approach is fabricating the liquid electrolyte DSSC by weaving the functional yarns into the woven textile, where each functional yarn represents a functional layer in the DSSC. Then the titanium oxide layer is printed on top of the woven textiles with dye loading and liquid

electrolyte injection to complete the PV cells' fabrication. This approach further increases the fabrication process compare to the previous work, which imposes great difficulty for large-scale manufacturing of the textile DSSC for wearable applications. In addition, the solid-state electrolyte should replace the liquid electrolyte to ensure the stability of the textile DSSCs for application purposes is also clarified in these papers.

3.4.3 Fully flexible textile based DSSC using ITO/PEN as top electrode

A high thermal resistant glass fibre textile was used as the substrate in this study, and a transparent conductive protective polyimide film was deposited via the roll-to-roll procedure as shown in figure 3.14. The titanium layer was grown by using the electron beam and sputtering deposition method on the polyamide film to maintain the substrate topography, and the TiO_2 paste was deposited by screen printing. The platinum cluster was deposited by a chemical reduction of $H_2P_tCl_6$ on the ITO/PEN substrate at room temperature. The device was sealed by special epoxy thermoplastic foils with a maximum PCE value of 1.8%. Durability test were taken over seven weeks, and no corrosion was found on the device performance.

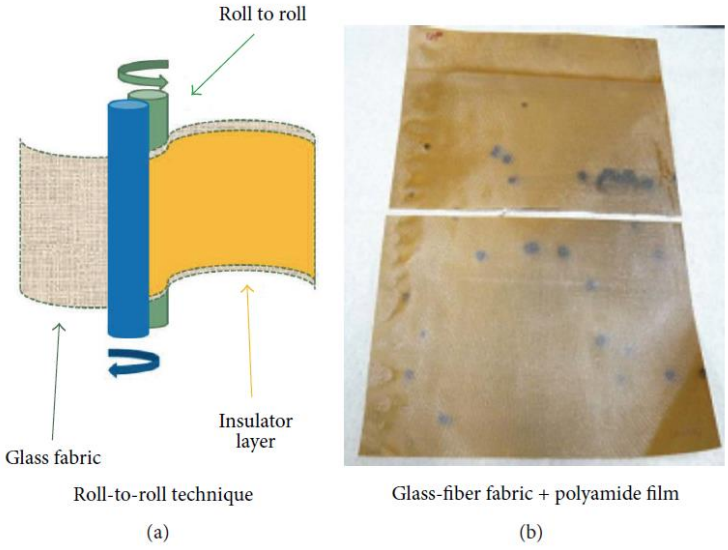

Figure 3.14. (a) Fabrication of polyimide film, (b) photograph of polyamide covered glass fibre fabric substrate[9].

This approach has successfully demonstrated a fully flexible DSSC based liquid electrolyte. The additional polyimide film was stacked on the glass fibre textile to reduce the surface roughness. However, the stacked polyimide film may cause less adhesion under the high

temperature thermal treatment. This paper also indicates that a low temperature titanium ink, and a solid-state electrolyte need to be investigated in future research.

3.5 Solid-state dye-sensitized solar cell

Although the liquid electrolyte dye-sensitized solar cell has exhibited state-of-the-art efficiency on different types of substrate, the leakage and evaporation of the liquid electrolyte affected the long-term stability of the DSSC device [71]. Solid-state dye-sensitized solar cells (ssDSSCs) have become a reliable alternative to overcome the leakage problem of the conventional liquid electrolyte based DSSCs [71]. The solid-electrolyte in ssDSSC is easy to package, and only needs one transparent electrode which enables the application on textile substrate. Therefore, the 2D structured ssDSSC and the solid electrolyte enables roll-to-roll printing on the textile substrate, which also reduces the manufacturing cost. The recorded efficiency of ssDSSC is relatively high up to 11% based on two FTO glass electrodes use copper(II/I) to improve the pore filling in the hole transporting material (HTM) [129].

3.5.1 High temperature processed ssDSSC

Solid-state dye-sensitized solar cells have demonstrated two key manufacturing advantages over the liquid – electrolyte based DSSCs. The solid-state electrolytes are easier to package and are therefore are potentially more stable than liquid electrolytes, and ssDSSCs only require one piece of transparent electrode to enable light to pass into the cell which enables application on the textile substrate [130]. The counter electrode of ssDSSC is usually deposited by thermal evaporated Au or Ag [131, 132]. However, the thick metal Au or Ag layer results in the incident light being either dissipated or reflected at the metal surface. Some research has recently tried to overcome this problem by using metal particles as the top electrode in ssDSSC [133, 134], but the spray coated Ag nanoparticles are require annealling at 150 ^{o}C – 200 ^{o}C, which cause the spiro-OMeTAD to crystallize and the dye molecules absorbed on TiO_2 film to peel off [130].

Silver nanowires have recently been developed and investigated as the top electrode to solve these problems in ssDSSC, an approach that uses the laminated AgNW as the reflective counter electrode via the solution process with a maximum achieved a PCE value of 2.7% compared to the thermal evaporated Ag film electrode of 2.8 %[130]. In order to improve the

conductivity, AgNW was deposited on a coverslip glass substrate and heated at 180 ^{o}C. It was then subsequently pressed onto the sipro-OMeTAD at a pressure of 1.6×10^4 psi for 30 seconds as shown in figure 3.15. The overall surface coverage of AgNW on the spiro-OMeTAD was 59% by employing using this method.

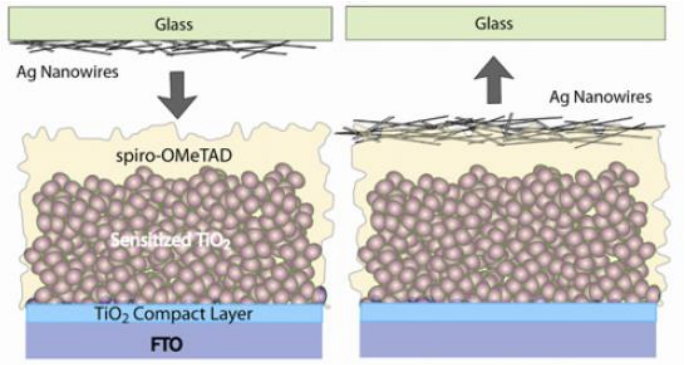

Figure 3.15. Structure diagram of ssDSSC using AgNW as the top electrode (a) before, and (b) after lamination[130].

The optical property of this AgNW coated ssDSSC has been successfully demonstrated by absorbing more incident light compare to the thermal evaporated Ag electrode. This present study shows that the thermal evaporated Ag electrode can be replaced by this AgNW mesh counter electrode in ssDSSC with a comparable PCE value. It also indicated that AgNW can be used as the semi-transparent front contact of a glass free electrode by a tandem structured ssDSSC. Based on this investigation, this research group has developed a highly transparent AgNW coated PEDOT:PSS conductive electrode by using this solution process. The structure of the device is shown in figure 3.16, along with the cross-sectional and planar view of the cell.

The structure of the cell is similar to the standard ssDSSCs, except the top electrode. In this ssDSSC, a silver nanowire coated poly (3,4-ethylenedioxythio-phene);poly(styrenesulfonate) (PEDOT:PSS) replaces the platinum coated FTO glasses [135]. The electrolyte used here is Spiro-OMeTAD, and the fabrication process is quite similar to the conventional ssDSSCs. The PEDOT:PSS layer is deposited by spin coating followed by the spray coating of silver nanowire to complete the top electrode. The SEM image in figure 3.16 (d), shows that the nanowires are embedded in the PEDOT:PSS. There are two important roles of PEDOT:PSS in this device, one is to improve the ohmic contact between the Sprio-OMeTAD and silver nanowire [135], enabling the working function between these two materials to be matched. The other is to improve the conductivity of the silver nanowire. The SEM image in figure 3.16 (c) shows the gap between the nanowires can be 500 nm, which results in a low conductivity. PEDOT:PSS could promote the charges transport between the nanowires.

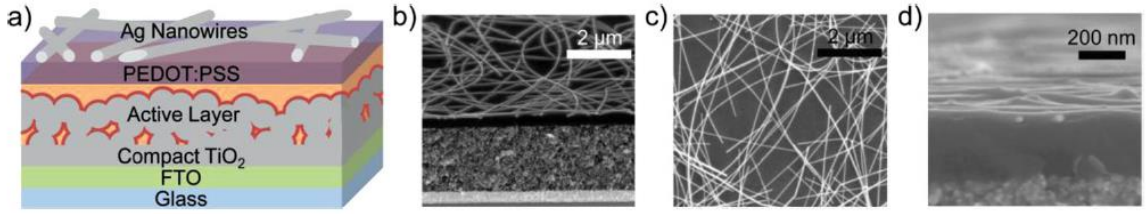

Figure 3.16. (a) Structure of ssDSSC with silver nanowire electrode. (b) SEM image of the ssDSSC with a 20º incident angle. (c) SEM image of the Ag NW/PEDOT:PSS electrode. (d) SEM image of the cross-sectional view of the Ag NW/PEDOT : PSS electrode [135].

The results from this device are shown in table 3.3. The efficiency achieved in this device is 3.6% which is quite similar to the reference ssDSSC device. This demonstrates that it is possible to replace the top glass electrode with a silver nanowire coated PEDOT:PSS electrode since it is just 0.1% less [135]. The spray coated AgNW/PEDOT:PSS layer also shows more than 92% peak transmittance without damaging the underlying ssDSSC. This development thus exhibited the possibility of a textile based ssDSSC device.

Table 3.3. Results of the ssDSSC with silver nanowire electrode and the reference ssDSSC [135].

Devices	Open circuit voltage (V_{oc}), V	Fill factor (FF)	Current density (J_{sc}), mA/cm^2	Efficiency %
Reference	0.82	0.60	7.6	3.7
Ag NW device	0.82	0.61	7.2	3.6

3.5.2 Low temperature processed ssDSSCs by atomic layer deposition method

The recent research on ssDSSC has demonstrated a reliable alternative to solve the leakage and evaporation problem of the conventional liquid electrolyte based DSSC, also brings an easier packaging way to widen the device application on flexible substrate. However, although there are several approaches have successfully demonstrated a low temperature processed mesoporous TiO_2 film, the TiO_2 compact layer still needs the high processing temperature (≥ 450 ºC) to form the crystalline. The crystallized TiO_2 compact can block the holes travelling

from the hole transporting material to the conductive film on the cathode substrate in order to prevent the device from short circuiting. Therefore, the key challenge of fabricating a low temperature processed ssDSSC is to solve the temperature issue to form the TiO_2 compact layer.

Low temperature processed ssDSSCs using the atomic layer deposition method to fabricate the TiO_2 compact (blocking) layer with an achieved efficiency of 1.3% was reported by Jiang et al [136], and an efficiency of 3.9% was achieved from the high temperature processed (conventional spray pyrolysis) ssDSSC device. In this study, the TiO_2 compact layer was deposited on the FTO glass substrate by the atomic layer deposition (ALD) method with a 150 ^oC processing temperature using $TiCl_4$ and DI water as the precursors. The device structure was shown in figure 3.17. The low temperature processed mesoporous TiO_2 film was synthesized by mixing TiO_2 nanoparticle powder in tert-butanol for 15 hours with no organic binders, and was further deposited onto the substrate by ALD. Spiro-OMeTAD was used as the hole transporting material, and Ag was deposited as the top electrode. This low temperature processed ssDSSC has successfully demonstrated a promising from of low cost flexible ssDSSC.

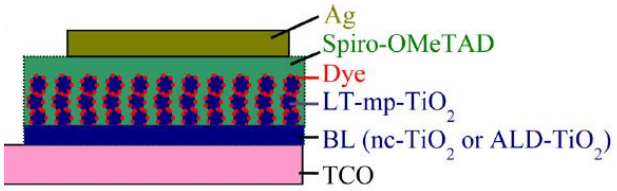

Figure 3.17. Structure of low temperature processed ssDSSC using atomic layer deposition method [136].

An improvement has been made on the polymer based ssDSSC by Xue et al [137]. In their work, the TiO_2 compact layer was deposited by ALD and the mesoporous TiO_2 film was deposited by the electrophoretic deposition method at low temperature. In this study, the ssDSSC is fabricated onto the FTO glass and ITO/PEN substrate respectively as shown in figure 3.18 (a) and (b) respectively. The TiO_2 compact layer is deposited by the ALD method at 150 ^oC on ITO/PEN substrate using $TiCl_4$ and DI water as the precursors, and deposited on the FTO glass substrate by the conventional spray pyrolysis method annealed at 450 ^oC to form the crystalline. The fabrication method of mesoporous TiO_2 film used in this approach is electrophoretic deposition by using ethanol, isopropanol, and butanol (1:2:4) based TiO_2 suspension. P3HT was used as the hole transporting material in this approach. A maximum efficiency of 1.93 % was achieved on ITO/PEN substrate with a fabrication processing

temperature lower than 150 ºC compared to the efficiency of 2.2% of the high temperature processed FTO glass device. This research successfully indicates the possibility of the roll-to-roll printing textile based ssDSSC for future research.

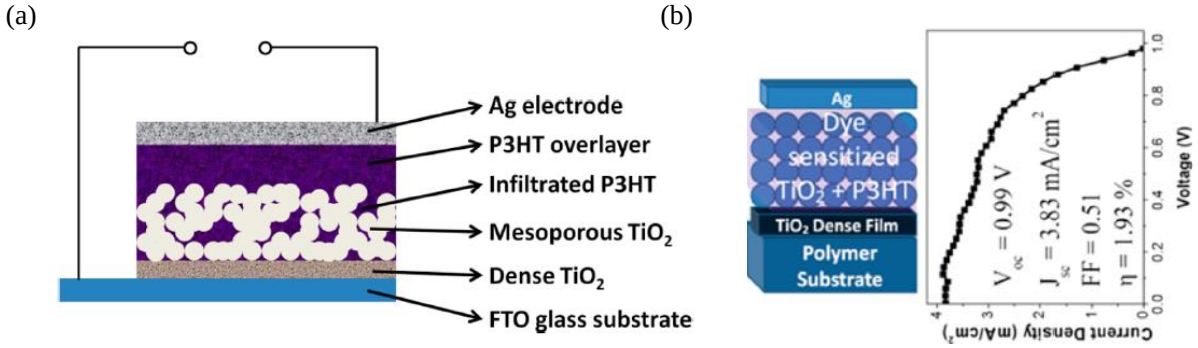

Figure 3.18. Cross-sectional view of (a) ssDSSC on FTO glass substrate, and (b) on ITO/PEN substrate [137].

The key challenge in both flexible ssDSSC and perovskite solar cells is to fabricate the compact layer at a low temperature (≤ 150 ºC). Another investigation based on different curing methods such as photonic curing and nearly infra-red curing was reported with an outstanding efficiency of 11.2%[138] on ITO/PET substrate. These approaches will enable the low-cost roll-to-roll manufacturing textile based solar cells in the future.

3.6 Conclusions

In summary, the efficiency of different types of DSSC and fabrication methods were summarised in Table 3.4. In order to achieve a textile based solar cell DSSC, the research work needs to focus on optimizing the morphology of the TiO_2 photoactive layer and the TiO_2 compact layer. The cell processing temperature is another concern of the textile based DSSC. A low temperature processed photoactive material (TiO_2 layer) can be synthesized by the colloidal sol-gel method, but the cell performance is not comparable to the ethanol or tert-butanol based TiO_2 paste since the acid is contained in the film which will degrade the flexible substrate. A good morphology of TiO_2 films needs to be investigated with solvent based formulation to achieve a fully solution processed DSSC on textile substrate. Therefore, in this research work, a non-acid based low temperature processed TiO_2 paste is formulated and developed for the flexible substrate, the rheological specification of the printing process of the functional layers is also investigated to achieving a flexible DSSC. For the long-term stability

of the flexible DSSC device, the characterization of ssDSSC needs to be investigated to fabricate the device on textile substrate.

Table 3.4. Summary of DSSC efficiency and fabrication method.

Device substrate	Processing method	Processing temperature	Device efficiency
FTO/Glass	TiO_2 sol-gel	150 ^oC	5.44%
FTO/Glass	TiO_2 sol-gel with $TiCl_4$ treatment	150 ^oC	8.54%
FTO/Glass & ITO/PET	TiO_2 sol-gel with $TiCl_4$ treatment	150 ^oC	4.0%
FTO/Glass & ITO/PEN	TiO_2 sol-gel with $TiCl_4$ treatment	150 ^oC	5.8%
ITO/PET	Cold isostatic pressing	35-200 MPa at room temperature	6.3%
ITO/PEN	Pressing	Room temperature	7.6%
ITO/PET & FTO/Glass	$TiCl_4$ treatment	500^oC	7.2%
ITO/PET & Graphene coated cotton fabric	$TiCl_4$ treatment	100^oC	2.52%
FTO/Glass & Multi-wall carbon nanotube coated polyester cotton fabric	$TiCl_4$ treatment	500^oC	5.69%
Carbon coated fibre	3D structure	500^oC	3.4%

Ti wire & Carbon coated fibre	3D structure	500ºC	8.45%
Textile	Sewing method	500ºC	5.8%
Glass fibre & Polyamide film	Film transfer method	500ºC	1.8%
FTO/Glass	Solid-state electrolyte with Ag film evaporation	500ºC	2.8%
FTO/Glass	Solid-state electrolyte with AgNW	500ºC	3.6%
FTO/Glass	Atomic layer deposition of TiO_2 compact layer, and $TiCl_4$ treatment of TiO_2 mesoporous film.	150ºC	1.3%
ITO/PEN	Atomic layer deposition of TiO_2 compact layer, and electrophoretic deposition of TiO_2 mesoporous film.	150ºC	1.93%

This page intentionally left blank

Chapter 4

4 Investigation of low temperature processed titanium dioxide (TiO_2) films for screen printing and spray coated dye-sensitized solar cells (DSSCs)

4.1 Introduction

A standard DSSC consists of a FTO coated substrate, a nano-crystalline porous TiO_2 film, a dye sensitizer, a liquid electrolyte and a platinum coated counter electrode on another FTO substrate. The conventional process for obtaining an efficient photo anode is high-temperature sintering of the nano-crystalline TiO_2 film. Since this process for obtaining an efficient photo anode is high-temperature sintering of the nano-crystalline TiO_2 film, and high temperature annealing process rules out the use of majority potential flexible substrates such as plastics and wearable textiles. Therefore, the development of a low temperature process-able TiO_2 layer is of great interest for the realization of DSSCs on flexible substrates. The state of the art in low temperature processed TiO_2 layer in DSSCs are: low temperature annealing of spin coated TiO_2 film [139], hydrothermal crystallization [140], chemical vapor deposition [104], microwave irradiation [141], room temperature compressing [142, 143], chemical bath deposition[105], electro-spraying[144]and electrophoretic deposition [145]. However, none of these methods can be adapted for large area DSSCs for the interest of commercialization. There are few low temperature processes with the potential to deposit a suitable TiO_2 layer in large areas, without needing an inert atmosphere, high temperature annealing and vacuum evaporation techniques.

Potential large area processes at suitable low temperatures are doctor blading, spray coating and screen printing. Low temperature treated plastic DSSCs were reported by Malekshahi et al [146]. The TiO_2 ink was applied by doctor blading on an indium tin oxide/polyethylene terephthalate (ITO/PET) substrate and annealed at 120^{o}C for 24 hours achieving an efficiency of 1.26%. Lu et al reported the annealing conditions of TiO_2 films at various temperatures from 120^{o}C to 450^{o}C using both binder and binder free TiO_2 paste deposited on a highly flexible titanium foil substrates by doctor blading [147]. The results showed that the devices sintered

at 120°C for 30 minutes, for both the binder and binder free TiO_2 systems, obtained a PCE of 0.22% and 3.4% respectively. Janne et al reported DSSCs on ITO/PET substrates in which TiO_2 films were spray coated using a 100°C substrate platen temperature, followed by room temperature compression of the film, achieving a solar cell PCE of 2.3% [148]. Shungo et al developed screen printed plastic DSSCs on an ITO coated plastic substrate using a conventional TiO_2 paste with binders, annealed at 150°C, that achieved a PCE of 0.1% and additional hot UV treatment with an achieved PCE of 3.1% [149]. A doctor blade processed TiO_2 layer which is air dried at room temperature has also been reported with 1.2% PCE [150].

This chapter systematically investigates low temperature (150°C) processed TiO_2 formulations, with and without a binder system, in two different solvents and the use of a Nano particle stabiliser for the textile and plastic substrate. The study applies to and benefits both screen printing and spray coating techniques which are considered as the promising large area electronics fabrication methods. Screen printing is the most widely studied printing technique within printing electronics research due to the wide commercially availability of functional materials in printable pastes and can scale up for volume manufacturing. Among the various solution process techniques, spray coating can accept a much wider range of rheological properties than the alternatives of inkjet printing and doctor blading. Other solution based processes such as spin coating are not compatible with large area fabrication and generate a large amount of material waste when processing. For this work, 150°C has been set as the temperature limit to be compatible with the majority of wearable textiles and flexible plastics. An optimised formulation for the screen printable paste and the spray coating ink of the TiO_2 materials for large area DSSC fabrication at low temperature was reported in this work.

Therefore, the aim of this study is to develop and optimize a screen printable and spray coatable TiO_2 formulation to give a smooth TiO_2 film. The devices are fabricated and tested on a FTO glass slide processed at temperature < 150°C, in order to solve the main challenge in this research work which is the limitation processing temperature of textiles.

The experiments in this chapter include the fabrication method of conventional DSSC with the standard configuration as the reference device, using the commercialized production TiO_2 paste contains binder. The TiO_2 film is deposited on the FTO glass substrate by pipette printing and heated at high temperature (450°C), and an efficiency value of 9.14% is indicating a promising method for the fabrication of DSSC. Then the TiO_2 paste is customised prepared by mixing the TiO_2 powder with and without organic binder (Triton X-100), and the organic compound

(Acetylacetone) and water or ter-butanol as the solvent. Triton X-100 is used as the organic binder also as the stabilizer in this formulation due to its special chemical properties. It is a nonionic surfactant that has a hydrophilic polyethylene oxide chain and a hydrophobic group, which makes it more soluble in the water than other organic binders. The TiO_2 pastes are deposited on the FTO glass substrates with both screen printing and spray coating and sintered at low temperature of 150^oC for half an hour. Both screen printing and spray coating are applied to deposit TiO_2 paste onto the glass substrate, a maximum efficiency of 4.3% was achieved by screen printing, and 2.58% was achieved by spray coating in low temperature (150^oC) processing.The electrolyte and the counter electrodes are the same with the high processed DSSC experiment above. The details of the results are compared and discussed in the sections below.

4.2 Device design and structure

The structure of the device designed in this experiment is shown in figure 4.1. The normal fabrication procedure of a conventional DSSC is preparing the working electrodes and the counter electrode first. Then add the electrolyte between the two electrodes, and finally sealing the two electrodes together to accomplish the cell.

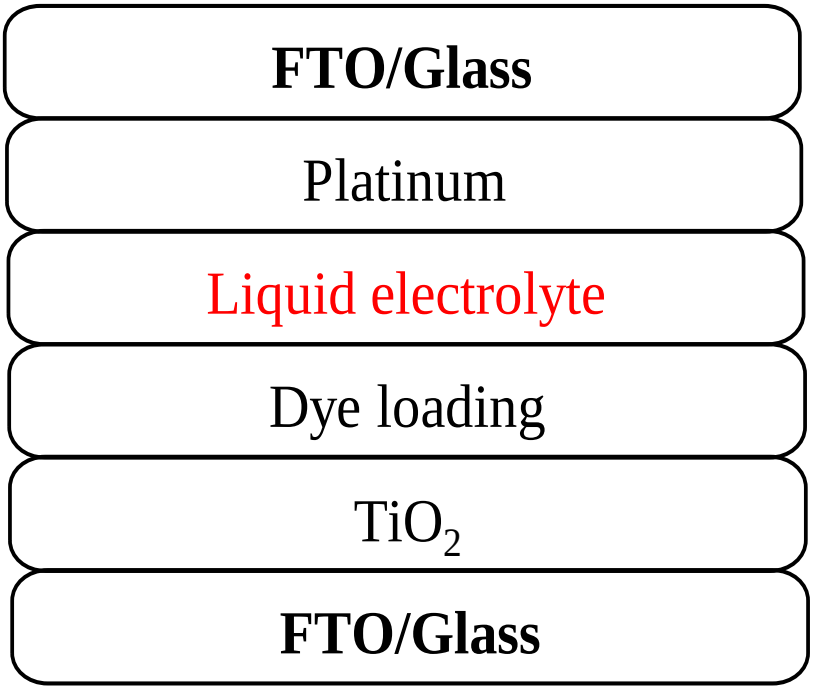

Figure 4.1. Structure of the conventional DSSC.

The working electrode is conventionally made of a FTO coated glass with a dye sensitized TiO_2 layer. The TiO_2 nanoparticles could be deposited onto the FTO glass substrate by many coating methods, such as screen printing, spray coating, doctor blading and spin coating. The most commonly used method is the screen printing since it is easy to control the position and thickness. TiO_2 Nanoparticles are normally prepared in paste type which normally contain the TiO_2 powder, binders, and solvent. Then, the TiO_2 paste is printing on the glass substrate. The paste needs to have a high viscosity so that it stays on the glass substrate properly after sintering at 450^oC for half an hour. The binder in the TiO_2 paste is removed by the high temperature, so that the conductivity of the cell could be improved. The working electrode is then finished by loading the TiO_2 substrates in the dye solution for a few hours at room temperature. The morphology of the TiO_2 nanoparticle layer is usually checked by the scanning electron microscope (SEM).

In the counter electrode fabrication, platisol is dropped on the FTO glass substrate to deposit the platinum layers, and then heated at 450^oC for half an hour. The electrolyte is added between the two electrodes. The cell is tested under 1 sun illumination by connecting the anode and cathode to the solar simulator to measure the output voltage and current.

4.3 Experiment of screen printing and spray coated devices

Figure 4.2 shows the flow diagram of the fabrication process, comprising both photo and counter electrode glass substrates with liquid electrolyte deposition in a sandwich structure assembly. The glass substrate is etched by the plasma cleaning. The TiO_2 formulation was either screen printed or spray coated onto the FTO coated glass substrates and cured at 150 ^oC and 450 ^oC for 30 minutes, respectively. The 450 ^oC process is carried out for comparison to the low temperature process. Then the dye loading process is carried out by immersing the sample into the pre-mixed dye solution for 12 hours. The last stage is to assemble the device by depositing the liquid electrolyte and sandwiching the two electrodes for testing. The TiO_2 film is deposited on the glass substrate by both screen printing and spray coating. The two electrodes are preparing separately, and sealed together for testing. The main steps for fabricating DSSC on two glass substrate are:

1) Preparing the working electrode.
2) Preparing the counter electrode.

3) Injection of the electrolyte.
4) Sealing and testing the cell.

The procedures for preparing the working electrode are:

1) Substrates cleaning.
2) Preparing the TiO_2 photo anode
3) Loading the TiO_2 glass substrate into the dye solution in a sealed and light tight box for several hours.

The procedures for preparing the TiO_2 photo anode are:

1) Preparing the TiO_2 film.
2) Depositing the TiO_2 film on the FTO glass substrate.
3) After drying, the TiO_2 coated FTO glass substrate is heated at 450^oC for half an hour.
4) Cool down the substrate to room temperature.

The procedures for dye loading are:

1) Preparing the dye solution (dye with ethanol) in petridish glass.
2) Sealing the petridish glass with kitchen film.
3) Putting the petridish glass in a sealed and light tight box for several hours or overnight.

The procedures for preparing the counter electrode are:

1) Add one or two drop of plastisol on the cleaned FTO glass substrate
2) Heating at 450^oC for half an hour.
3) Cool down to room temperature

The two electrodes are bounding together by the clips, and one or two drops of electrolyte is added between the two electrodes. The anode and the cathode of the cell are connected to the solar simulator to measure the output voltage and current by a probe. The evaluation parameters are calculated from the data recorded by solar simulator.

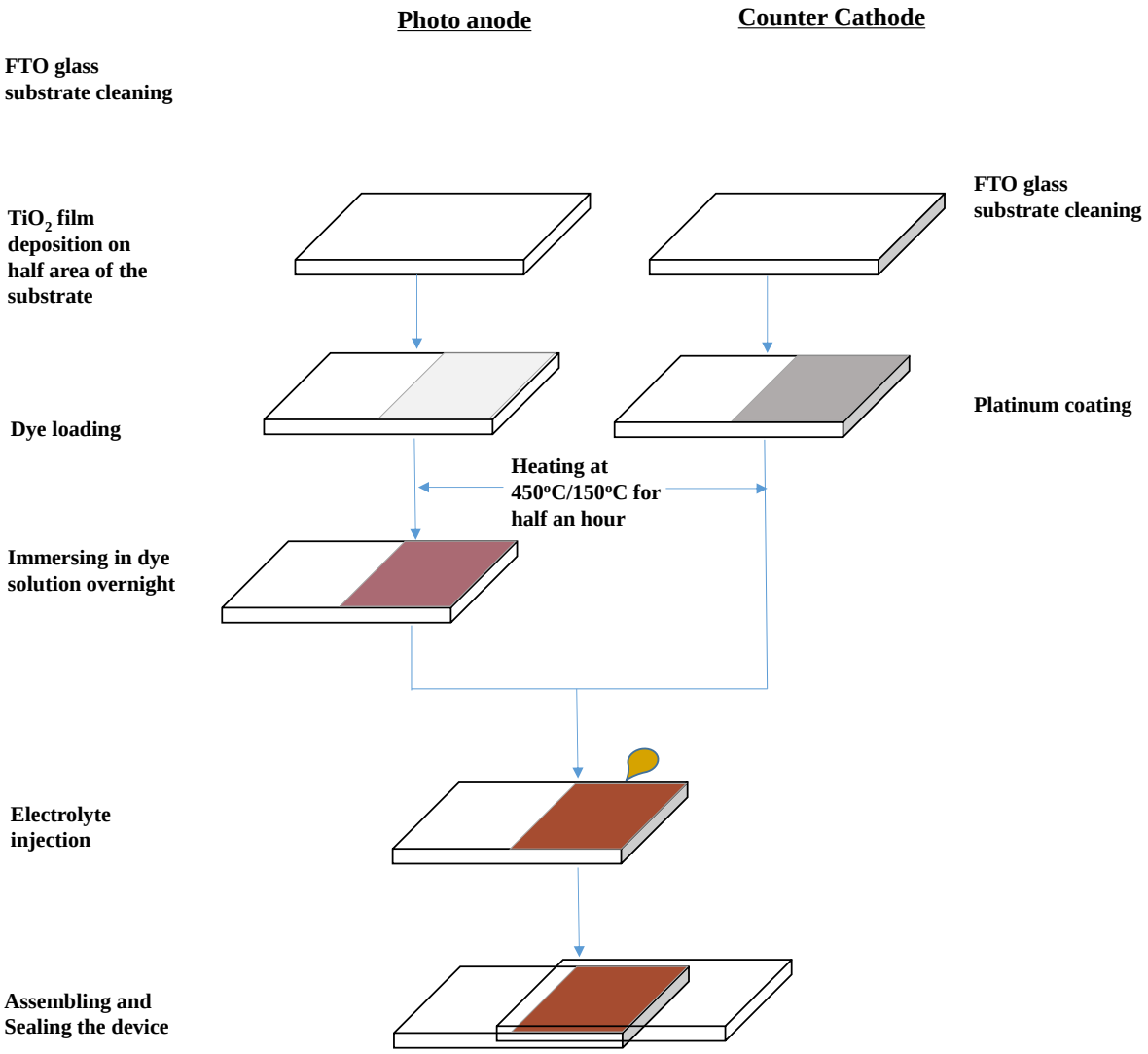

Figure 4.2. Fabrication process for standard DSSC [144].

4.3.1 Materials

Pre-coated fluorine-doped tin oxide (FTO) coated glass substrates (TCO 22-7, supplied by Solaronix) were used for the photo anode and cathode and has high transmittance in the range of 400 nm to 700 nm. The thickness is 1.0 mm with a resistivity of 7 ohm/sq. Titanium oxide (TiO_2, Aeroxide P25) nanoparticles of primary particle size 21 nm supplied by Sigma Aldrich are used to formulate the electron transporting layer (ETL) in the DSSCs. The rare polymorphs of TiO_2 used in this experiment is anatase. The Ruthenizer 535-bis TBA and N719 dye was supplied by Solaronix. The material is commercialized in dark purple powder, and the chemical name is cis-dissothiocyanato-bis (2, 2'-bipyridyl-4, 4'-dicarboxylato) ruthenium (II) bis (tetrabutylammonium). The structure is shown in figure 4.3 (a). The HOMO level is located

around -5.34 eV, and the LUMO level is located around -3.43 eV. The non-ionic surfactant binder used was Triton X-100, the chemical structure was shown in figure 4.3 (b) and the particle stabiliser was acetylacetone, both supplied by Sigma Aldrich and used to prevent the nanoparticles aggregating formulations. The absorption for the visible light is up to 750 nm with the TiO_2 film. Platisol-T from Solaronix was used as the precursor of the platinum layer for the counter cathode. Iodide/Iodine (I^-/I^{3-}) redox solution was used as the liquid electrolyte, supplied by Solaronix. All these above materials were used as supplied with no further modifications.

(a) (b)

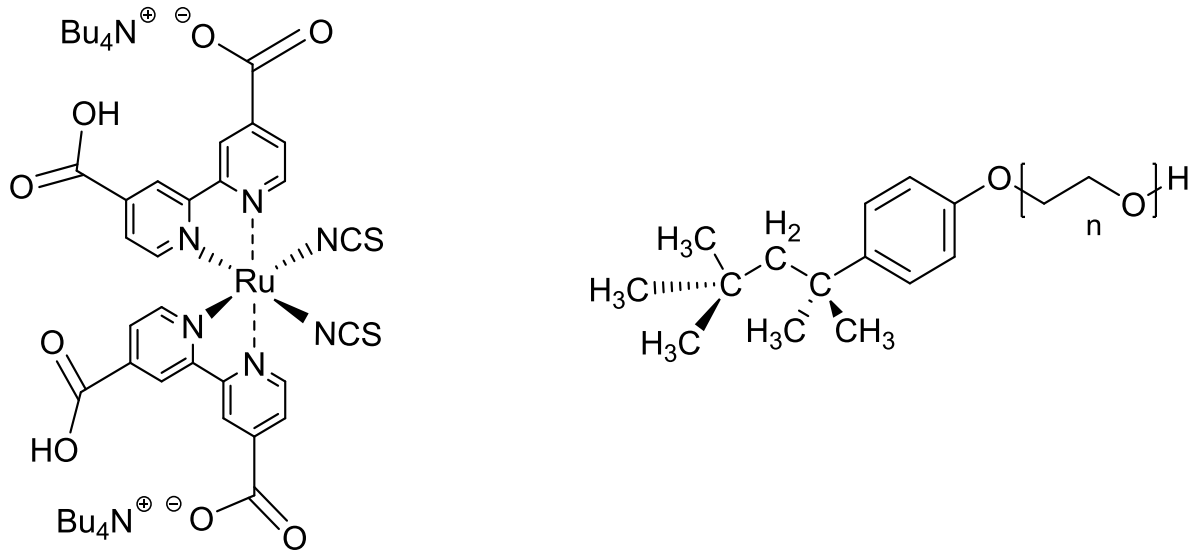

Figure 4.3. Chemical structure of (a) Ruthenizer [98] and (b) Structure of Triton X-100.

4.3.2 Substrates

The substrate (TCO22-7 from solaronix) used in this experiment is Flurin doped tin oxide (FTO, SnO2: F) coated soda lime glass, with the thickness of 2.2 mm. The FTO is coated on one side of the glass, and the resistivity is 7 Ω/sq. The glasses are cut into small pieces with the dimensions of 1.5 cm x 1.5 cm/piece.

The FTO coated glass substrate is transparent and able to transmit the light in visible range (400nm ~700nm). The FTO glass are the most commonly used substrate in conventional DSSC. It is a good start point for the investigation of new structure DSSC. A low temperature process will be tested on the glass substrate first, and will then move onto the fabric in the next stage. The glass substrates are going to use at the early stage of this research, as it is easy to test the

TiO_2 formulation and method of DSSC. The glass substrates will be replaced by the other material such as plastic, fabric and textile for the future work.

4.3.3 TiO_2 formulation study

This work investigated 8 formulations of low temperature TiO_2 evaluated at an annealing temperature of 150 ^oC. These formulations were used de-ionised water or tert-butanol as the solvent with no binder or with a Triton X-100 binder. The solvents water and tert-butanol were chosen as a rich oxygen provider; while annealing the TiO_2, they can contribute oxygen to prevent any TiO_2 oxygen loss. Both formulations were prepared with the same concentration of acetyl acetone as the particle stabiliser, as described in the following paste formulation. Formulations were then made suitable for screen printing and spray coating by varying the viscosity. The formulations used in this experiment are as follows. The TiO_2 screen printing paste was formulated using TiO_2 powder (6g) + acetyl aceton (0.2mL) + de-ionised water or tert-butanol (4mL) + Triton X-100 (0.1 mL). The TiO_2 spray coating ink was obtained from TiO_2 powder (6g) + acetyl acetone (0.2mL) + de-ionised water or tert-butanol (10 mL) + Triton X-100 (0.1mL). When deposited, these films were processed at 150 ^oC and compared with samples processed at 450 ^oC, as shown in the formulation system in figure 4.4. Other processes and the device architecture remained unchanged. The TiO_2 powder is mixed with the solvent of de-ionised water or tert-butanol, and acetyl acetone as stabiliser, plus the binder Triton X-100 or without a binder. Triton X-100 was chosen since it influences TiO_2 clusters towards a uniform size with well-defined particles. In addition, Triton X-100 increases the surface area which helps dye molecules to attach to the TiO_2 film.

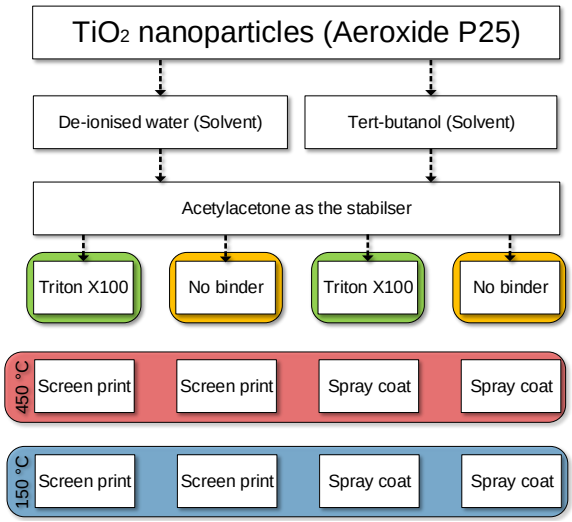

Figure 4.4. Systematic study of different low temperature processed titanium oxide formulations in relation to the curing temperature and the deposition methods.

4.3.4 Fabrication process of FTO

4.3.4.1 Cleaning the glass substrate

The FTO glass substrates were cleaned in acetone and de-ionised water for 5 minutes and plasma cleaned using a TEPLA Plasma 300 machine for 5 minutes in a cleanroom environment. The glass substrate is etched by the plasma cleaning using Plasma 300 machine in cleanroom for 5 minutes, and then washed by acetone and water. After wiping the substrates, it is important to check the conductive side by measuring the resistance value (around 18Ω) of the glass substrate. The cleaned glass substrates were kept in the Petri dish glass with the conductive side upwards and prepared for printing.

4.3.4.2 Screen printing of TiO_2 photo anode

In this experiment, two solvent based formulations are applied in preparing the TiO_2 paste, one is water-based paste with and without organic binder, the other is tert-butanol based paste with and without organic binder. Both of these four kinds of TiO_2 paste are tested under AM 1.5 condition and the results are compared in the following sections. Water is firstly used to prepare the TiO_2 paste since it was the most commonly-used and cheap material. The aim of using tert-butanol is to try to improve the TiO_2 paste to give a good morphology film.

The formulation of the water based or tert-butanol TiO_2 paste with organic binder and without organic binder used in this experiment are shown below:

With organic binder: [TiO_2 powder (6g)] + [Acetyl-acetone (0.2 ml) + water/tert-butanol (2 ml)] + [Triton X-100 (0.1ml)] + [water /tert-butanol (4ml)].

Without organic binder: [TiO_2 powder (6g)] + [Acetyl-acetone (0.2 ml) + water/tert-butanol (2 ml)] + [water /tert-butanol (4 ml)].

The TiO_2 powder is mixed with the solvent which contains water, acetyle-acetone and the organic binder Triton X-100. The water is later replaced with tert-butanol to improve the paste quality. The idea of the TiO_2 formulations is coming from the other papers. The organic binder Triton X-100 is dielectric material which is used to increase the viscosity of the TiO_2 paste. The reason for using this organic binder is that it contains hydrophilic group (refer to fig.4.4 - 2) which will not reduce much conductivity of the TiO_2 compared to the other organic binders. The acetyle-acetone is used as the stabilizer to make everything soluble in the system.

The sequence of preparing the TiO_2 paste is shown in figure 4.5. The TiO_2 powder of 6.0g is placed in a sealed plastic bottle, and weighted by a digital chemistry scale. Next, 0.2 mL of acetyl-acetone, 0.1 mL Triton X-100, and 6mL of water are dispensed into the TiO_2 powder. Lastly, the bottle contains TiO_2 powder, and the relative solvents is placed into the digital mixer for stirring at rpm 1500 for half a minute. Then the TiO_2 paste is ready for screen printing.

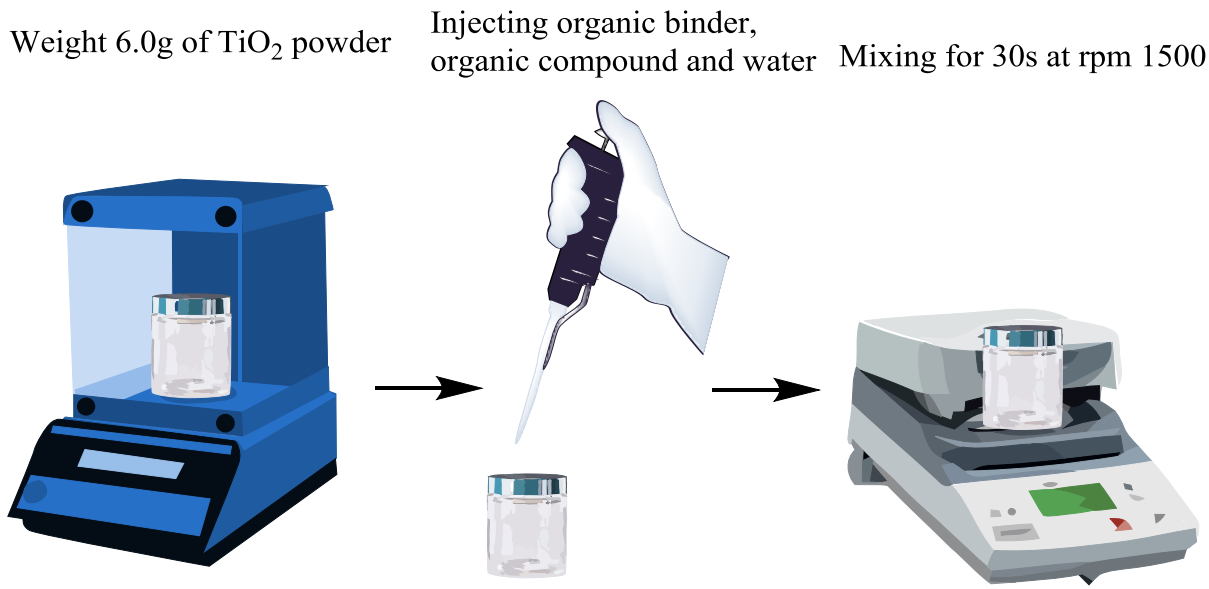

Figure 4.5. Preparation of TiO_2 paste.

The TiO_2 paste is deposited on the FTO glass substrate by hand screen printing method, the working electrodes are sintered at low temperature of 150^oC, and a high temperature of 450^oC for comparison. The counter electrodes are coated with platinum and heated at high temperature of 450^oC. The liquid electrolyte is applied between the working electrode and counter electrode.

The sequence of screen printing is shown in figure 4.6 and the photograph of the hand screen process was shown in figure 4.7. The glass substrates are fixed on the block by taps which also covering half area of the substrate; The screen is placed on the top of the substrate and should be fully contact with substrate, so that the paste can be printed on the substrate through the pattern on the screen. Some TiO_2 film is placed on the top of the pattern on the screen as well on the squeegee, forcing the squeegee from the top to bottom of the screen. The TiO_2 film is printed on the substrate through the mesh, and then the screen is removed from the top with the ink deposited on the substrates. A thickness of 4.47 µm is achieved by two deposits.

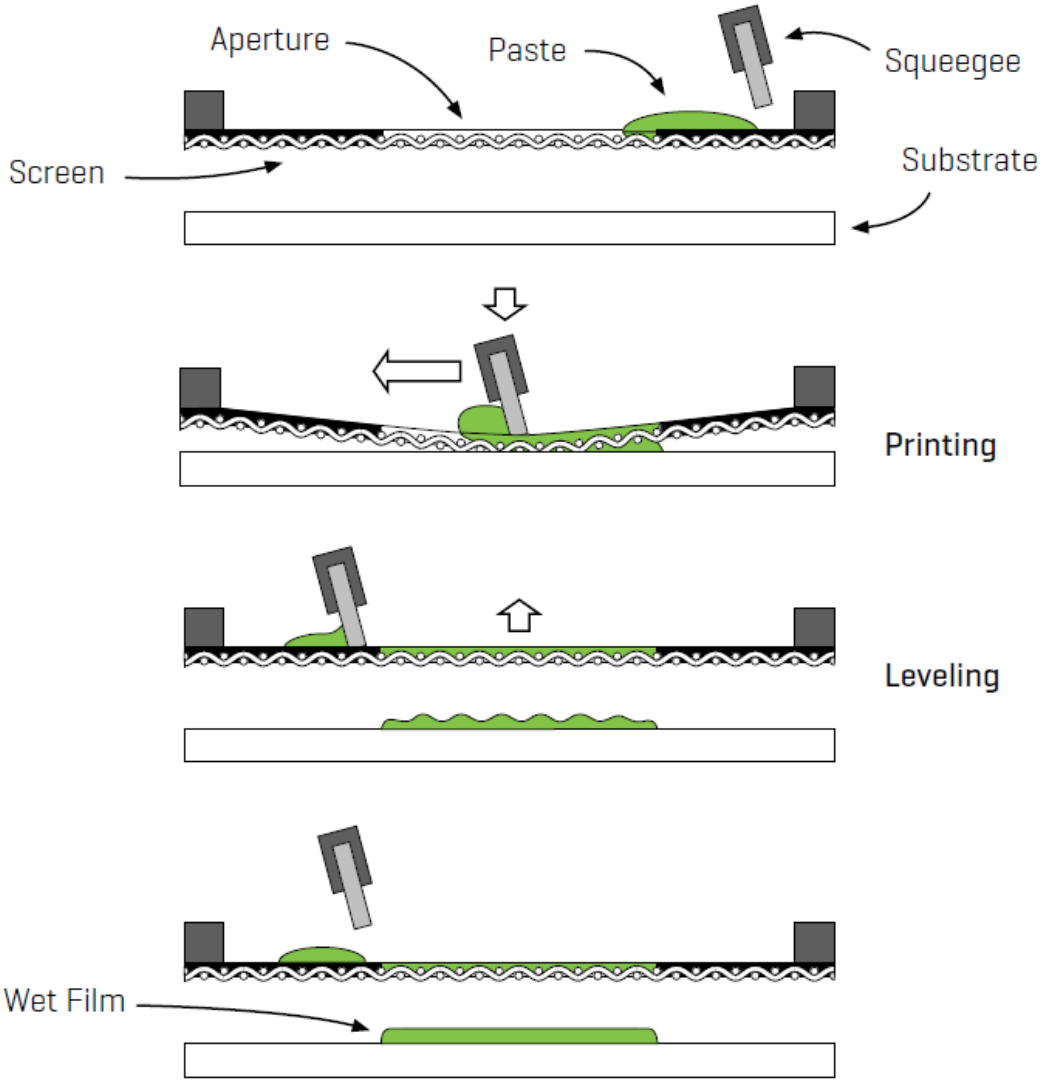

Figure 4.6. Screen printing sequence.

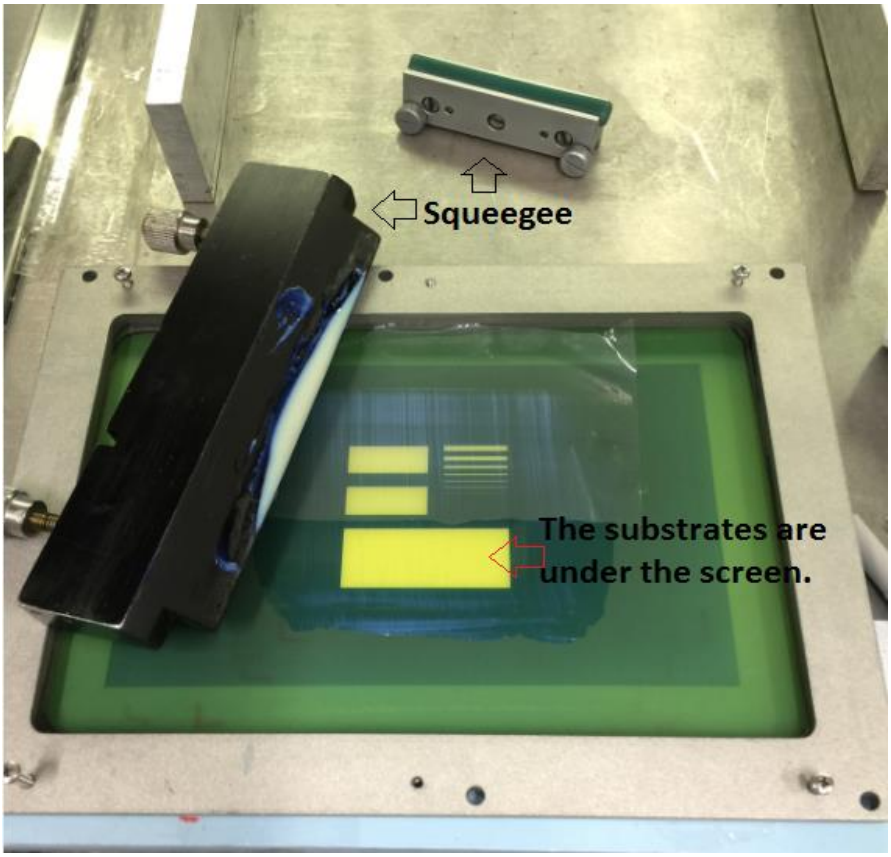

Figure 4.7. Photograph of screen printing process of TiO_2 film on the glass substrate.

4.3.4.3 Spray coating of TiO_2 photo anode

The TiO_2 paste for spray coating is prepared in two forms in this experiment, one is the paste with organic binder and the other is the paste without organic binder. The TiO_2 ink is a mixture with and without an organic binder, organic compound, and water. The spray coating method is applied to deposit the TiO_2 ink to the glass substrates, and the substrates are heated at low temperature of 150^oC, and at high temperature of 450^oC for comparison. After dye loading for 12 hours, the TiO_2 electrode is assembled with a counter electrode by injecting one drop of liquid electrolyte in between them.

The formulation of the TiO_2 paste with organic binder and without organic binder used in this experiment is shown below:

With organic binder: [TiO_2 powder (6g)] + [Acetylacetone (0.2mL) + water/tert-butanol (2mL)] + [Triton X-100 (0.1mL)] + [water/tert-butanol (10ml)].
Without organic binder: [TiO_2 powder (6g)] + [Acetylacetone (0.2mL) + water/tert-butanol (2mL)] + [water/tert-butanol (10ml)].

The organic compound acetylacetone of 0.2 mL, organic binder Triton X-100 of 0.1 mL, and water of 12mL are dispensed into 6g of TiO_2 powder. The TiO_2 ink without a binder is just removing the Triton X-100 from the mixture solvent. The powder is placed into separated plastic bottles and mixed by a digital chemical mixer for half minute. Then, the two types of TiO_2 ink are ready for spray printing.

The spray coating process is shown in figure 4.8. An air spray coating gun is used to spray the TiO_2 ink to the glass substrates. The glass substrates are placed into a holder and hung onto a stage, and the air gun is kept 10 cm away from the stage. The spray distance 10 cm was chosen based on Table 4.1 with 1 spray deposition for 1 second, which results in the required TiO_2 thickness. The spray time was controlled by a digital timer, the time was tested for 1 second and 2 seconds with 1-3 spray depositions. The spray pressure was set to 2.5 bar. The higher deposition times and spray coating time results in higher thickness and film cracking. The TiO_2 ink is sprayed onto the substrates by pressing the air gun. The image of spray coated TiO_2 electrodes with an organic binder is shown in figure 4.9. The substrates are subsequently heated in the oven at a low temperature of 150^{o}C for half an hour.

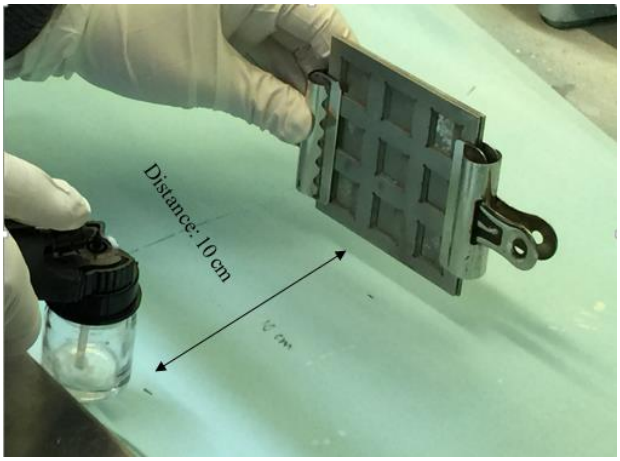

Figure 4.8.Spray coating process for low temperature processed DSSC.

Table 4.1. Spray coating specification summarizing.

Spray distance	TiO_2 thickness	Number of sprays	Spray time (s)
5 cm	10~12 µm	1	1
10 cm	4~6 µm	1	1
15 cm	2~3 µm	1	1
20 cm	0~1.5 µm	1	1
5 cm	11~13 µm	2	1
10 cm	7~8 µm	2	1

15 cm	6~7 µm	2	1
20 cm	3~4.2 µm	2	1
5 cm	13~14.3 µm	3	1
10 cm	8.5~9.2 µm	3	1
15 cm	8.7~9.8 µm	3	1
20 cm	5.2~7.4 µm	3	1
5 cm	8.8~11.2 µm	1	2
10 cm	4.9~6.8 µm	1	2
15 cm	3.2~4.6 µm	1	2
20 cm	1.2~2.5 µm	1	2
5 cm	15~17.6 µm	2	2
10 cm	8.2~9.6 µm	2	2
15 cm	6.2~7.3 µm	2	2
20 cm	5.0~6.5 µm	2	2

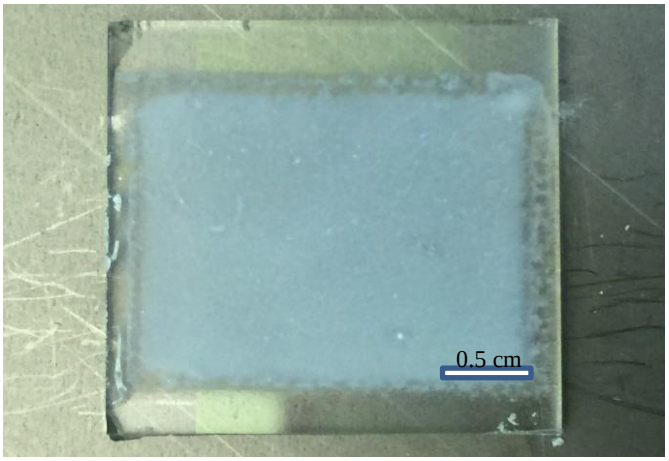

Figure 4.9. Photograph of spray coated device.

4.3.4.4 Staining process

Dye solutions are prepared with mixing dry dye powders and the required mount of ethanol. Firstly, the dye powders are weighted to the amount of 50mg by the digital chemistry weight scale, and placed into a sealable glass bottle. Next, 5ml ethanol are mixed to the dye powders. The mixer is stirred at room temperature until all the powders are dissolved in the ethanol, the solution is now claret-coloured and poured. It is poured into a petridish for staining.

The electrodes are immersed fully into the dye solution with the TiO_2 surface facing up. The solution should cover the whole surface of TiO_2 electrodes to enable enough dye molecules to be adsorbed on the TiO_2 surface. Next, the petridish glass with dye solution and TiO_2 electrodes

are sealed with a transparent kitchen film and put in a sealable black box to avoid light exposure (refer to figure 4.10). Dye loading takes 12 hours which is the maximum loading time.

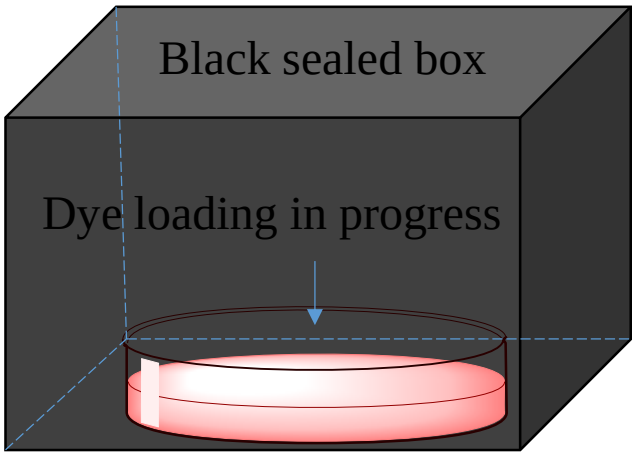

Figure 4.10. Dye loading staining process.

The TiO_2 electrode surface should be claret-coloured, that indicates a good staining and also a good porous property of TiO_2. When the entire surface of the TiO_2 electrode becomes claret-coloured, the electrodes are ready to take out. The electrodes are rinsed by a small amount of ethanol, and kept in a sealed container to avoid light exposure. The photograph and SEM photo of TiO_2 electrode after staining with dye solution is shown in figure 4.11 (a) and (b) respectively. Cross-section SEM photographs of both the TiO_2 working electrodes of screen printing are shown in figure 4.12.

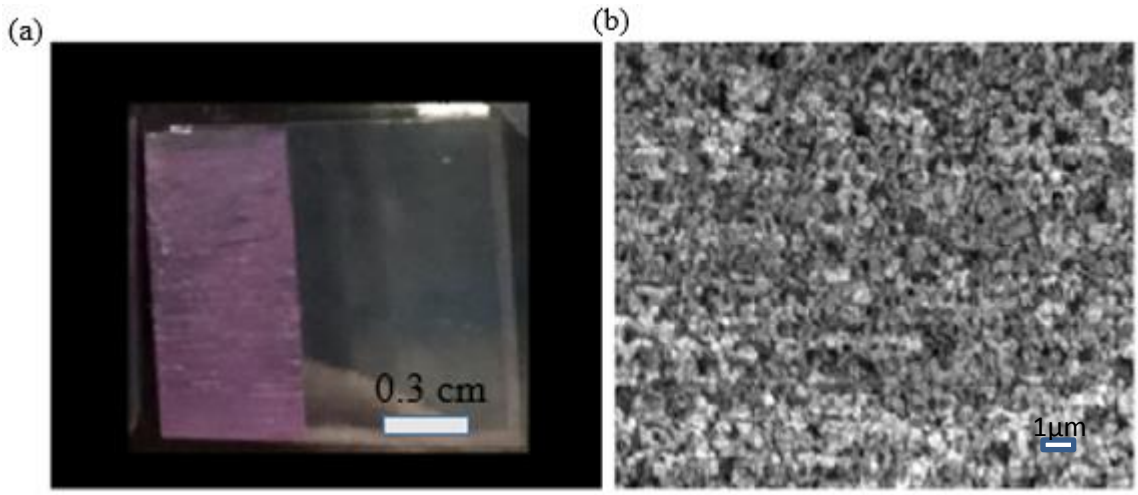

Figure 4.11. (a) Photograph and (b) SEM plan view of screen printed DSSC processed at high temperature after staining with dye solution.

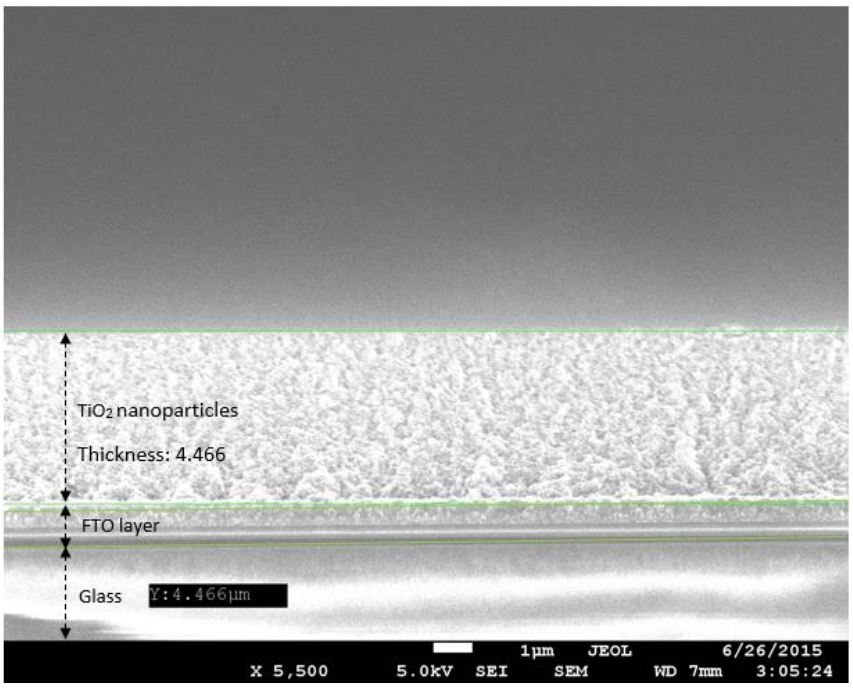

Figure 4.12.SEM image of the cross-sectional view of screen printed DSSC working electrode. The thickness of the TiO_2 film is 4.466 µm.

4.3.4.5 Preparing the counter electrode

The preparation procedure of the counter electrode is similar to the working electrode; the half area of the electrode is covered by the tape, and the other half is coated with platinum. One or two drops of platisol T is applied to the electrode, and then put on the hot plate at 50^{o}C for 5-10 minutes. Lastly, the counter electrodes are heated at 450^{o}C for half an hour in the oven. The working electrodes and counters electrode are kept together for testing.

4.3.4.6 Assembling the device

The working electrode is placed on a flat surface, applying one or two drops of electrolyte is applied to the active area of the working electrode which is the stained TiO_2 surface. In order to get a better performance from the cell, the electrolyte should be stain the entire area of TiO_2 surface. Subsequently, the counter electrode is placed face to face with the working electrode. The active layer of both electrodes should contact each other. After that, the two electrodes are pressed together by a clip. Figure 4.13 shows the assembled DSSC device.

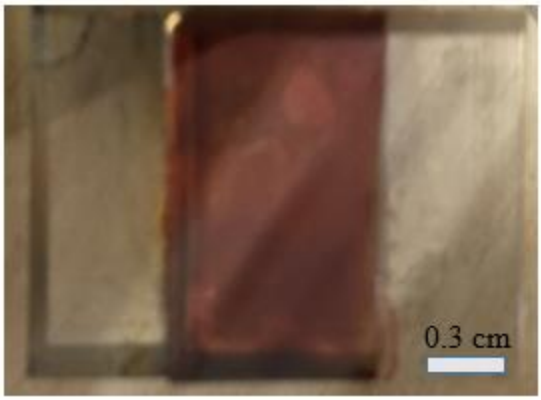

Figure 4.13. The final device of a standard DSSC, the working electrode and counter electrode assemble together.

4.4 Device testing

The method used to test the DSSC is to measure the output current and voltage of the device. Firstly, the devices need to be set up with the relevant instruments. Figure 4.14 shows the device being set up for measurements. All the devices are measured under dark and illuminated condition by using a digital source meter (Keithley, Model 2400) as shown in figure 4.15, and a solar simulator (ABET Sun 300) to provide illumination of AM 1.5 conditions. The digital source meter is connected to the computer and the device, the output current and the voltage data is measured by the controller as shown in figure and processed to the computer via the software Lab View. The device is putting into the solar simulator under the lamp, the distance between the device and the lamp is about 15 cm.

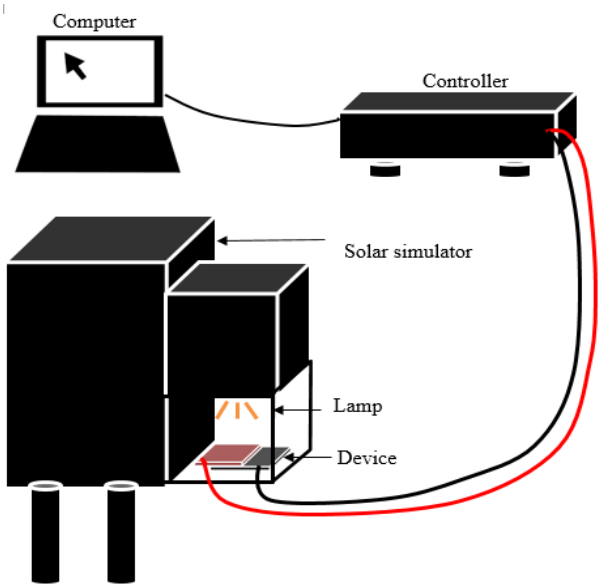

Figure 4.14. Device measurements set up. The device is put into the solar simulator to absorb the light which gives a standard sun irradiance AM 1.5 G. The controller is connected to the device to measure the output current and voltage of the device, and to send the data to the computer.

Figure 4.15. The controller of the device. This controller is connected to the cell and records the output current and voltage of the device.

The devices are tested by connecting the two terminals of the cell by a crocodile clip, and the probes are connected to the digital source meter, as shown in figure 4.16. The solar simulator used in this research work is ABET Sun 3000 as shown in figure 4.17 (a); it provides an artificial light (AM 1.5) within the lamp and the devices are put under this lamp before testing as shown in figure 4.17 (b). A reference silicon based solar cell was firstly tested by the solar simulator to find out the exact location of device to have the maximum light intensity. The output current and voltage of the is measured by the controller and recorded via the software Lab view. The program is run after the lamp is turned on. The output current and voltage is automatically rerecorded by the system as shown in figure 4.18.

Figure 4.16.DSSC device is connected to the controller by using crocodile clips.

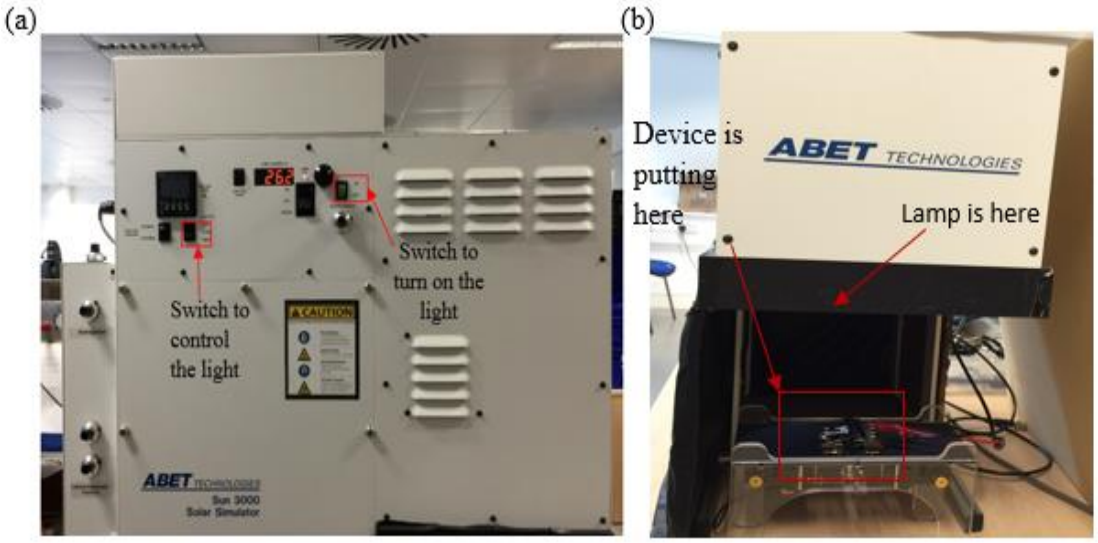

Figure 4.17. (a) Photograph of the front view of solar simulator. The switch on the right is used to turn on the lamp, and the button on the left is used to turn the light on and off. (b) Photograph of the solar simulator on the right side; the devices are put under the lamp for testing.

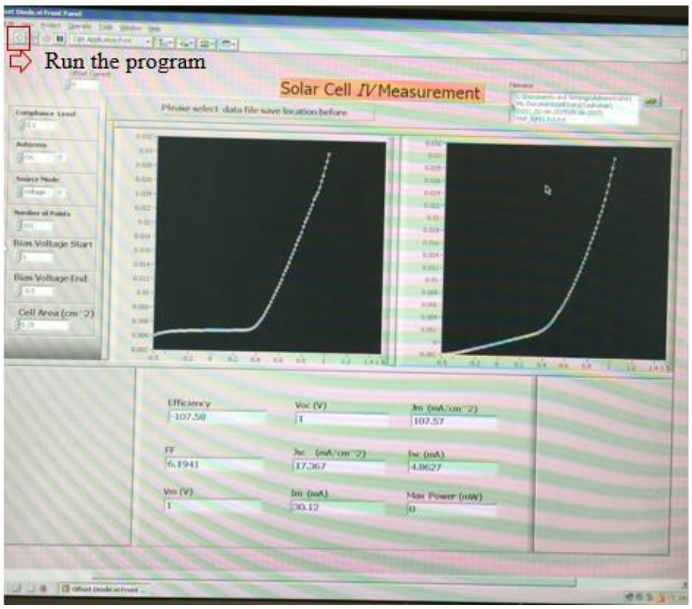

Figure 4.18. Solar cell IV measurement system.

4.5 Results and discussion

4.5.1 Results of standard devices

A conventional DSSC was first fabricated using the commercialized TiO_2 and processed at high temperature of 450^oC by screen printing as the standard device. The results of the standard DSSC device 1 and device 2 with conventional structure are summarized in Table 4.2. The highest efficiency of 9.14% is achieved, with the open voltage of 0.69. These results are calculated based on the current and voltage data generated from the solar simulator with the relevant formulas. The cell area is defined by the pre-designed solar cell mask.

Firstly, the current and voltage data are imported to the Origin software to plot the power and J/V curve of the device. The maximum power can be found from the power curve; the maximum point gives the maximum power (P_{max}) value which is 0.00256 W for device 1, and then the corresponding current and voltage is the maximum current (I_{max}) and voltage (V_{max}). The current and voltage curve is plotted based on the data measured from the device, and J/V curve. The short circuit current is the point where voltage is zero, and the open circuit voltage is the point where the current is zero. Based on the J/V curve shown in figure 4.6 -1, the short

circuit current density (J_{sc}) and open circuit voltage (V_{oc}) for device 1 is 21.7 mA/cm^2 and 0.69 V respectively.

The calculations are based on these values, since the maximum current and voltage, and the short circuit current and open circuit voltage are obtained, therefore the fill factor could be calculated based on the formula Fill factor = $(V_{max} \times I_{max})/(I_{sc} \times V_{oc})$, which is 0.61 in this case. The efficiency could be calculated by the formula $\eta = P_{max} / P_{in} = I_{sc} \times V_{oc} \times FF / P_{in}$, where the irradiance is the cell active area times the standard irradiance value 100 mW/cm^2 since the cell is testing under 1 sun condition. The current density (J_{sc}) value is calculated by the formula $J_{sc} = I_{sc}$/ cell area. The calculations could be summarized in the following steps:

(1) Importing the current and voltage data to Origin software.
(2) Calculating the power by writing the formula P = I × V.
(3) Plotting the power curve and find the maximum power.
(4) Based on the maximum power find the corresponding maximum current and voltage value.
(5) Plotting the J/V curve and find the short circuit current and open circuit voltage.
(6) Calculating the fill factor, efficiency, and current density based on the value found in the above steps.

The following experiment sections will be following the same steps to calculate the results.

Table 4.2. Results of pipette printed high temperature processed standard DSSC.

Devices	**Open circuit voltage (V_{oc}), V**	**Fill factor (FF)**	**Current density (J_{sc}), mA/cm^2**	**Efficiency %**	**Cell area (cm^2)**
1	0.69	0.61	21.7	9.14	0.28
2	0.69	0.61	21.52	9.0	0.28

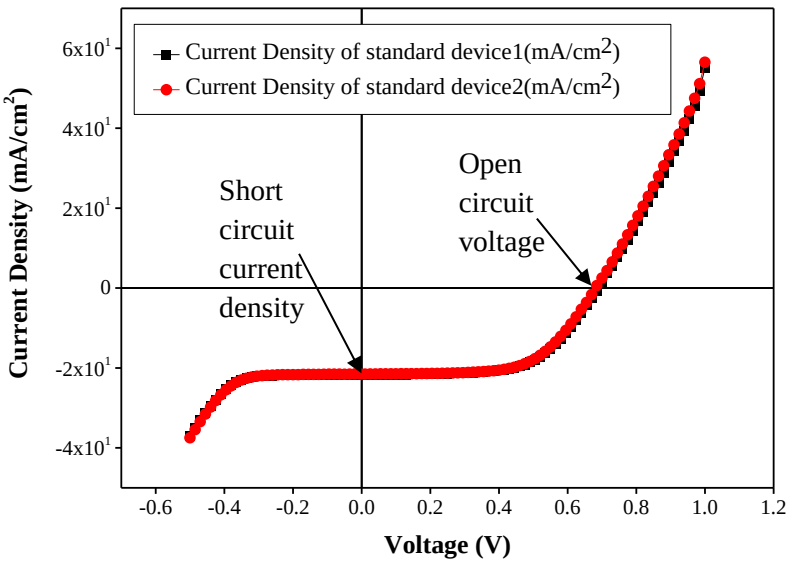

Figure 4.19. J/V curves of the high temperature processed standard DSSC.

4.5.2 Results of screen printed and spray coated devices

Surface and film morphologies of different photo anodes are measured by FESEM and shown in figure 4.20 and figure 4.21. The SEM sample were prepared by coating a thin layer of gold on the cross-sectional area of the device. The samples were pre-cut in the middle and put into the coating machine for 30 seconds/sample. The coating time is restricted on 30 seconds to improve charging problem. The SEM machine was set to low resolution mode first to choose the scan area of the TiO_2 film, and then adjusted to the high-resolution mode to view the TiO_2 nanoparticles inside film. Figure 4.20 (a, b) shows the FESEM images of screen-printed water based TiO_2 films with and without binder system on FTO glass substrates respectively. Both indicate the film thicknesses of ~10µm, which is an ideal thickness for the flexible substrates. The ideal thickness of 10µm allows sufficient dye molecule adsorbed on the TiO_2 film which results in more current. However, the thicker thickness of the TiO_2 film will lead a long way for the electrons to pass to the FTO glass, and cause the film cracking. Therefore, the ideal thickness of the TiO_2 film is ~10µm which is approved by the experiments as well. In addition, these films are uniform, crack-free and well adhered on FTO glass substrates. Figure 4.20 (c, d) shows the FESEM images of screen printed tert-butanol based TiO_2 films with and without binder system on FTO glass substrates respectively. Both indicate the film thicknesses around ~40µm which is over the ideal thickness for the flexible substrates hence the appearance of a

crack on the screen-printed films. Moreover, these films showed the significantly amount of fragility and poor uniformity along the top surface and the cross sectional FESEM images as shown in figure 4.20 (c, d). For the spray coated TiO_2 films on FTO glass substrates, a similar trend of film appearance has occurred, as shown in the FESEM images in figure 4.21 (a, b) using water as the solvent and in figure 4.21 (c, d) using ter-butanol as the solvent. The reason for these non-uniform films is due to the high melting point (25^oC ± 1) and the low boiling point (82^oC ± 1) of the tert-butanol solvent. The tert-butanol solvent is frozen when the room temperature is below 25^oC. As the deposition process carried out in the room temperature either by screen printing or spray coating technique, part of the tert-butanol solvent is under the frozen condition or being evaporated which will prevent the settling of the printed TiO_2 paste or ink on the glass substrate to form the uniformed layer and cause the fragility in the annealed TiO_2 layer. In essence, it is clearly seen that the de-ionised water based system with and without binder would benefit much more in the layer's uniformity and interconnected TiO_2 nanoparticles as a layer.

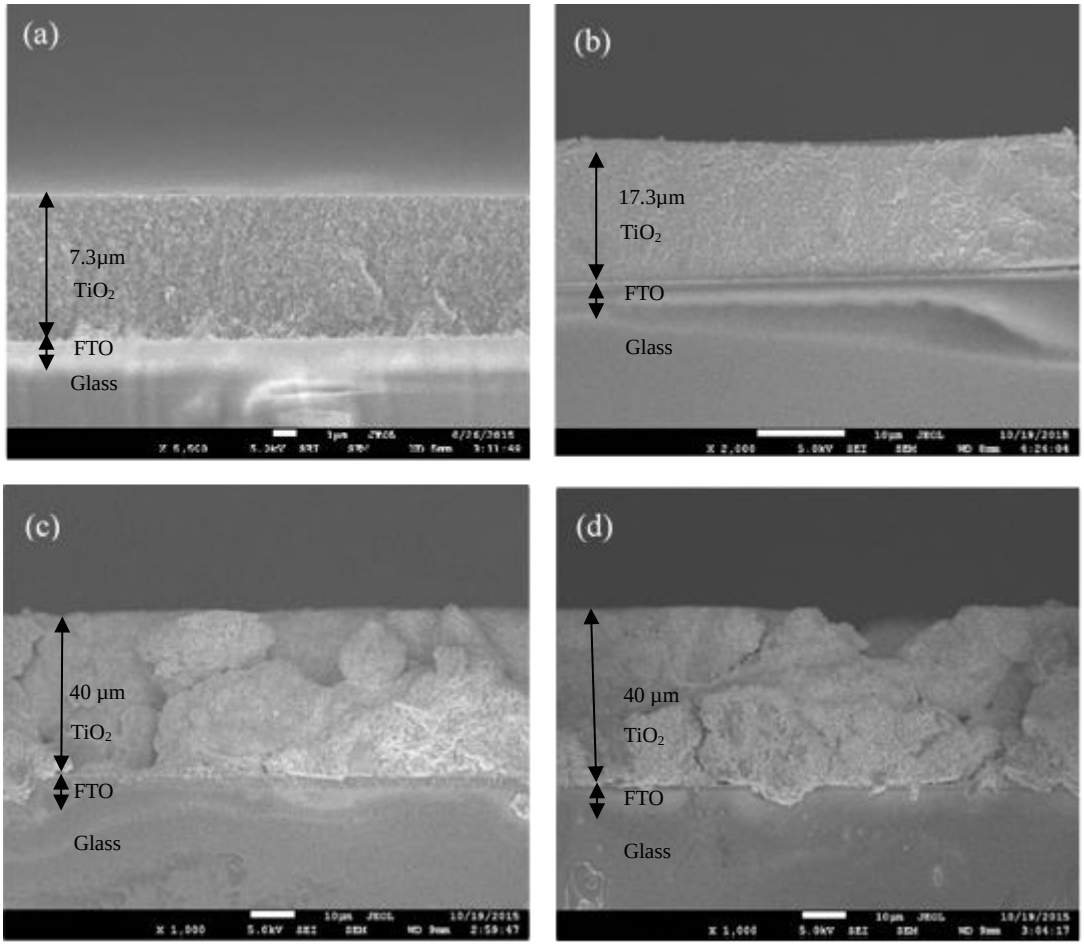

Figure 4.20. Cross-sectional SEM image of screen printed titanium oxide layer on FTO glass substrates, (a) de-ionised water based with Triton X-100, annealed at 150^oC for 30 minutes, (b)

de-ionised water based without binder, annealed at 150°C for 30 minutes, (c) tert-butanol based with Triton X-100, annealed at 150°C for 30 minutes and (d) tert-butanol based without binder, annealed at 150°C for 30 minutes.

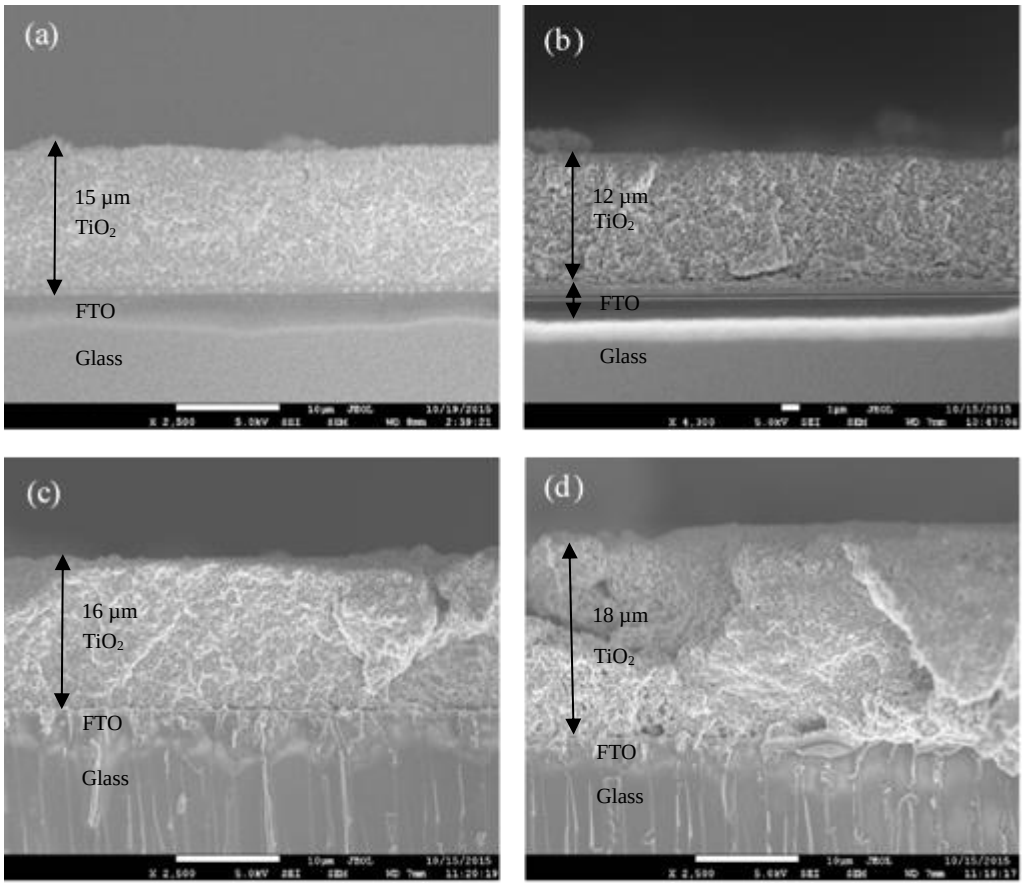

Figure 4.21. Cross-sectional SEM image of spray coated titanium oxide layer on glass substrates, (a) de-ionised water based with binder system, annealed at 150°C for 30 minutes, (b) de-ionised water based without binder system, annealed at 150°C for 30 minutes, (c) tert-butanol based with binder system, annealed at 150°C for 30 minutes and (d) tert-butanol based without binder system, annealed at 150°C for 30 minutes.

The J/V curves of DSSCs in which TiO_2 films were screen printed and annealed at 150°C and the corresponding devices were annealed at 450°C for comparison as shown in the figure 4.22 (a, b) respectively. DSSCs studied in this research work and their measurement results are summarised in Table 4.3. At 150°C, the PCE of 0.77% and 4.3% were obtained from the water solvent with and without binder systems whereas the PCE of 0.41% and 1.04% were obtained from the tert-butanol solvent with and without binder systems. In the above cases, the formulation with binder system delivered lower efficiencies when compared to without binder system. This indicates that the binder, Triton X-100 may remain in the dried TiO_2 film, acting

as the insulating layer and blocking the movement of the charges. The maximum efficiency of 4.3% obtained from the TiO_2 formulation without binder indicates the uniformity and level of TiO_2 particle interconnection as shown in Figure 4.20(b) even at the low temperature annealing. However, the PCE of 1.04% obtained from formulation with the tert-butanol as the solvent without binder system may reflect the non-uniform films as can be seen in the FESEM image in Figure 4.20(d). As a whole, the lower efficiencies obtained by tert-butanol with and without binders can be explained by the thickness of TiO_2 films over 30µm, non-uniform films and eventually reduce the PCE values.

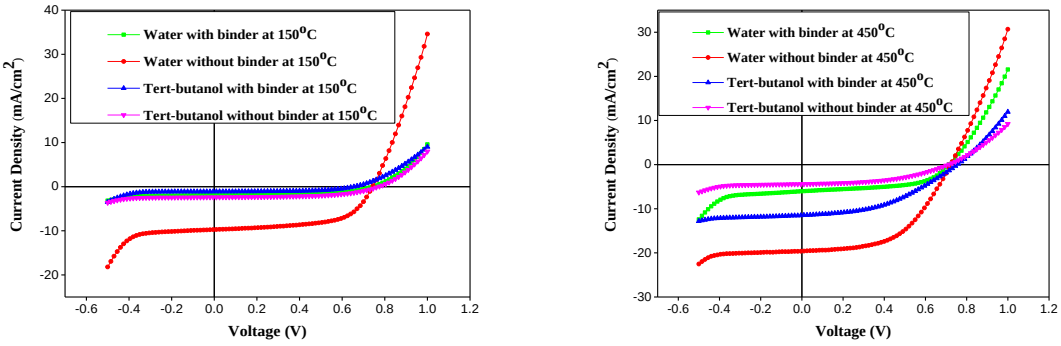

(a) (b)

Figure 4.22. J/V curves of the screen printed DSSCs processed at temperature of (a) 150°C and (b) 450°C, respectively.

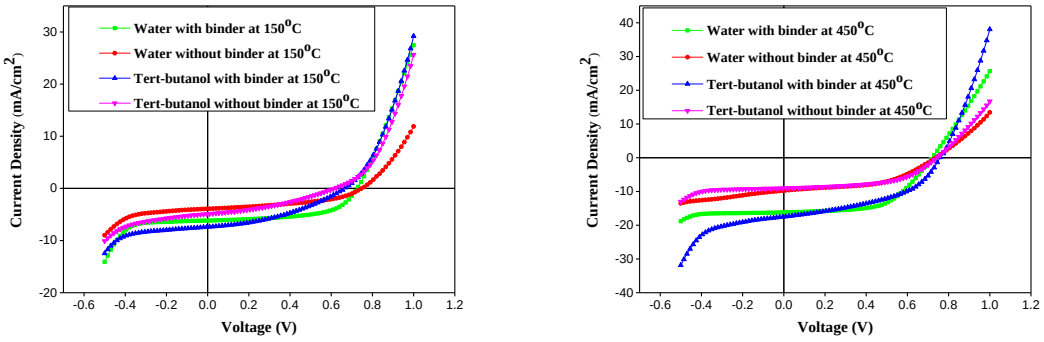

(a) (b)

Figure 4.23. J/V curves of the spray coated DSSCs processed at temperature of (a) 150°C and (b) 450°C, respectively.

The J/V curves of DSSCs in which TiO_2 films were spray coated and annealed at 150°C and the corresponding devices were annealed at 450°C for comparison as shown in the Figure

4.23(a, b) respectively. At 150°C, the PCE of 2.58% and 1.29% were obtained from the formulation with water solvent with and without binder systems whereas the PCE of 1.89% and 1.06% were obtained from the formulation with tert-butanol solvent with and without binder systems. In this case, the systems with binder delivered higher efficiencies when compared to without binder and contradict the results obtained from the screen printing technique. This could be explained by the use of the spray coating ink which has less viscosity and lower concentration of the Tinder X-100 binder than the screen printing paste formulation. Due to the lower concentration of the binder, it leads to the high porosity of the spray coated TiO_2 film resulting in more dye molecules attaching onto the TiO_2 nanoparticles hence higher the efficiency for the systems with binder Triton X-100 using water and tert-butanol solvents.

Table 4.3. The summary of open circuit voltage (V_{OC}), short circuit current density (J_{SC}), fill factor (FF) and power conversion efficiency (PCE) of the screen printed and spray coated dye sensitised solar cells on FTO coated glass substrates, in relation to the formulation binder system, solvent used and its curing temperature. (A: de-ionised water and B: Tert-butanol).

		Solvent	TiO_2 Paste	Annealing T, °C	V_{OC}, V	FF	J_{SC}, mA/cm^2	PCE, %	Area, cm^2
Screen printing	1	A	With binder	450°C	0.71	0.54	6.04	2.36±0.3%	0.31
	2		Without binder	450°C	0.72	0.54	19.63	7.41±0.1%	0.21
	3	A	With binder	150°C	0.74	0.54	1.91	0.77±0.4%	0.33
	4		Without binder	150°C	0.74	0.59	9.72	4.30±0.1%	0.21
	5	B	With binder	450°C	0.76	0.42	11.50	3.70±0.1%	0.18
	6		Without binder	450°C	0.71	0.46	4.41	1.14±0.1%	0.26
	7	B	With binder	150°C	0.65	0.57	1.09	0.41±0.05%	0.36
	8		Without binder	150°C	0.77	0.56	2.40	1.04±0.1%	0.29
Spray coating	9	A	With binder	450°C	0.71	0.57	16.18	6.65±0.15%	0.30
	10		Without binder	450°C	0.73	0.49	9.74	3.52±0.2%	0.30
	11	A	With binder	150°C	0.73	0.57	6.16	2.58±0.3%	0.28

	12		Without binder	150°C	0.74	0.44	3.92	1.29±0.3%	0.4
	13	B	With binder	450°C	0.76	0.45	17.54	6.10±0.25%	0.12
	14		Without binder	450°C	0.74	0.53	9.02	3.61±0.2%	0.42
	15	B	With binder	150°C	0.67	0.38	7.40	1.89±0.4%	0.21
	16		Without binder	150°C	0.62	0.34	4.92	1.06±0.2%	0.24

By comparing the cells performances across different processing temperature in regards to the same formulation and deposition method, the PCE obtained from the high temperature processed TiO_2 cells exhibits around double the value of the PCE obtained from the low temperature processed cells, as shown in Table 4.3. The reason for this is the binder burn off and the further nano-crystallisation of the TiO_2 film under high temperature, which benefits the dye loading and charges transporting. Based on PCE results obtained from screen printing and spray coating techniques under low temperature process, the following statements can be made. Screen printing offers the best performance devices as it needs high viscous TiO_2 paste for printing and may help to attach more dye molecules than a spray coated TiO_2 layer. The operation mechanism of the screen printing is to compress the paste between the screen and the squeegee, and then press the screen down to the substrate which helps to form the uniform and fairly condensed film but still allows the dye loading. Therefore, the screen printed cells without binder system exhibit better performance than the spray coated cells, but a lower performance than the screen printed cells with binder system. However, the spray coating benefits from the low concentration of the binder system, higher film porosity and better control over the film thickness down to sub 10 μm scale. The crystalline structure of TiO_2 thin film was shown by XRD measurement in Figure 4.24 (b). A typical peak orientation was achieved as compared with Figure 4.24(a), the peaks indicates the presence of the anatase structure of TiO_2.

(a)

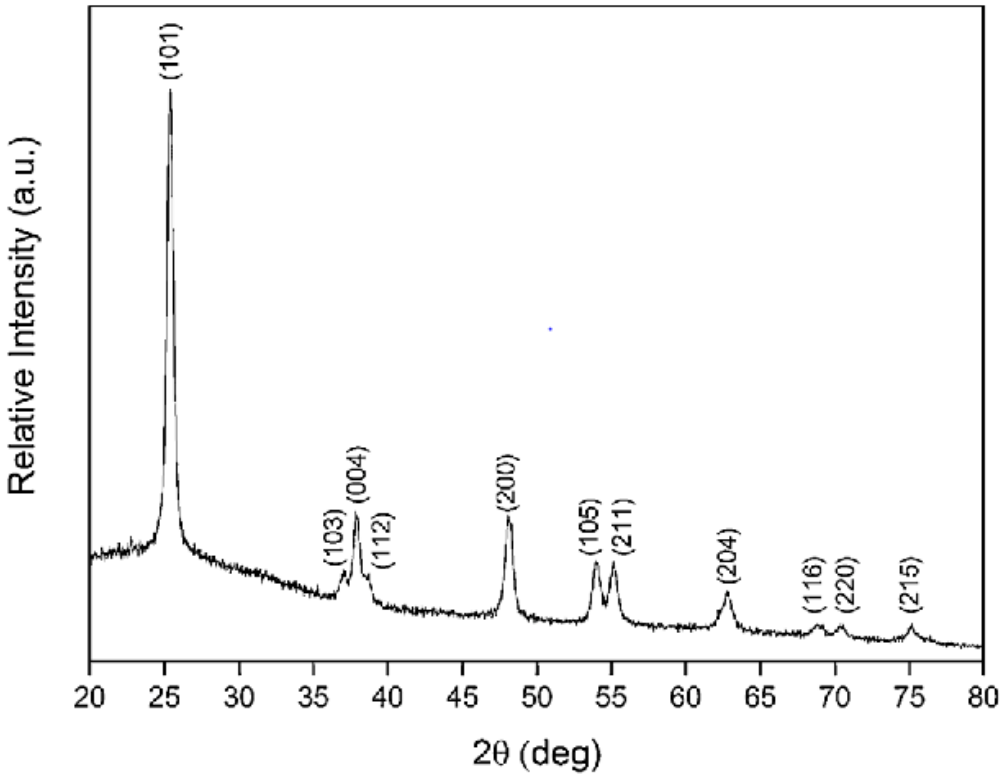

(b)

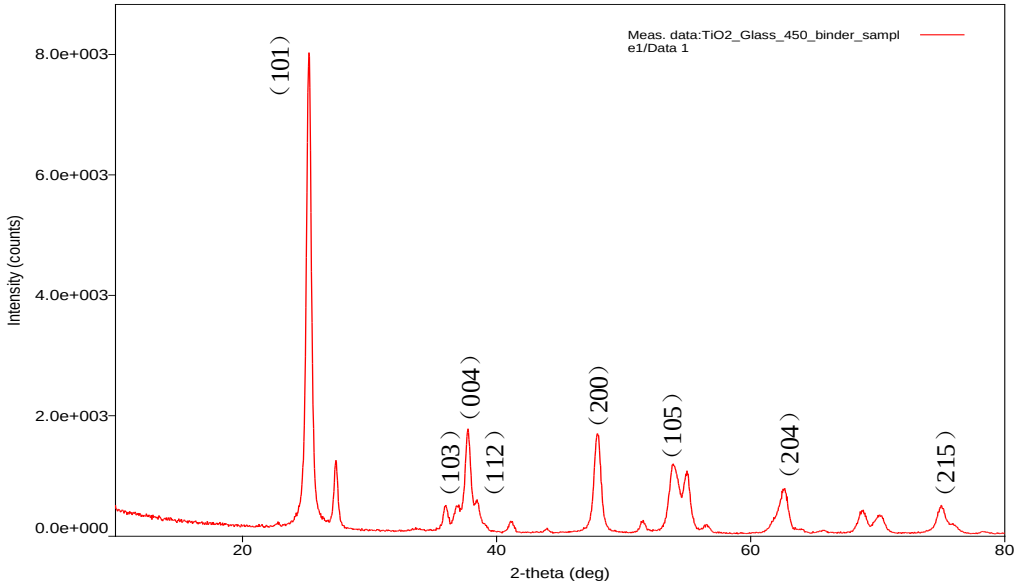

Figure 4.24. X-Ray Diffraction (XRD) pattern of the (a) literature anatase TiO_2 spectrum, and (b) TiO_2 particles under low temperature processing at 150^{o}C with organic binder have been coated onto the FTO glass.

4.6 Conclusions

In conclusion, different formulations of low temperature processed TiO_2 film are developed and investigated in this study for both screen printing and spray coating techniques. The high temperature processed DSSCs is successfully achieved with an efficient value of 7.41% based on the formulated TiO_2 paste/ink via screen printing and 6.65% via spray coating, at the same time, low temperature processed DSSCs has been achieved 4.3% via screen printing and 2.58% via spray coating. Both screen printed and spray coated DSSCs on glass substrates have demonstrated reliable results using a low temperature annealing process, which can significantly reduce the manufacturing cost in production. This optimized formulation is suitable for mass production and can provide low cost processing photo anode materials suitable for a wide range of potential flexible substrates, such as flexible plastics and wearable textiles. This formulated low temperature processed TiO_2 paste and ink is investigated to apply on Kapton and polyester cotton fabric as the intermediated stage towards the final target textile substrate. In order to achieve a textile based DSSC, the printing rheological specification on kapton and interface surface is studied in next chapter.

Chapter 5

5 Screen printed dye-sensitized solar cells (DSSCs) on woven polyester cotton fabric

5.1 Introduction

A low temperature processed TiO_2 paste was investigated and obtained in chapter 4. In this work, the first optimized fabrication method to obtain reproducible photovoltaic textiles using screen printing with low temperature materials compatible onto Kapton and the standard 65/35 polyester cotton fabric was claimed. The results demonstrate a state of the art PV efficiency of 7.03% was achieved on Kapton and 2.78% was achieved on fabric.

In this chapter, the development of DSSC on fabric was mainly investigated. The screen printing was used as the main fabrication method to fabricate the DSSC on the Kapton and woven cotton fabric substrates. The performance of different conductive film Ag and AgNW was also compared and discussed in this chapter. Design and structure.

5.2 Design and structure

The structure of the devices designed in this experiment of the DSSCs is shown in figure 5.1. There are four types of devices based on Kapton and fabric with interface substrates, using Ag and AgNW as the conductive film. The thickness of AgNW was thinner than the Ag and fabrication procedure was less complicated. Therefore, four types of devices are designed and fabricated to compare these two conductive films on kapton and fabric with interface substrates. For the kapton based devices, the conductive film silver paste and AgNW ink was directly screen printed and spray coated onto the substrate without any coatings. For the fabric based devices, an interface was firstly printed on the fabric before depositing the conductive film Ag or AgNW. The top electrodes for these four types of devices is platinum coated FTO glass

substrate, this semi-flexible structured DSSC is investigated as the intermediate stage towards the final target fully flexible DSSC device.

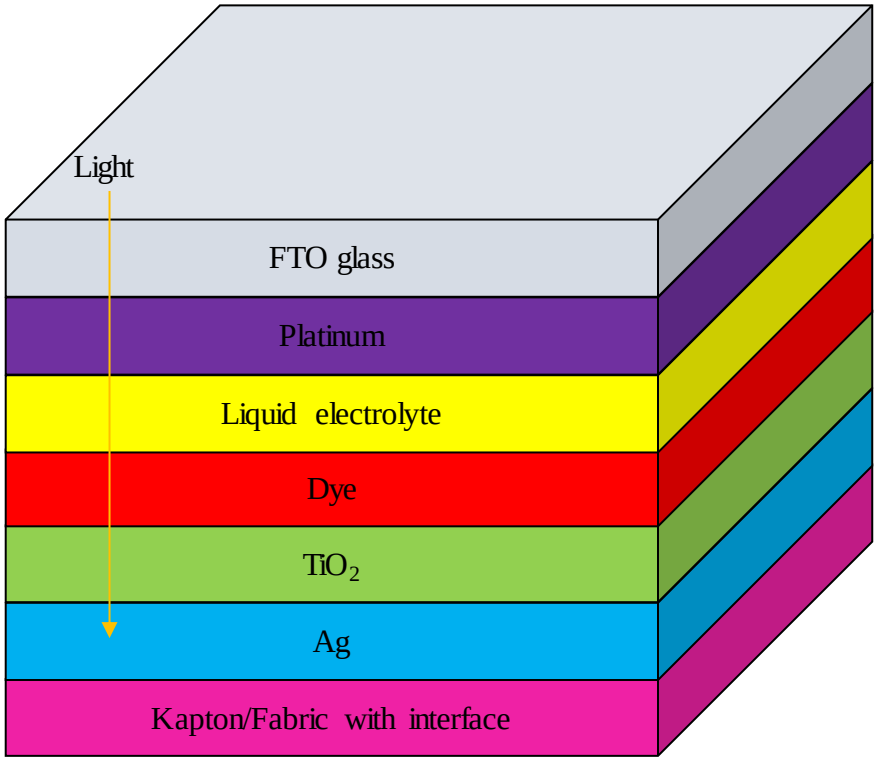

Figure 5.1. Structure of the screen printed DSSC on Kapton / fabric substrate.

5.3 Experiment

In this experiment, screen printing and spray coating are the main printing techniques to deposit the functional layer on the substrate. The spray coating depositing method remain the same in Chapter 4. A semi-automatic screen printer of TF01 DEK 248 was used in this experiment to deposit the interface, silver and TiO_2 paste on the substrate. The photograph of the screen printer is shown in figure 5.2. The screen was predesigned with the desired pattern and bought from MCI Precision Screen Ltd. The fabrication process was similar to the glass based DSSC in chapter 4. The photo anode was firstly prepared, followed by the counter electrode: the two electrodes were assembled using the clip with the liquid electrolyte in between. A semi-automatic screen printer was used to deposit the conductive film Ag and the TiO_2 paste instead of by hand printing. The pressure and speed of the squeegee, and the printing gap was set by

the computer, once the sequence was started, the substrate plate will automatically drive the substrate under the screen. The squeegee subsequently pressed the paste forward and backward on the screen returning to the original place with the pre-set printing gap, speed and number of printing deposits. A homogenous film was deposited by the semi-automatic screen printer with a sub-micrometre thickness. The key advantages of screen printing is not restricted to the only wrap and weft the directions, any pattern can be printed on the substrate based on the design of the screen. Besides these, the printing time is efficient compare to the inkjet printing and dispenser printing, which enable large area production. It can be maintained by the good flexibility and breathability, and is easy to combine into the fabric manufacturing process.

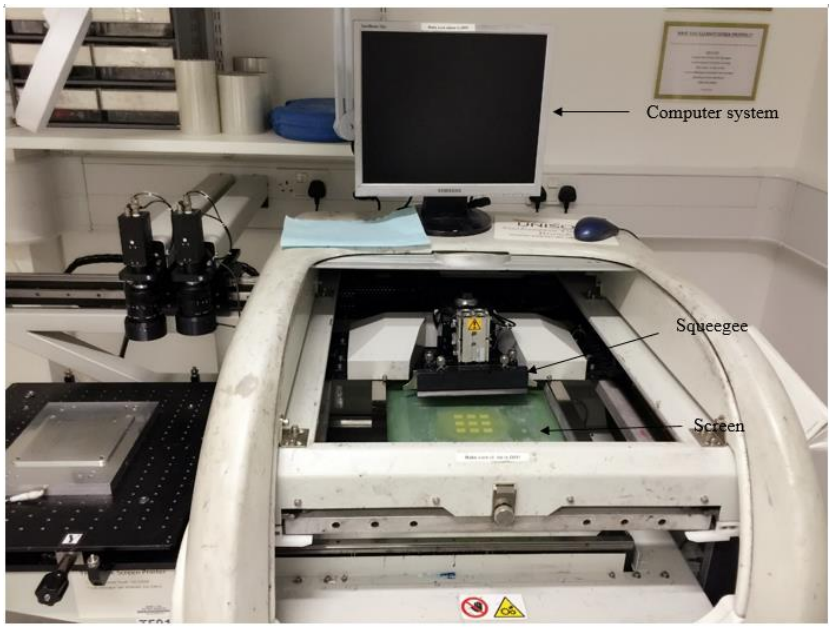

Figure 5.2. Photograph of semi-automatic screen printer DECK 248.

5.3.1 Materials

Two different flexible substrates are used in this research: a polyimide film (Kapton) supplied by Dupont and standard woven 65/35 polyester cotton fabrics was supplied by Klopmann International. The approach described in detail below uses a screen printable polyurethane based interface paste (Fabink-UV-IF1, supplied by Smart Fabric Ink Ltd.) to smooth the fabric surface. The origin of the interface paste is polymer, and developed and optimized by mixing three two types of polymer for 2 hours. It is flexible after annealing by UV light. The conductive film used in the bottom electrode is a screen printable Ag paste from Dupont 5000, and spray coating metallic AgNW suspension in isopropyl alcohol (IPA) from Nanopyxis. Titanium oxide (TiO_2, Aeroxide P25) nanoparticles used in this experiment was the same in

chapter 4. The non-ionic surfactant binder Triton X-100 and the particle stabilizer acetylacetone used in this chapter are the same in chapter 4. De-ionised water was used as the solvent for low temperature annealing of TiO_2. A FTO pre-coated glass slide, Ruthenizer N719, Platisol-T, and iodine/iodide solution (I^-/I^{3-}) are also same with chapter 4. All the above materials were used as supplied with no further modifications for functional ink formulation and fabrication. In addition, alumina tiles, supplied by Hybrid Laser Tech Ltd. are used to hold the fabric and Kapton substrate flat during processing. The self-adhesive expanded neoprene sponge strip which is used to make the chamber to hold the dye solution is from DELTA RUBBER. The spray mount glue is used to stick the substrates on the aluminium oxide tiles is purchased from 3M.

5.3.2 Fabrication process

The two types of substrates used as the photo anode are kapton and standard 65/35 polyester cotton fabric. The 65/35 woven polyester cotton fabric is the most commonly used fabric in clothing. The Kapton and 65/35 polyester cotton fabric was cut into the 12cm × 12cm square pieces, and stick on the aluminium tile using the 3D spray glue. The fabric substrate needed to be ironed before stuck onto the tile.

In order to reduce the surface roughness of the polyester cotton fabric, a polyurethane layer was pre-coated onto the fabric substrate as shown in figure 5.3. It was defined as the interface layer to provide a smooth surface for the following functional layer. A stain-steel screen is designed to print the interface covered desired surface area of the fabric. The surface energy of the interface layer was measured by a tension-meter (Kruss DSA30B) of about 35 mN m^{-1}; this value presents the interaction between the ink and the substrate. It means that it is suitable for the solvent-based electronic printing ink which have a lower surface tension normally around 30 mN m^{-1}. The interface coated fabric also have good thermal resistance which can heat up to 150 ^oC for half an hour.

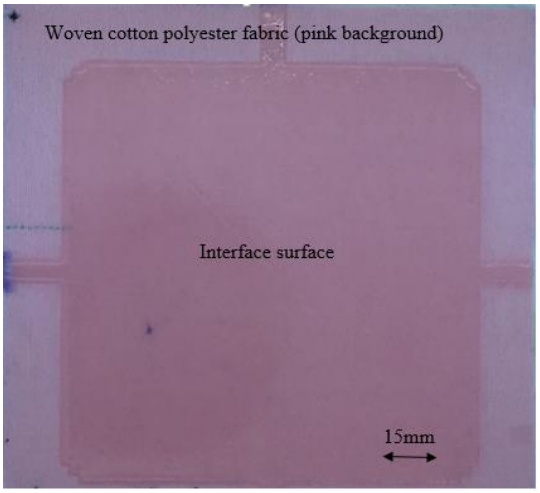

Figure 5.3. Photograph of woven cotton polyester fabric with interface.

5.3.3 Fabrication process of semi-flexible DSSCs

The fabrication process of Kapton based and the polyester cotton fabric based DSSC are similar; the difference is the polyester cotton fabric substrates need to print an interface layer to make the fabric surface smooth. Figure 5.4 -3(i)-(vii) shows all the steps of the whole fabrication process of fabric based DSSC photo anode. There are mainly three depositing stages; deposition of interface, deposition of conductive film Ag or AgNW, and deposition for TiO_2 film.

The 65/35 polyester cotton fabric was ironed before cut into small pieces; both Kapton and fabric are cut into 12cm × 12cm pieces. The fabric and Kapton were stuck onto the aluminium oxide tiles to keep the substrate flat for printing each following functional layer. The aluminium oxide tiles were wiped by acetone, and the glue was sprayed onto the tile from top to bottom twice. Then the Kapton and fabric substrates are stuck onto the aluminium oxide tiles, and left under some books for 1 or 2 days to let the glue go through the entire surface and also make the surface as flat as possible. This step is necessary since it will result in a nice screen printing layer on a smooth and flat surface. Then the substrates are ready for screen printing the functional layer.

The substrates will peel off from the aluminium tile at the testing stage; the cells are tested without the aluminium tile. The Kapton or fabric was peeled off at a small angle at the edge of the substrate, and then a small amount of acetone was applied to the gap between the substrates

and the aluminium tile. The glue was dissolved in the acetone and left for 2 minutes. Additionally, the tile was heated at 50^{o}C to minimize the damage of the functional layer.

Figure 5.4 (i) – (iii) shows the fabrication process of printing the interface on the fabric, a printable polyurethane based interface paste (Fabink-UV-IF1) was used to print the interface layer. The printer squeegee was set to pressure 5.5, and the printing gap was changed with the deposit times. The printing gap was first set to 1.6 mm for 8 times depositing, then the printing gap was changed to 1.8mm for 4 times depositing since the thickness of the interface is increased, and then the printing gap was increased to 2.0mm for 2 times depositing. The substrate was put into the UV curved cabinet for half a minute for every two deposits. The photograph of the interface layer was shown in figure 5.3. The feel and appearance of the interface did not change much from the fabric; it was still a flexible substrate.

For the purpose of comparison, there are two conductive films used in this experiment; the silver ink and the silver nanowire ink. The silver nanowire ink was sprayed onto the Kapton and fabric with interface substrate using the spray gun with 0.3 bar air pressure and 10cm spray distance, and heated at 150^{o}C for 20 minutes.

The silver paste was a commercially available product from DUPONT, and was deposited on the Kapton and fabric with interface substrate by screen printing. The squeegee pressure was set to 5.0, and the printing gap was set to 0.9 to 1.0 for 1 deposit for both Kapton and fabric substrate. The printing pressure, gap and the deposit time was decreased since a thinner silver layer at this stage to ensure a flat surface for the following functional layer. Then the substrates are annealed at 150^{o}C for 20 minutes.

The formulation of TiO_2 pastes is based on the previous experiment, but with a different percentage of each material. The water based solvent which contains organic binder Triton X-100 is used to mix the TiO_2 powder. Ethanol is added to the solvent as the surfactant to improve the surface tension between the TiO_2 film and the substrate. All the solvent are mixed and stirred first before being added to the TiO_2 powder to make the powder sufficiently mix with the solvent. The formulation of the TiO_2 paste is shown below.

Formulation of the solvent: [Water (48mL) + ethanol (12mL) + Acetyle-acetone (2mL) + Triton X-100 (1mL)].

Formulation of the TiO_2 paste: [TiO_2 powder (3g) + combined solvent (4mL)].

The solvent was prepared first and then added to the TiO_2 powder for mixing by using the automatic speed mixer at 1500 rpm for half minute. The TiO_2 paste was screen printed onto the silver or silver nanowire layer by setting the printing pressure at 5.5kg, with printing gap of 1.6mm for 1 deposit. Then the TiO_2 film was annealed at 150^oC for half an hour. The photographs of the Kapton and fabric with interface The screen mesh was pre-designed and ordered from MCI Precision Screens Ltd with mesh density of 78/cm^2, 9 piece of 1.5cm × 1.5cm small cell of TiO_2 film are printed on each alumina oxide held substrate due to the pattern of the screen. The 9 small cells are then cut into each individual cell by scissors after the staining process.

For the glass substrates DSSC, the whole substrates are directly immersed into the dye solutions, and stained overnight. In this experiment, the whole Kapton and fabric substrates cannot be immersed into the dye solution; since the substrates bend during the staining process. Therefore, the alumina oxide tiles are not peeled off at this stage because it was still used to support the Kapton and fabric substrate to keep flat, and it will peel off after staining process. A chemical resistant tape is applied to the 9 TiO_2 film square, as shown in figure 5.4 -5. The dye solutions are 100mg mixing of dye powders with 20ml ethanol and heated at 50^oC on the hot plate for 10 minutes. Then the dye solutions are poured into the tape made chamber on the substrate and kept for 2-4 hours, and washed by ethanol. The whole Kapton and fabric substrates are peeled off after staining and cut into 9 pieces following the pattern. Then the photo anode is ready for testing.

The fabrication of the top electrode was the same with the experiment in chapter 4, a FTO glass substrate was coated with platinum and heated at 450^oC for half an hour. To complete the cell, liquid electrolyte was injected between the photo anode and top electrode.

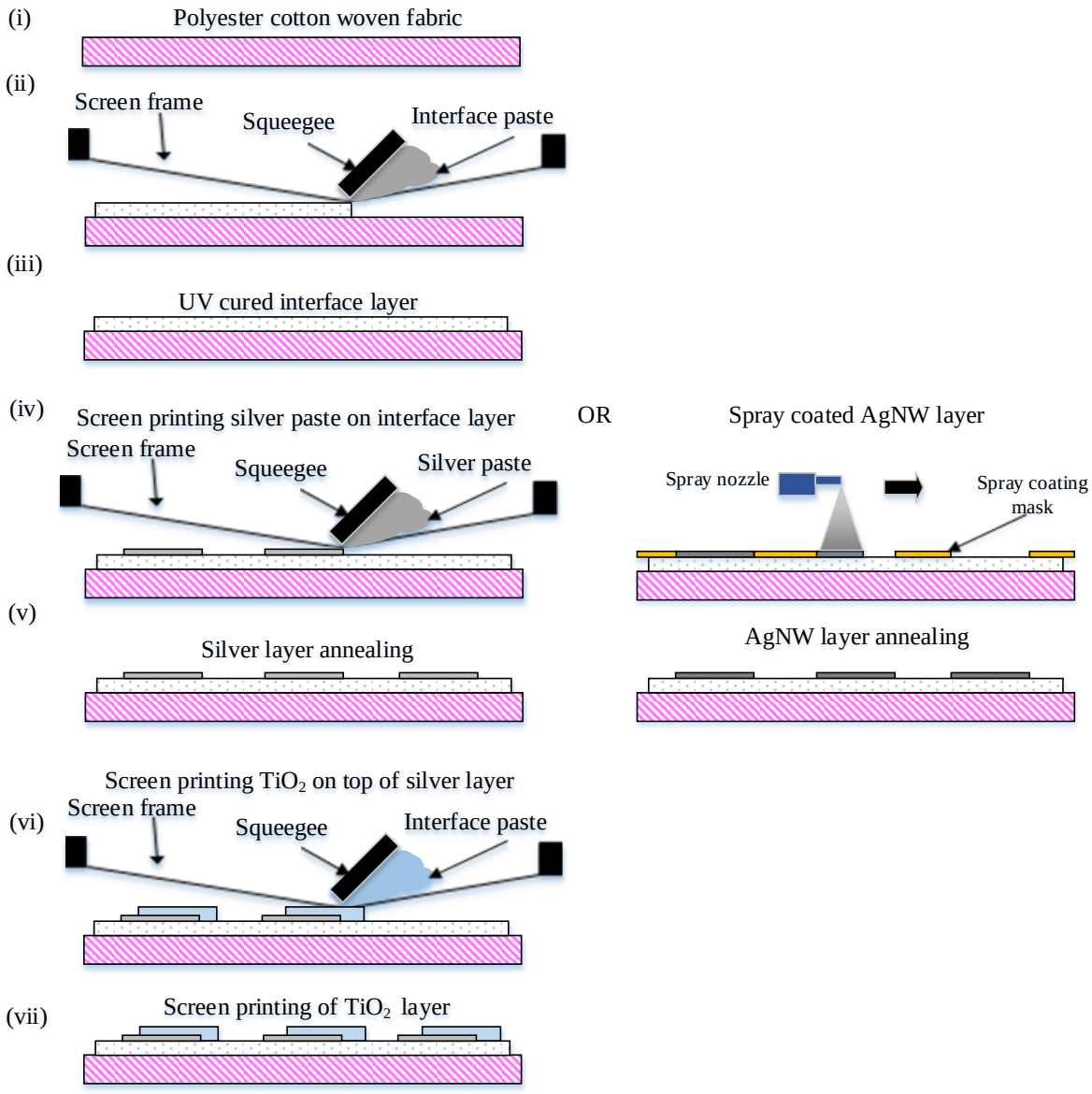

Figure 5.4. Fabrication process of fabric based DSSC using Ag and AgNW as the conductive film.

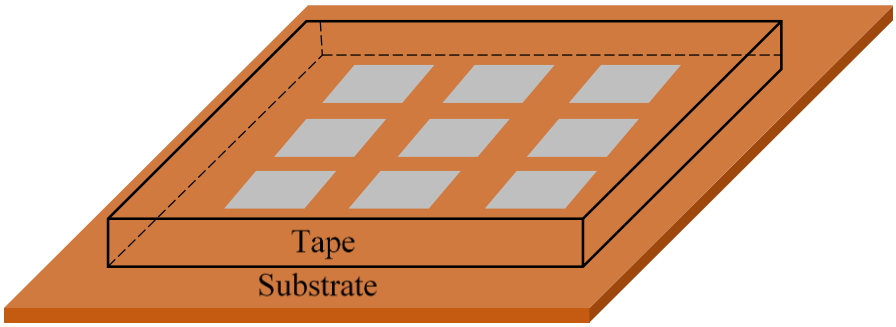

Figure 5.5. Staining process of kapton and fabric based DSSC photo anode.

5.4 Results and discussions

There are four types of DSSCs fabricated and tested in this experiment with the same TiO_2 formulation, hence four batches of results presented and discussed in the section 5.5.1-5.5.4. The fabric interface DSSC with AgNW was firstly fabricated before bringing the DSSC onto the target fabric substrate. Silver paste was changed instead of the AgNW in the second batch of the fabrication since AgNW was peeling off by the liquid electrolyte. Then the DSSC was moved onto the fabric interface substrate; both Ag and AgNW are use the conductive film for comparison. There are 9 devices fabricated from each type of DSSCs, only the best ones are present in the following section, and all the devices are tested under AM 1.5 conditions using an ABET solar simulator. The cell area is defined by using the pre-designed printing mask, and the cell area is measured by the active area of the cell.

5.4.1 Results of devices using AgNW as the conductive film

The conductive film AgNW ink was spray coated onto the Kapton and fabric interface substrate firstly to investigate a comparison with the silver paste. The thickness of the AgNW was much lower than the screen printed Ag, and the fabrication procedure was less complicated. The liquid electrolyte was added to the dye-sensitized TiO_2 film, and then the platinum coated FTO glass electrode was put on top of the TiO_2 film to complete the cell. The photograph of the AgNW based DSSC bottom electrodes were shown in figure 5.6 (a) and (b).

Table 5.1 summarises the measured and characterised results of the both spray coated AgNW based DSSCs on Kapton and the interface coated fabric substrates under the low temperature fabrication process. Both types of DSSCs were measured under the same conditions with the cell area of 0.04cm^2. Kapton based DSSCs achieve the highest PCE of 1.24 % with a V_{OC} of 0.61 V, a FF of 0.21 and a J_{SC} of 8.52 mA/cm^2. Interface coated fabric based DSSCs have a PCE of 0.48 %, with a V_{OC} of 0.60 V, a FF of 0.32 and a J_{SC} of 2.5 mA/cm^2. Figure 5.6 (c) and (d) demonstrate the J/V curve of the spray coated AgNW based DSSCs under the low temperature process on both Kapton and interface coated fabric substrates. The efficiency of this type of DSSC was much lower compare to the glass substrate devices because the AgNW started to peel off when injecting the liquid electrolyte between the two electrodes. Therefore, there was an interrupt between photo anode and cathode, which made the device short circuit. It is needed to test the device immediately after injecting the liquid electrolyte before the

AgNW was fully peeled off. To prevent this problem silver was screen printed on the interface instead of AgNW.

Table 5.1. Summary of the measured results on the Kapton and interface coated fabric based DSSCs with AgNW as the conductive bottom electrode.

Devices	Temperature	Open circuit voltage (V_{oc}), V	Fill factor (FF)	Current density (J_{sc}), mA/cm^2	Efficiency %	Cell area (cm^2)
Kapton	150^{o}C	0.61	0.21	8.52	1.24±0.05%	0.04
Fabric	150^{o}C	0.60	0.32	2.5	0.48±0.1%	0.04

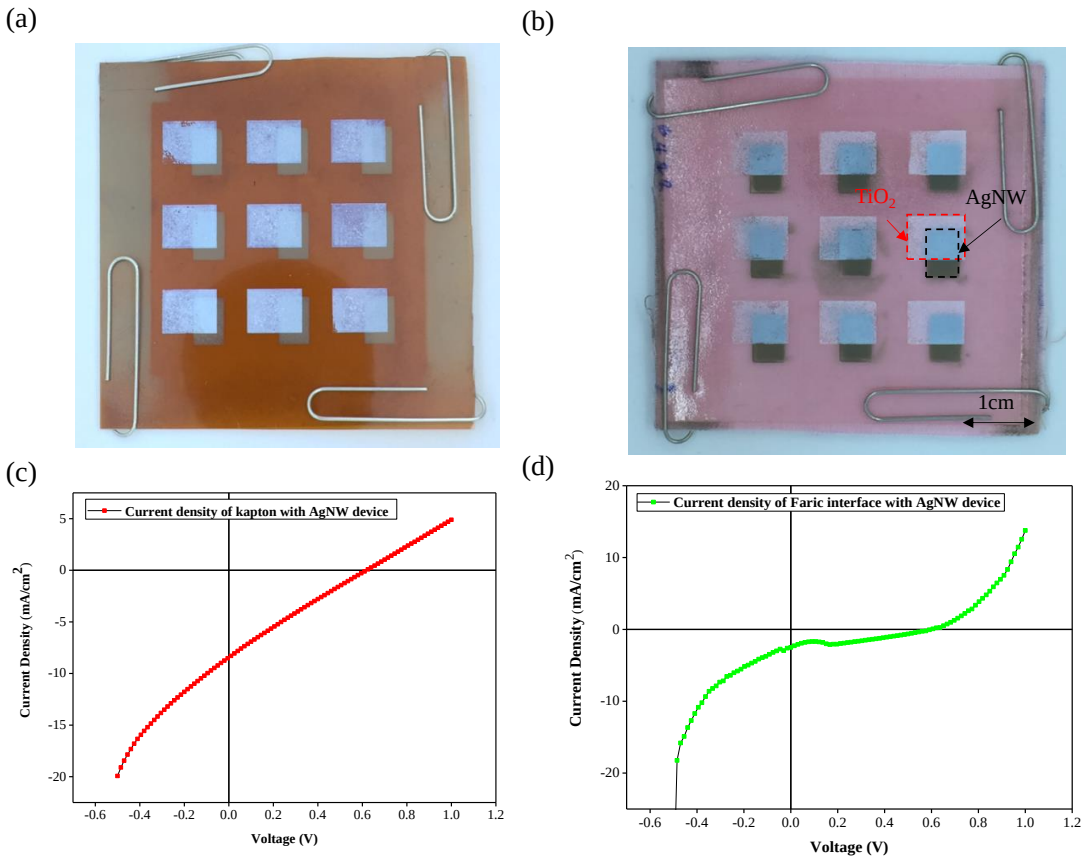

Figure 5.6. Photograph of (a) Kapton based AgNW DSSC device, (b) fabric interface based AgNW DSSC device; JV graph of (c) kapton based AgNW DSSC device, and (d) fabric interface based AgNW DSSC device.

5.4.2 Results of devices using Ag as the conductive film

Figure 5.7 (a, b) shows the top view images of the screen printed TiO_2 and silver layers on Kapton and interface coated fabric substrates. Figure 5.7 (c) shows the SEM cross sectional view of the interface coated fabrics with a smooth top layer. Figure 5.7 (d) shows the FESEM cross sectional view of the screen printed TiO_2 and silver layers on the Kapton and interface coated fabric substrates, indicating that the thickness of the screen printed TiO_2 is around 20 - 25 µm. Both FESEM images were taken before the dye loading process. Both indicate a film thicknesses above the ideal thickness of 10-12 µm [151, 152] and hence cracks are observed on the screen printed films. Moreover, the printed TiO_2 films on the fabric substrate bulged due to deformation of the interface layer after annealing and demonstrated fragility and poor uniformity. However, a good quality flat printed TiO_2 film is observable on the Kapton substrate after annealing.

Table 5.2 summarises the measured and characterised results of both screen printed DSSCs on Kapton and the interface coated fabric substrates following the low temperature process. Both types of DSSCs were measured under the same conditions with the cell area of 0.04cm^2 for Kapton and 0.02cm^2 for fabric substrates. Kapton based DSSCs achieve the highest PCE of 7.03% with a V_{OC} of 0.6V, a FF of 0.36 and a J_{SC} of 32.85 mA/cm^2. Interface coated fabric based DSSCs have a PCE of 2.78%, with a V_{OC} of 0.3V, a FF of 0.25 and a J_{SC} of 36.56 mA/cm^2. Figure 5.8 (a) shows the J/V curve of the screen printed DSSCs following the low temperature process on both Kapton and interface coated fabric substrates. It can be seen from the J/V curves that the fabric DSSC shows a linear behaviour but with a current offset. It is believed the TiO_2 layer was damaged as a result of the fabric substrate deformation caused by the annealing and dye loading stages. The dye loading in particular significantly changes the fabric interface uniformity as the entire fabric rolled up resulting in delamination and flake-off of the printed TiO_2 layer which suffers from the weak bonding forces to the substrate. Alternative approaches need to be investigated to avoid the interface coated fabric substrate deformation as a result of annealing. The transmittance spectra plot of the platinum coated FTO glass substrate is shown in Figure 5.8 (b) alongside a standard counter electrode FTO glass substrate for reference. Topside illumination is used through the platinum/FTO glass substrate. It indicates that platinum coated electrode shows high transmittance characteristics in the visible region of 450 – 750 µm.

Although silver demonstrate a higher efficiency with more stable performance, but the degradation and formation of silver halides caused by the directly contacting between liquid electrolyte and Ag when TiO_2 film is peeling off. The Ag/AgCl system require the presence of chloride in the electrolyte, and the mobility of the anions and cations in the electrolyte must be comparable in order to prevent the formation of diffusion potentials as well. Therefore, a liquid electrolyte contains chloride need to investigate to overcome this problem in the future work.

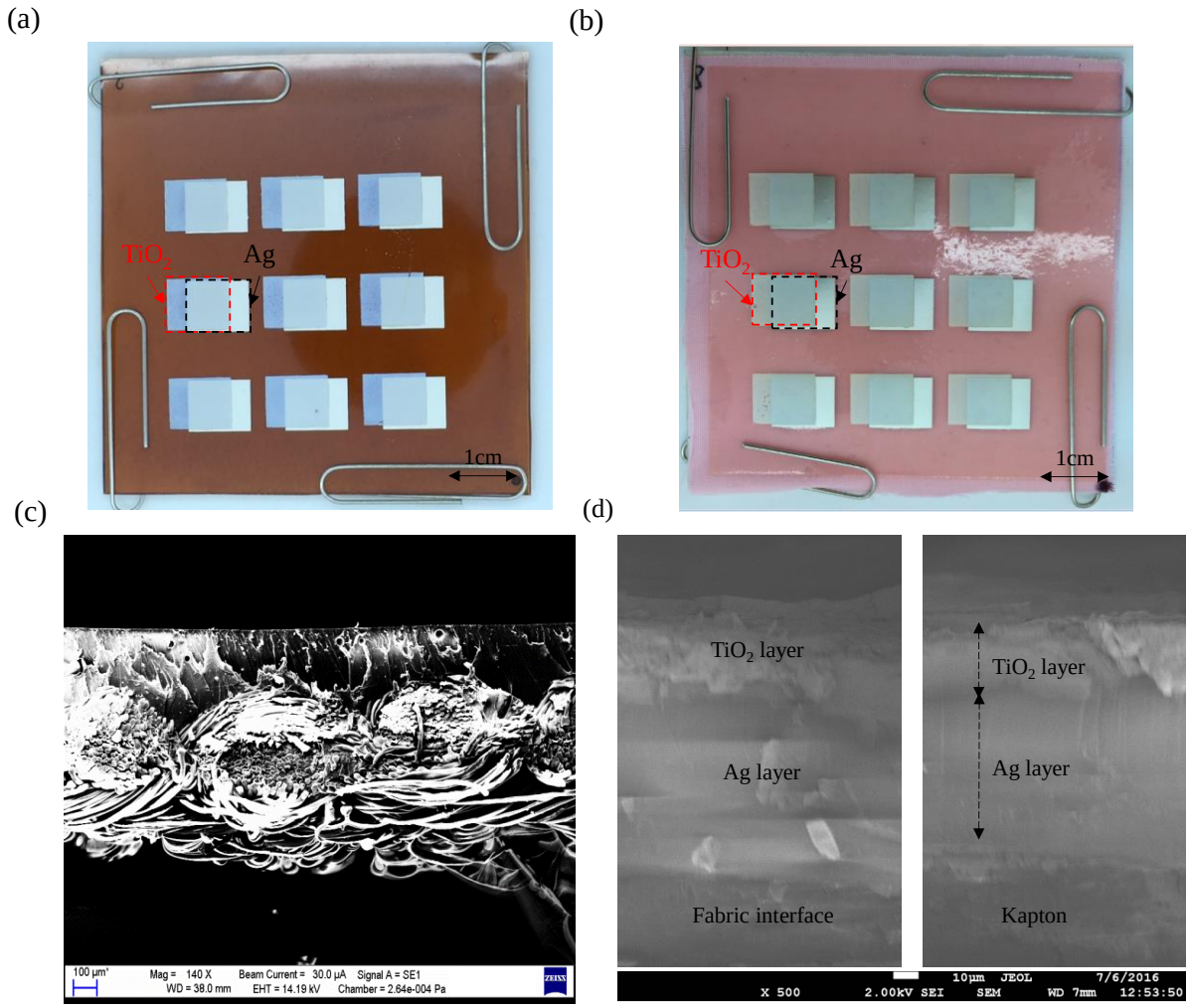

Figure 5.7. Plan view of the screen printed photo anodes on (a) Kapton and (b) interface coated fabrics, Cross sectional SEM view of (c) the standard woven 65/35 polyester cotton fabric and (d) the screen printed TiO_2 and Ag layers on Kapton (left) and interface coated fabric (right) substrates.

Table 5.2. Summary of the measured results on the Kapton and interface coated fabric based DSSCs with Ag as the conductive bottom electrode.

Devices	Open circuit voltage (V_{oc}), V	Fill factor (FF)	Current density (J_{sc}), mA/cm^2	Efficiency %	Cell area (cm^2)
Kapton	0.60	0.36	32.85	7.03±0.1%	0.04
Fabric	0.30	0.25	36.56	2.78±0.25%	0.02

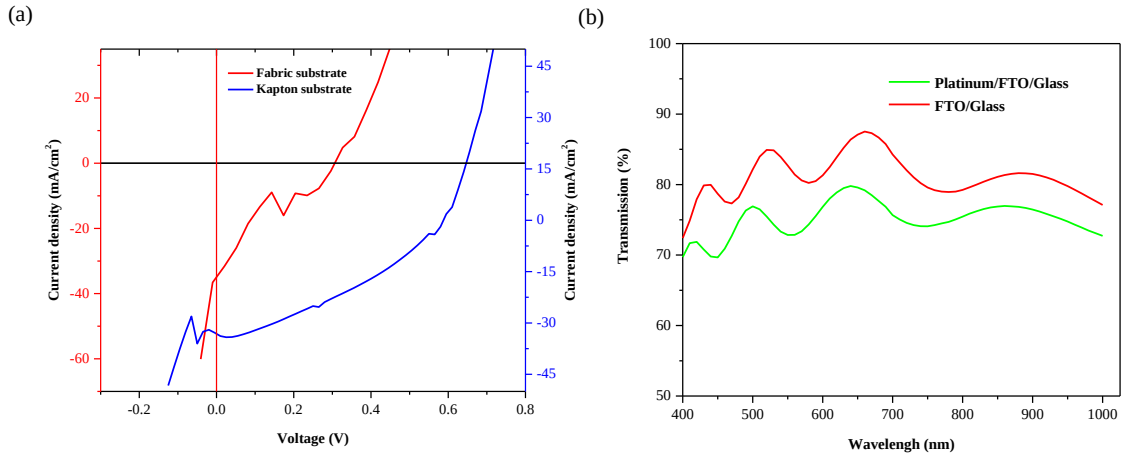

Figure 5.8. (a) J/V characteristics of the screen printed DSSCs following the low temperature process on both Kapton and fabric substrates and (b) Transmittance spectra of glass/FTO and Glass/FTO/platinum substrates.

5.5 Conclusions

There are four types of DSSC were fabricated based on the fabric and Kapton substrates with the two types of conductive layer. The highest efficiency achieved was 7.03% from Kapton based DSSC with Ag as the conductive film. This result demonstrates a successful DSSC which was fabricated onto flexible substrate using the screen printing method. The investigation of the Kapton based DSSC was towards to the fabric substrate; the maximum efficiency achieved on fabric was 0.48% with the AgNW film, and 2.78% with the Ag film. The results of fabric with Ag film was much higher than the AgNW devices on both Kapton and fabric substrate, since Ag was more stable in the liquid electrolyte compare the AgNW. The fabric DSSC could

be improved by achieving a thinner Ag layer, a different staining method, and a high viscosity TiO_2 paste in the future work.

Kapton substrate is firstly investigated as the non-conductive flexible DSSC substrate to enable the application of plastic DSSC. Since the Kapton is high temperature and non-conductive substrate which is suitable to investigate as the intermediate stage for the further research on textile substrate. Interface coated polyester cotton fabric is low temperature processed non-conductive cotton fabric substrate which is the final target substrate. The two conductive film AgNW and Ag is chosen to investigate as the conductive film which is spray and screen printable. AgNW results in a thinner thickness which make sample more flexible, but the lower efficiency and unstable morphology of the film makes it incompatible with Ag. This work indicates the possibility to achieve a fully flexible DSSC using liquid electrolyte. In next chapter, the top electrode FTO glass was replaced with a flexibile ITO/PET substrate to achieve a fully flexible DSSC.

Chapter 6

6 Screen printed DSSCs on woven polyester cotton fabric and glass fibre textile with ITO/PET as top electrode

6.1 Introduction

A fabric based DSSC using rigid glass as the top electrode was investigated and obtained in chapter 5. The purpose of this chapter is to achieve a fully flexible textile based DSSC. The rigid top electrode needs to be replaced by flexible substrate based on the results achieve in chapter 5. In this chapter, a fully flexible DSSC was demonstrated on polyester cotton fabric and glass fibre fabric substrate, using indin tin oxide coated polyethylene terephthalate (ITO/PET) substrate as the top electrode. The development of a fully flexible textile based DSSC was mainly investigated. The screen printing was used as the main fabrication method to fabricate DSSC on woven cotton fabric and glass fibre textile substrates. Cotton fabric and glass fibre fabric is using as the low temperature textile and high temperature textile to investigate DSSC fabrication on different processing temperature.

6.2 Design and structure

The DSSC device structure applied in this chapter is shown in figure 6.1. There are two types of DSSCs are designed and investigated based on polyester cotton fabric and glass fibre textile. The polyester cotton fabric was daily wearable textile which is investigated as the main target substrate via low temperature processing. Glass fibre textile was chosen as the high temperature textile to investigate the DSSC on textile via normal processing temperature. It is also investigated to compare with the low temperature processed cotton fabric textile based DSSC to enable more applications. The surface roughness is studied on these two types of textile, and the methods are investigated to reduce the surface roughness hence to improve the morphology of the functional layered material. The surface roughness is measured using the same method in Chapter 5.

The surface roughness is a main concern for textile substrate to deposit thin film layers. The glass fibre textile and polyester cotton fabric based DSSC device uses an additional coating layer to reduce the surface roughness and also to improve the breathability of the textile. The liquid polyimide is pre-coated on the glass fibre textile, and the polyurethane which is interface layer is pre-printed on the polyester cotton fabric to reduce the surface roughness of the textiles. The commercially available screen printing TiO_2 paste is deposited after the liquid polyimide layer is placed on the glass fibre textile substrate and annealed at high temperature (450^oC). The low temperature processed TiO_2 ink which is formulated in Chapter 4 is spray coated on polyester cotton fabric interface substrate. The graphite coated ITO/PET is used as top electrode instead of the rigid platinum FTO glass substrate, and the liquid electrolyte in injected between the bottom fabric electrode and top plastic electrode.

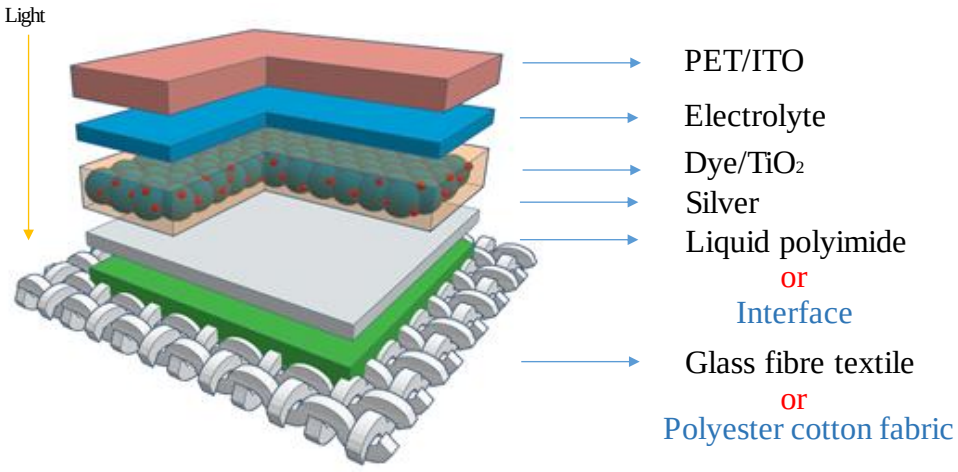

Figure 6.1. Schematic representation of the dye sensitized solar cells using PET/ITO as the top electrodes.

6.3 Experiment

6.3.1 Material

The polyurethane-based interface paste was screen printed on the woven polyester cotton (65/35) fabric used in this experiment was the same with chapter 5. The maximum temperature this fabric can withstand is 150^oC. The plain-woven composite glass fibre textile (FK144) was supplied by Valmiera Glass and this can withstand 1200^oC. This was planarised using a screen

printable liquid polyimide paste (TV-1003) purchased from Epoxy Technologies Inc. Liquid polyimides are synthetic polymers containing two acl groupd (C=O) bonded to nitrogen (N); Polyimides are commonly used as a coating due to their solvent containing formulation. It is suitable for large surface area printed instead of adhesive glue joints. The origin of polyimides is thermoplastic. Screen printed liquid polyimide is treated as the same function with the interface to reduce the surface roughness of the glass fibre textile. The surface roughness is significantly reduced by screen printed interface and polyimide layer and discussed in section 6.4. Screen printable silver paste was the same with chapter 5 used for the bottom electrode. Two types of TiO_2 material have been developed for the electron transport layer. For the glass fibre variant, the TiO_2 paste comprised a mixture of rutile and anatase, (Sigma-Aldrich 700355) with an average pore size of around 15 nm to 20 nm. For the lower temperature process using the polyester cotton, the paste formulation used in this experiment was investigated in chapter 4 contained TiO_2 powder (6 g), acetylacetone (0.2 mL), de-ionised water (4 mL) and Triton X-100 (0.1 mL). The paste was prepared in a SpeedMixer^{TM} (DAC 150.1 FV-K) for 1 minutes at a speed of 2000 rpm. The TiO_2 powder used in the low temperature paste was the same in chapter 5. This was mixed with the non-ionic surfactant binder (TritonX-100) and the particle stabilizer is acetylacetone. De-ionised water was used as the solvent for low temperature TiO_2. The ruthenizer 535-bisTBA dye sensitizer in powder form, Iodine/iodide solution (I^-/I^{3-}) liquid electrolyte and a 25μm thick thermoplastic sealant, Meltonix (42432), were supplied by Solaronix. The PET/ITO flexible film was supplied by Sigma Aldrich. A thin layer of graphite was added by rubbing the top surface of ITO with an HB pencil.

6.3.2 Substrate

There are two types of textiles investigated in this chapter. The glass fibre textile can allow the annealing temperature up to 800^{o}C, which is used as the high temperature textile to investigate the device performance at high processing temperature (450 ^{o}C). The polyester cotton fabric is used to investigate the device performance at low temperature (150 ^{o}C) processing. The liquid polyimide and polyurethane interface was pre-treated on the glass fibre textile and polyester cotton fabric textile before depositing the functional layers.

The textile is cut into 15 cm $\times$15 cm and stuck on the aluminium tiles to provide a flat and smooth surface as mentioned in Chapter 5.

6.3.3 Fabrication process of flexible DSSCs on textile substrates

For the woven polyester cotton fabric, the fabrication of the textile DSSCs starts with the screen printing of the interface layer. The purpose of the interface layer is to reduce the surface roughness of the fabric and present a smooth layer to support the subsequent screen printed functional films. The screen design ensures that the interface layer is only printed where subsequent layers are required thereby maintaining the fabric's flexibility and maximizing breathability when compared to commercially available pre-coated fabrics. The interface layer was printed 8 times and UV cured for 30s each time as previous reported [153, 154].

After printing the interface layer, the functional films are built up as a stack on top of the interface layer. The conductive silver paste was screen printed on to the interface layer forming the bottom electrode layer and was cured at 150°C for 20 minutes. The TiO_2 electron transport layer was then screen printed on top of the silver electrode. The screen printed TiO_2 layer was annealed at 150^oC in a conventional box oven for 30 minutes. The annealed TiO_2 film was then immersed into the prepared dye solution (100mg of Ruthenizer 535-bisTBA dissolved in 10 ml of ethanol) for 8 hours. The graphite coated flexible PET/ITO film was used as the top electrode. The sandwiched bottom and top electrodes were subsequently sealed using the Meltonix Sealent, which was solidified at 60°C. The sealed devices were injected with the liquid electrolyte I^-/I^{3-} through a small hole in the PET/ITO layer which was sealed afterwards. The device structure is shown schematically in figure 6.2.

To fabricate the flexible DSSC on the glass fibre textile, the liquid polyimide (Kapton) paste was screen printed on the fabric surface to obtain a smooth surface on the textile. The film was cured at 150°C for 15 minutes and 250°C for a further 20 minutes. The silver paste was screen printed on the liquid polyimide layer and annealed at 150°C for 20 minutes to form the bottom electrode. The high temperature TiO_2 paste was then screen printed onto the electrode and annealed at 450^oC for half an hour. The deposition of the dye, the liquid electrolyte, and sealing of the flexible ITO top electrode are the same as described for the polyester cotton fabric. Several batches of devices were fabricated for each textile to optimise the thickness of the functional layers to maximise PCE. After initial optimisation, 20 devices were fabricated on each of the polyester cotton and glass fibre textile and all functioned correctly.

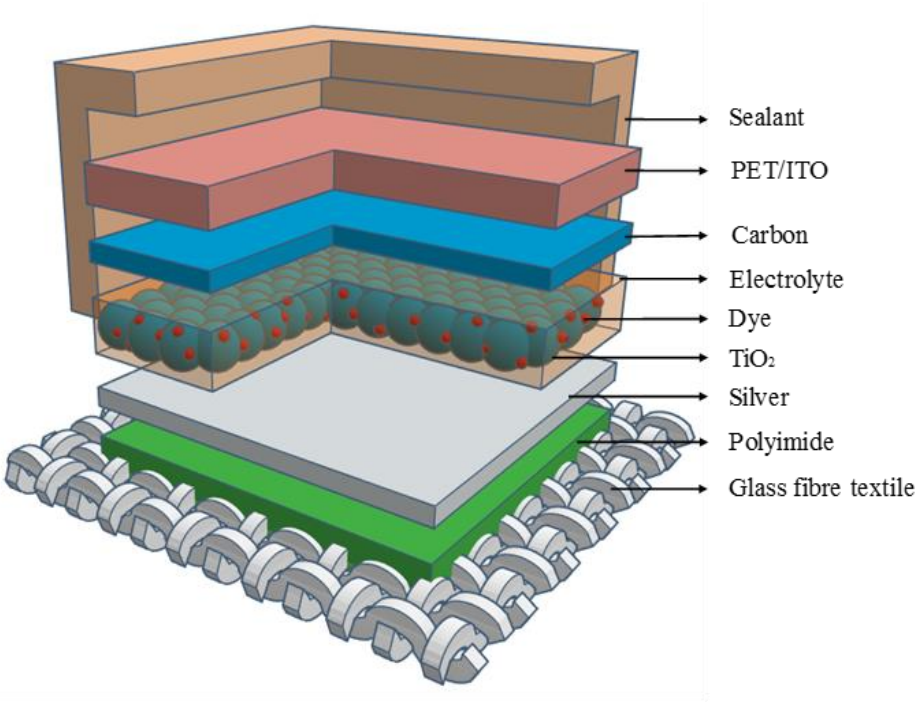

Figure 6.2. Schematic representation of the dye sensitized solar cells using PET/ITO as the top electrodes.

6.4 Results and discussion

6.4.1 Woven polyester cotton fabric devices

The surface roughness (R_a) of the polyester cotton fabric was initially 143.3 µm and this was reduced to 20 µm by the interface layer. The average surface roughness is measured by using the profilometer in cleanroom. The sample is placed on the stage plate, and pin was set to start with the fabric and cross the edge between the interface and fabric, and then move onto the fabric. The average surface roughness (R_a) was calculated based on the results chosen from the interface value.

The thickness of the interface layer was 35 µm as shown in figure 6.3(a). The R_a of the printed silver electrode was measured 3 µm with 20 µm thick layer whilst the TiO_2 film was 15 µm thick. Although the TiO_2 layer was cured at a relatively low temperature of 150^oC, the particles have formed a consistent and crack free film which is necessary for efficient electron transfer. After dye loading of the TiO_2, the flexible PET/ITO substrate was clipped to the textile photo anode to enable characterisation of the cell. A PCE value of 3.24% was observed with an open circuit voltage (V_{OC}) of 0.67, a fill factor (FF) of 0.5 and a current density (J_{SC}) of 9.6 mA/cm^2.

Figure 6.3(b) shows the J/V curves for the sealed polyester cotton fabric DSSC device being shown in figure 6.3(c). The sealed device was kept in air at room temperature for a period of 4 months and performance was measured every 4 weeks. During the first 4 weeks, the device had suffered from a slight evaporation of the liquid electrolyte, and therefore further electrolyte solution was injected into the cell. The efficiency of the cells demonstrated no change in the PCE value. The device was measured again at 8 weeks at which point the electrolyte was again topped up. The device obtained a PCE value of 3.18%, which is still comparable to the device PCE value recorded immediately after fabrication. The cell maintained the same V_{OC} and FF values but there was a slight decrease in current density of 9.4 mA/cm^2. After a further 4 weeks, it was found that the liquid electrolyte had completely dried out and the device again required injection of the liquid electrolyte. After the injection of the liquid electrolyte for the third time, it was observed that some of the dye loaded TiO_2 film around the edges had cracked and peeled off and were floating in the electrolyte. The TiO_2 film was annealed at 150°C meaning the TiO_2 particles are loosely bound together resulting in a fragile film that was being damaged by the repeated addition of the electrolyte. Because of this, the effective surface area of the device was reduced to 0.28 cm^2 as discussed in Table 6.1. The device was fabricated by using the pre-designed mask to define the cell area, and the effect cell area is determined by the cell area covered by the liquid electrolyte. The device showed PCE of 1.03% with V_{OC} of 0.66 FF of 0.28 and J_{SC} of 5.5 mA/cm^2. The PCE is lower than the previous measurements at 4 and 8 weeks' due to the deterioration in the TiO_2 film. After 16 weeks, there is no visible TiO_2 film on the textile substrates and no further photovoltaic response could be obtained which suggest the TiO_2 has slowly peeled off by the electrolyte. To explore the durability of the TiO_2 film, the results can be compared to these obtained from the DSSC on glass fibre textiles.

(a)

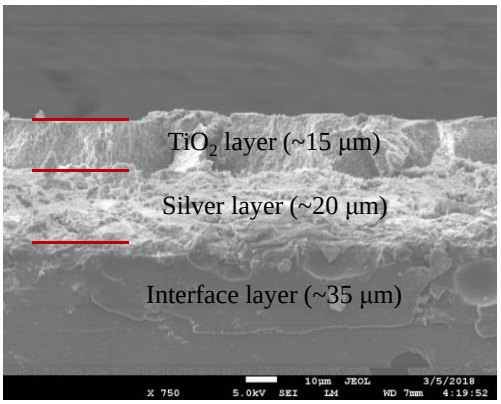

(b)

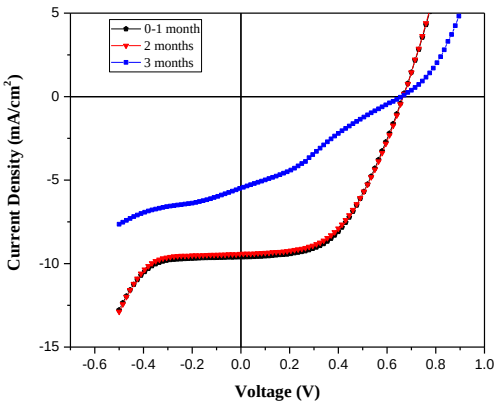

(c)

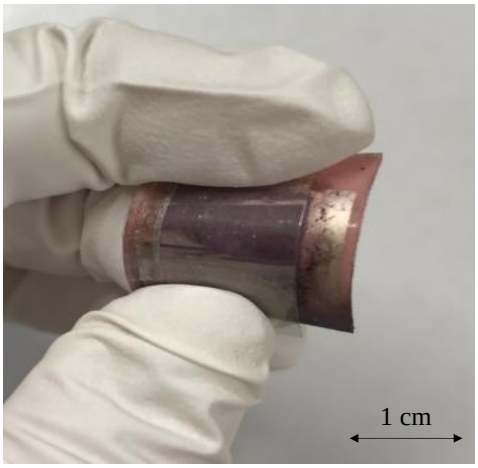

Figure 6.3 SEM image (a) of polyester cotton fabric DSSCs, (b) J/V graph of cotton fabric interface devices, photograph of (c) cotton fabric sample.

Table 6.1. Photovoltaic results of woven polyester cotton fabric DSSC device left in ambient conditions tested over 3 months.

Months	V_{oc}, V	FF	J_{sc}, mA/cm^2	PCE, %	Cell Area, cm^2
0-1	0.67	0.5	9.6	3.24 ± 0.1%	0.4
2	0.67	0.5	9.4	3.18 ± 0.2%	0.4
3	0.66	0.28	5.5	1.03 ± 0.5%	0.28

A fully flexible DSSC based was achieved on interface coated cotton fabric substrate which indicates the possibility of a daily wearable portable energy source. However, the efficiency and stability of the cell needs to be improved in the future work. A property encapsulation needs to be investigated, and the TiO_2 formulation needs to be optimized to achieve a more stable film. In order to achieve a more reliable textile based DSSC, high temperature processed TiO_2 film still needs to be fabricated to interface the surface area of TiO_2 and the

interconnection of the TiO_2 nanoparticles. Therefore, the high temperature processed textile such as glass fibre is worth to be investigated as more reliable method to enable the application on textile.

6.4.2 Woven glass fibre textile devices

The low temperature (150^oC) processed TiO_2 layer showed poor mechanical stability which reduced the long-term stability of the device. To overcome this problem and achieve a more homogenous and stable TiO_2 film on the textile substrate, the commercially available high temperature TiO_2 paste was screen printed directly on the silver coated glass fibre textile and sintered at 450^oC. The R_a of the bare glass fibre textile is 70.5µm and this can be reduced by printing a thicker silver bottom electrode. An electrode thickness of 33µm reduces the R_a to 26.1 µm, but this is still greater than the R_a of the silver electrode on the poly cotton fabric and therefore a much thicker TiO_2 layer is required to achieve a continuous film with consistent morphology. Figure 6.4(a) shows the SEM micrograph of a cross sectional DSSC on the bare glass fibre textile with a 31µm thick nanoporous TiO_2 film. The increased thickness of the TiO_2 film reduces the DSSCs efficiency to 1.2% which is less than the PCE of the poly cotton DSSCs. The increased thickness leads to charge recombination and resistance in the dye/TiO_2 layer reducing PCE. Therefore, the R_a of the glass fibre textile must be reduced further to achieve a stuiable functional layer. The approach adopted to reduce R_a and planarise the glass fibre textile surface was to screen print a polyimide interface layer. It also soaks into the glass fibre textile and bonds the glass fibre yarns together creating a more stable substrate.

Figure 6.4(b) shows the SEM micrograph of the cross section of the DSSC on the polyimide coated glass fibre textile. The photograph of the bare glass fibre textile used in the experiment and the completed sealed device is shown in figure 6.4(c) and (d) respectively. A 40 µm thick polyimide layer was screen printed onto the glass fibre textile and this was successful in reducing the surface roughness down to 10 µm. This was further reduced to 5 µm by the 20 µm thick printed conductive silver bottom electrode. This smoother surface enabled the thickness of the TiO_2 layer to be reduced to an average of 15 µm which reduced on the resistance and the charge recombination in the functional layer. The device was assembled with the top flexible PET/ITO substrate and achieved a maximum PCE of 4.04% with a V_{OC} of 0.73V, a FF of 0.54 and J_{SC} of 10.24 mA/cm^2 as shown in table 6.2. The JV graphs of the bare textile devices and the polyimide coated glass fibre devices are shown in figure 6.5. The

PCE of the textile devices improved significantly because of the smoother and flatter surface that enabled the subsequent functional layers to be deposited evenly across the device. The improved efficiency may also be due to the higher annealing temperature for the TiO_2 layer. The high temperature removes more of the binder enabling greater surface coverage of the dye and improved carrier mobility. The high temperature also improves the mechanical constancy of the film when achieving a nanocrystalline structure.

To study the stability of the devices in air, the textile DSSCs were stored in ambient condition after sealing with the top ITO/PET electrode. The PCE was measured periodically and the device demonstrated good stability with the no change in PCE after a period of 8 weeks. The J/V characteristics of the woven glass fibre textile devices are shown in figure 4 and the photovoltaic analysis is summarised in Table 6.2. After 12 weeks storage, the sealed device again suffers from the evaporation of the liquid electrolyte and dries out. After injection of the electrolyte, the device showed a lower PCE of 2.37% and 1.8% after 16 weeks. This was due to the TiO_2 functional layer cracking and peeling off during the injection of the electrolyte. This reduced the cell area from 0.5 cm^2 to 0.3cm^2. Other than this, the high temperature TiO_2 functional layer was still staying on the substrate in the electrolyte and remained intact. Future work will focus on fabricating the DSSCs with a solid electrolyte to avoid loss of the liquid electrolyte and the associated issues with the functional layer peeling off. Investigation of the packaging approach will also be undertaken to better protect the PV cells on top of the textile. A suitable encapsulate will be used that places the active layers close to mechanical stresses that arise from bending the textile.

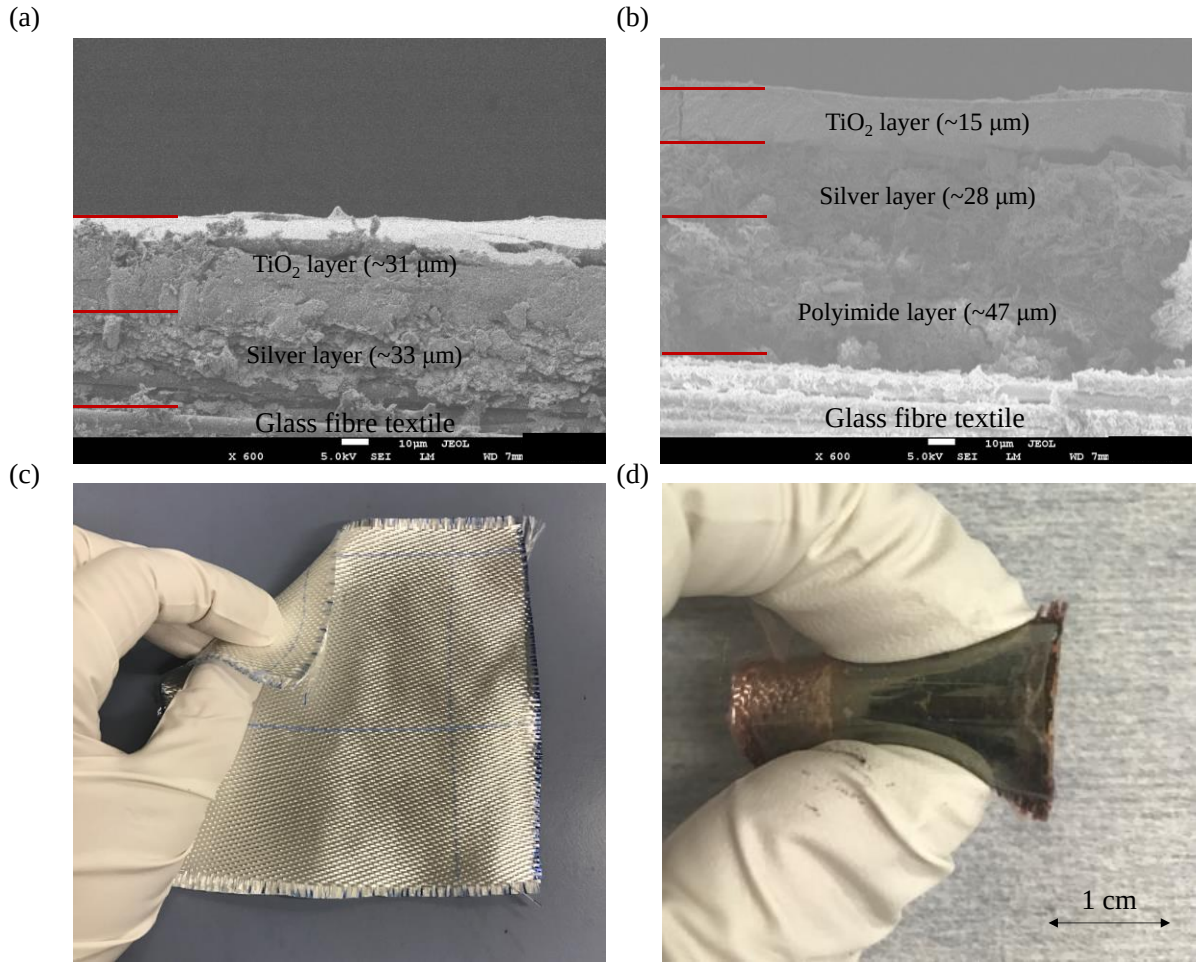

Figure 6.4. FESEM images of DSSC fabricated on (a) bare glass fibre textile, (b) liquid polyimide coated glass fibre textile, photograph of (c) glass fibre textile sample and (d) glass textile devices using PET/ITO top electrode.

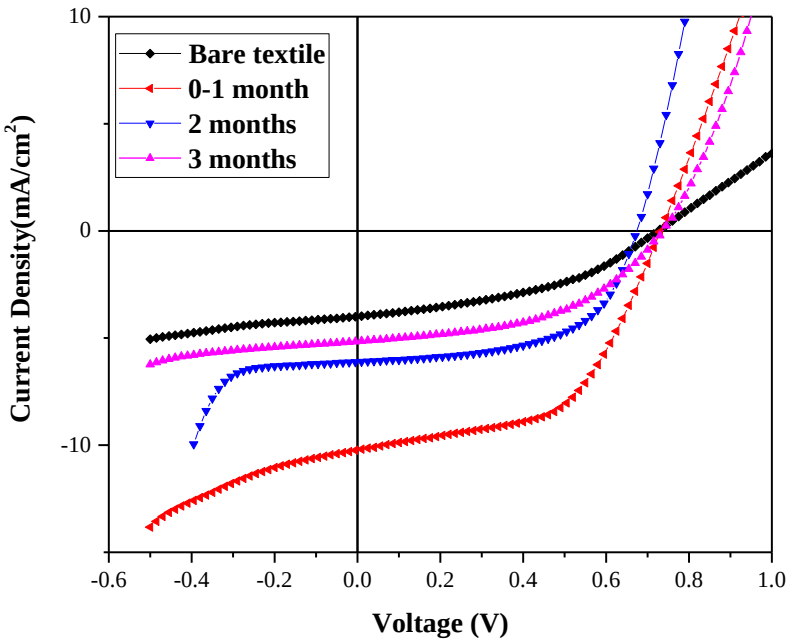

Figure 6.5. J/V curves of bare and polyimide coated glass fibre textile DSSCs.

Table 6.2. Photovoltaic results of glass fibre fabric DSSC device stored in ambient air conditions tested over 4 months.

Glass fibre textile	Months	V_{oc}, V	FF	J_{sc}, mA/cm^2	PCE, %	Cell Area, cm^2
Bare textile	0	0.73	0.41	4.0	1.2 ± 0.32%	0.5
Polyimide coated textile	0,1,2	0.73	0.54	10.24	4.04 ± 0.12%	0.5
	3	0.67	0.57	6.12	2.37 ± 0.31%	0.3

	4	0.73	0.48	5.16	1.8 ± 0.32%	0.3

6.5 Conlusions

The processing temperature of 150 ^{o}C associated with standard fabrics such as polyester cotton requires a low-temperature TiO_2 functional layer. Whiles this was found to function initially, the film is not durable and peeling off in the electrolyte. This can be solved by high temperature TiO_2 layer but this requires the use of high temperature glass fibre textiles and is not suitable for standard fabrics. This work has demonstrated promising PCEs from the textile cells but further work is required to package devices and improve their robustness as well as undergoing the use of solid-state electrolytes for use on standard fabrics. In next chapter, the characterization of the ssDSSC was investigated on the glass substrate before fabrication the device on the textile.

This page intentionally left blank

Chapter 7

7 Investigation of solid-state dye-sensitized solar cell (ssDSSCs) on glass substrate

7.1 Introduction

The ssDSSC is not only overcome the volatile liquid electrolyte evaporation and leakage, but also enables the solar cell device to be fabricated on the flexible substrates such as fabric since the HTMs can be easily packaged and more reliable compared to the liquid electrolyte. 2,2',7,7'-tetrakis(N,N-di-*p*-methoxyphenylamine)-9,9'-spirobifluorene(spiro-OMeTAD) is one of the most promising solid-state electrolyte with a relevant high efficiency and was therefore used in this experiment. It is solution based which is easy to deposit by spray coating and spin coating.

In this chapter, the ssDSSC was first fabricated on the glass substrates, like the standard devices, which will be later replaced with a fabric substrate. Spiro-OMeTAD was used as the HTM with lithium salts as the additives, and the PEDOT:PSS [poly (3, 4-ethylenedioxythiophene): poly (styrenesulfonate)] with AgNW layer were used as the top electrode instead of the platinum coated FTO glass substrate[155]. This device was fabricated as the reference device with a high temperature (450 ^{o}C) processing, and the maximum efficiency achieved was 2.83% by spray coating method, which is investigated toward the final target of printing on the fabric substrate. In order to achieve a fully flexible ssDSSC on a single textile substrate, the conductive film Ag is investigated to replace conductive film FTO on glass substrate. In this experiment, the conductive film Ag is deposited on the plain glass substrate by screen printing and spray coating.

7.2 Design and structure

There are three types of devices that are designed and fabricated on the FTO glass and glass substrates. The schematic diagram of the device structure designed in this experiment is shown in figure 7.1. The device was processed at a high temperature of 450^{o}C, and the device was first fabricated on the FTO glass substrate for investigating the characteristics of the ssDSSCs. The structure of FTO based ssDSSC is shown in figure 7.1 (a). It was subsequently moved onto plain glass substrate with Ag as the conductive film, as shown in figure 7.1 (b), and will finally move onto the fabric substrate in the next stage. The structure was similar to the fully flexible liquid electrolyte based DSSCs in chapter 6, the difference was ITO/PET was replaced with AgNW coated PEDOT:PSS layer and liquid electrolyte was replaced with solid-state electrolyte. Both PEDOT:PSS and AgNW are solution based inks which can be deposited by spray coating[135]. The spiro-OMeTAD was used as the HTMs in this device, and lithium salt was added to the sprio-OMeTAD as the additives to improve the conductivity of the spiro-OMeTAD. The staining process was exactly the same as the conventional DSSC with liquid electrolyte, and the TiO_2 layer was fabricated using screen printing method as introduced in chapter 5.

The bottom electrode of the ssDSSC was similar to the conventional DSSC except for the additional TiO_2 compact layer between the FTO and the HTMs. For the ssDSSC, a TiO_2 compact layer is fabricated to avoid the short circuit of the device and the losses of the current in the charge recombination between the HTMS and the FTO[155]. It creates a blocking layer between the HTMs and the FTO. Since the solid-state electrolyte (spiro-OMeTAD) was used instead of the iodine-iodide redox couple[75], a significant difference exists between the FTO electrode and the electrolyte[155]. In the conventional DSSC devices, the liquid electrolyte was strong enough to generate the barrier at its surface to prevent the recombination of charges generated by the photons[155]. In the ssDSSC devices, HTMs and FTO creates an ohmic contact, the electrons will recombine at the FTO interface with the holes in the HTMs which will make the cell inefficient. Therefore, an additional TiO_2 compact is necessary to achieve a good performance of the ssDSSC device. The best thickness of compact layer reported so far was around 100nm, a thicker layer will result in a low fill factor since the series resistance was increased. On the other hand, a thicker layer will also result in the difficulties of the transportation of the electrons to reach the FTO electrode.

The spiro-OMeTAD was one of the most efficient solid-state electrolyte, it was a p-type organic HTM. The work function of the spiro-OMeTAD was around 5.2eV, and the hole mobility of the spiro-OMeTAD was 1×10^{-4} cm^2/Vs. Lithium salt was a common additives used to improve the conductivity of the spiro-OMeTAD. The hole mobility of spiro-OMeTAD can be increased to 1×10^{-3} cm^2/Vs by adding the lithium salt into the spiro-OMeTAD.

The most important function of the PEDOT:PSS layer is to create the ohmic contact between the spiro-OMeTAD and the AgNW. The work function of the AgNW was around 4.5eV, the spiro-OMeTAD was about 5.2 eV, while the PEDOT:PSS was 5.0eV, which gives a better energetic match with the spiro-OMeTAD. The other role of the PEDOT:PSS layer is to reduce the series resistance so that to improve the lateral charge transport between each of the nanowires. The role of AgNW in the device is facilitating the charges, and also make the contact to the external load. The other important issue of using AgNW is it is semi-transparent material and can be spray printable, the transmittance diagram is shown in Figure 7.6 (b).

The FTO glass substrate was used as the bottom electrode in this device; the TiO_2 compact layer was deposited on top of the FTO by spray pyrolysis method and heated at high temperature of 450°C. The TiO_2 ink was applied onto the glass substrate on top of the TiO_2 compact layer by spray coating and then annealing at 450°C. Then the substrates was dip coated in the dye solutions for several hours. The solid electrolyte was deposit on the dye-sensitized TiO_2 film by drop casting. The PEDOT:PSS and AgNW was deposited by spray coating method.

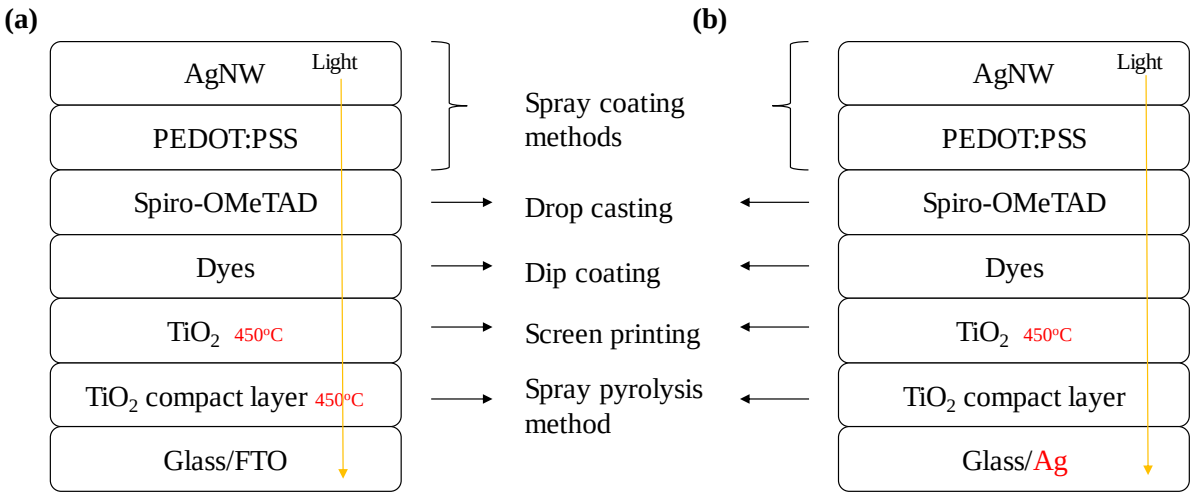

Figure 7.1. Schematic of (a) conventional ssDSSC, (b) ssDDSSC with Ag as the conductive film.

7.3 Experiment

7.3.1 Materials

The TCO glass substrates, P25 TiO_2 powder, Ruthenizer N719, ethanol, used in this experiment was the same with previous chapters. Titanium diisopropoxide bis (acetylacetonate 75%) was purchased from SIGMA-ALDRICH, it was used to fabricate the TiO_2 compact layer. The structure of the Titanium diisopropoxide bis (acetylacetonate) is shown in figure 7.2. Bis(trifluoromethane)sulfonimide lithium salt was used as the additives in spiro-OMeTAD, which is purchased from SIGMA-ALDRICH. Acetonitrile was used as the solvent to mix with the lithium salt was purchased from SIGMA-ALDRICH. Cholorobenzene and tert-butylpyridine was used as the solvent to mix with the spriro-OMeTAD which was also bought from SIGMA-ALDRICH.

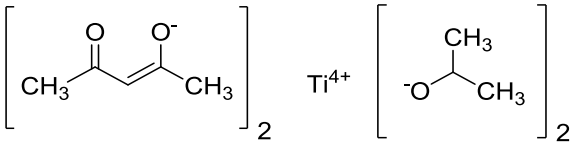

Figure 7.2. Structure of the Titanium diisopropoxide bis (acetylacetonate).

7.3.2 Substrates

There are two types of glass substrates used to investigate the characterization of the ssDSSC devices. The FTO glass substrates were cut into small pieces 1.5cm 1.5 cm x 1.5 cm/piece by the scriber machine in the cleanroom, and then washed in acetone and cleaned using a wipe. The non-coated glass substrates were cut into the same size with the FTO glass substrates and used to investigate the performance of the conductive layer by different deposition methods. The conductive silver paste and silver ink was deposited on the glass substrates by screen printing and spray coating respectively, then annealing at 150 ^oC before depositing the following functional layers.

7.3.3 Fabrication process

The fabrication procedure of standard ssDSSC was different from liquid electrolyte based DSSC. The addition layer TiO_2 compact layer was deposited on the FTO glass substrate, screen

printed silver glass substrate, and spray coated silver glass substrate by spray pyrolysis method as shown in figure 7.3. The TiO_2 compact layer was deposited by the spray coating of titanium diisopropoxide bis (acetylacetonate 75%) diluted 10 times onto the FTO glass substrates, and then heated at the hot plate for drying. The pressure of the spray coating was set to 2.5 bar, the spray time is 1 second per deposition which is the shortest deposition time for hand spray coating. The spray time is controlled by digital time, the spray distance is 10 cm (based on the investigation in Chapter 4) from the spray nozzle to the substrate. The spray deposition time with different TiO_2 compact layer thickness is summarized in Table 7.1. Subsequently, the TiO_2 compact were annealing at 450^{o}C for half an hour in the box oven. The spray times was chosen to achieve non-conductive TiO_2 compact layer with lower thickness.

The TiO_2 porous layer was deposited by spray coating with same formulation as stated in Chapter 4 using water as the solvent with an organic binder. The formulation of the spray coating TiO_2 ink was [TiO_2 powder (6g)] + [Acetylacetone (0.2mL) + water (2mL)] + [Triton X-100 (0.1mL)] + [water (10ml)]. The TiO_2 ink was put into a glass spray vial, spray coated onto the glass substrate and heated at 450^{o}C for half an hour.

The staining process was the same with previous glass substrate devices as stated in chapter 4. The glass substrates were dipped into the dye solution overnight for staining. The dye powders were mixed with ethanol and poured into a petridish glass, and the glass substrates were immersed into the dye solution for staining. The substrates were washed by ethanol after staining.

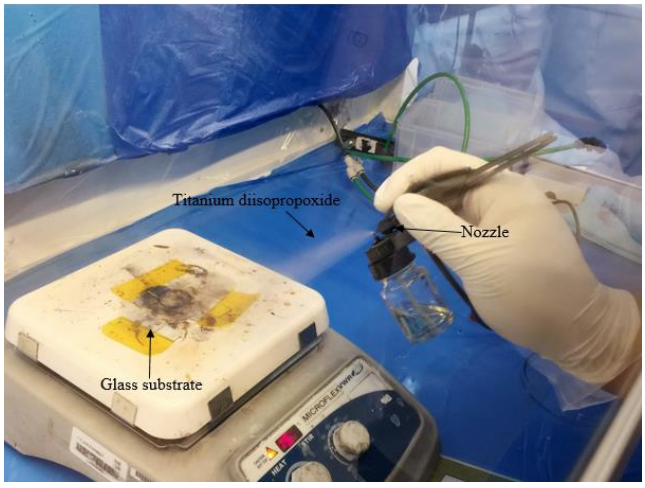

Figure 7.3. Fabrication process of TiO_2 compact layer.

Table 7.1. Summarization of the spray times optimization.

Number of sprays	Spray times (s)	TiO_2 compact thickness	Conductivity
5	1	100 pm	Conductive
10	1	300 pm	Non-conductive
15	1	600 pm	Non-conductive
20	1	1 µm	Non-conductive

The spiro-OMeTAD solution was used as solid electrolyte in this experiment. The spiro-OMeTAD contains spiro-OMeTAD, lithium salt solution, chlorobenzene and tert-butylpyridine. The lithium salt solution was pre-solved in the acetonitrile, 0.6 molar was needed to added into the spiro-solution [130]. Since milli-moles/molar = millilitres, and milligrams/molecular weight = milli-moles, so 172mg of lithium salt is added into 1ml of acetonitrile in the glove box (the molecular weight of lithium salt was 287.09g/mole). The formulation of spiro-OMeTAD was

[Spiro-OMeTAD (625mg)] + [Chlorobenzene (1.2ml)] + [Tert-butylpridine (25µl)] + [Lithium salt solution: lithium salt (172mg) + acetonitrile (1ml)][156, 157].

The fabrication process of spiro-OMeTAD needs to be in the glove box since most of the solvents are not stable in the air. The spiro-OMeTAD was deposited on top of the TiO_2 film by drop casting and was left for 12 hours for oxidation.

The top electrode consisted of the PEDOT:PSS layer with AgNW on top. The PEDOT:PSS layer and AgNW layer was deposited by spray coating. PEDOT:PSS solvent was poured into a glass vial and spraying onto the TiO_2 film and left for 10 hours. The AgNW ink was sprayed onto the PEDOT:PSS layer subsequently and left under the room temperature.

7.4 Results and discussions

7.4.1 Results of FTO glass ssDSSC

Figure 7.4(a) shows XRD results for the TiO_2 CL compared with FTO reference glass substrates. For XRD, the films were illuminated at a constant incidence angle of 0.2° with a wavelength of 1.54 Å (Cu Anode) and incident energy of 40 keV. The XRD patterns of FTO/glass with the CL TiO_2 layer, shows a strong diffraction peak of TiO_2 at 25.5°, which is

due to the lower thickness of TiO_2 layer. The CL TiO_2 sharp peak is attributed to the existence of a crystalline surface compared to the FTO reference glass substrates. The similar XRD pattern for the CL TiO_2 and FTO was reported by Charbonneau et al. [158] The crystalline properties of the TiO_2 CL was further confirmed by observing the morphology of the CL film in an Atomic Force Microscope (AFM) as shown in Figure 7.4(b). The surface of the film shows a granular domain interface with an RMS surface roughness value of 131 nm. The CL is well densified with the small crystals formed as desired each estimated to be a few tens of nanometres in length. Moreover, the 1×1 μm region scanned in the AFM appears to be free of pinholes despite its low thickness.

To measure the thickness of each functional layer, a cross-sectional image of the ssDSSC was obtained using a SEM as shown in figure 7.5 (a). The CL TiO_2 is not clearly visible as it is only 100-200 nm thick. A 7 μm thick layer of TiO_2 paste was screen printed directly onto the CL, which was previously identified as the ideal thickness [29]. As can be seen in figure 7.5 (a), PEDOT: PSS and AgNW were spray coated with a thickness of 100 nm. The photograph of the ssDSSC device is shown figure 7.5 (b). Table 7.2 summarises the measured and characterised results of the both FTO glass based and textile based devices. Figure 7.6 (a) shows the J/V curve for the FTO glass based device. The device demonstrated an efficiency of 2.8% with an open circuit voltage (V_{OC}) of 0.44 V, fill factor (FF) of 0.34 and current density (J_{SC}) of 18.5 mA/cm^2. The J/V curve shows a decrease in series resistance (current going through the device) that suggests there is no barrier to the charge transport between the optimized functional layers. The transmittance spectra plot of PEDOT: PSS/AgNW/glass substrate is shown in Figure 7.6 (b) alongside a standard FTO electrode on a glass substrate for reference. Transmission measurement results is achieved mainly by two steps, collecting a baseline by measuring the reference standard light source without the sample and measuring with sample. Deviation between these measurements define the spectral transmission characteristics of the sample. For transmission measurements procedure, a detector and reference light source is to emit the entire desired wavelength range of the sample under test. For all translucent material, a part of the light will be reflected, apart absorbed and a part transmitted. The characteristics of the sample define the deviation between these three variables at different wavelengths. The total amount of light emitted by a light source directed towards the sample equals the sum of absorption, transmission, and reflection of the sample. Topside illumination is used through the PEDOT: PSS/AgNW layers and therefore, it should be as

transparent as possible. It indicates that the PEDOT: PSS/AgNW coated electrode shows high transmittance characteristics of 70-80% in the visible region of 450-850 nm.

The testing procedure of the ssDSSCs are the same with the previous devise, all the samples are tested under the AM 1.5 condition. This type of device was fabricated as the reference device under the high temperature processing (450 ^{o}C). An efficiency of 2.83% was achieved from this type of ssDSSC with PEDOT:PSS as the top electrode. Some other methods will be investigated to fabricate the TiO_2 compact layer in the next stage.

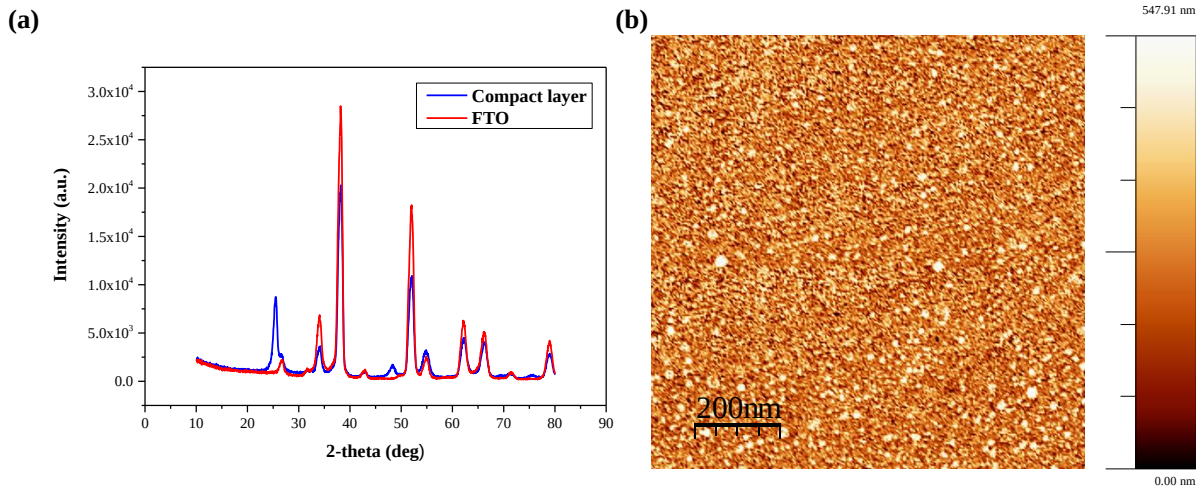

Figure 7.4. (a) XRD spectra of the CL TiO_2 film prepared by spray pyrolysis on FTO glass substrates. (b) AFM graph for TiO_2 compact layer (CL) on FTO glass substrates.

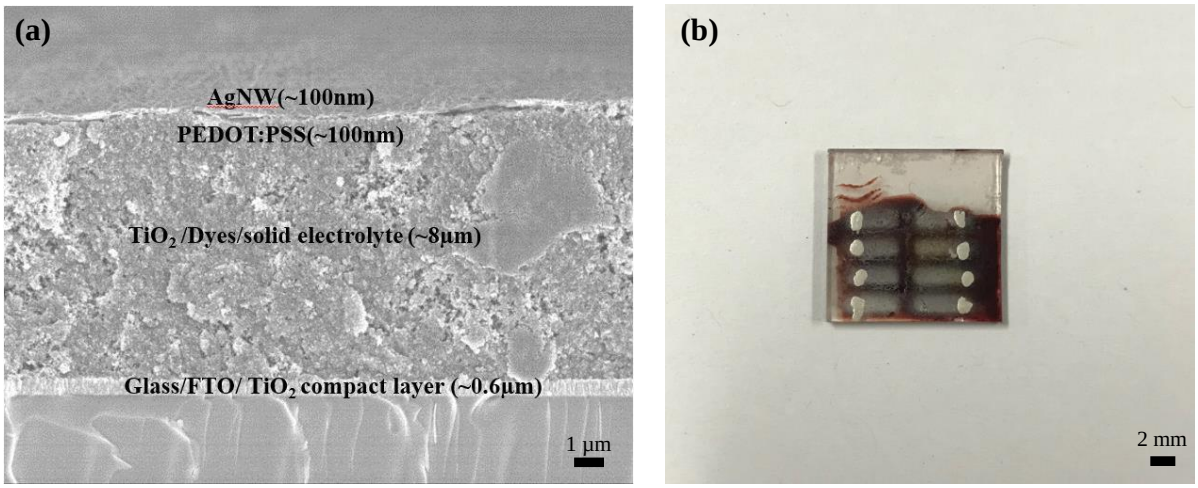

Figure 7.5. (a) FESEM for the cross sectional solid-state DSSC device on FTO glass substrates, (b) photograph of the solid-state DSSC device.

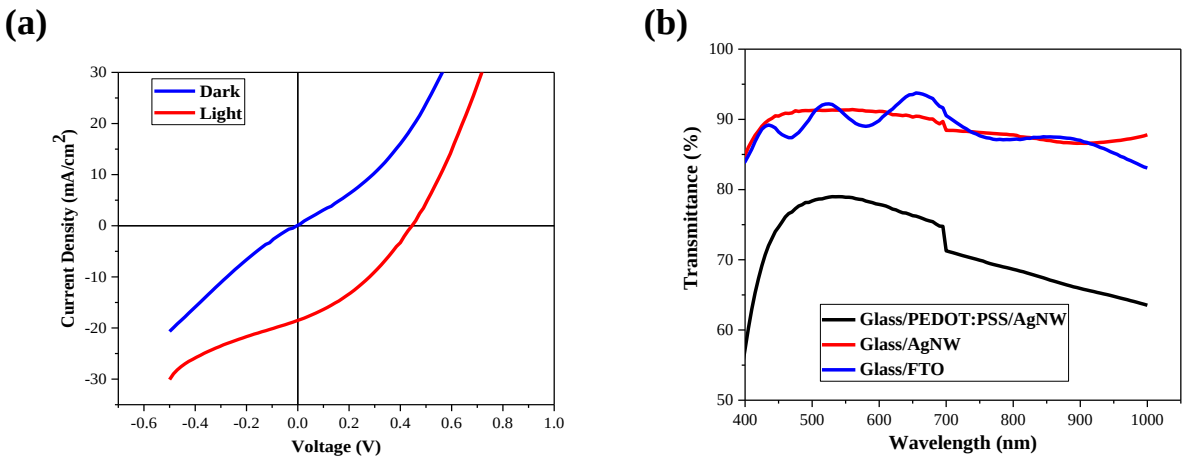

Figure 7.6. (a) J/V graph for the FTO glass substrates, and (b) transmission graph for the AgNW and PEDOT:PSS/AgNW glass substrates.

Table 7.2. Results of FTO ssDSSCs standard devices.

Devices	Temperature	Open circuit voltage (V_{oc}), V	Fill factor (FF)	Current density (J_{sc}), mA/cm^2	Efficiency %	Cell Area, mm^2
Device 1	450^{o}C	0.44	0.34	18.59	2.83±0.2%	3

7.4.2 Results of screen printed silver glass based ssDSSC

The screen-printed silver glass substrates were investigated as the intermediate stage towards the final textile substrate. A maximum PCE of 0.94 % was achieved by screen printed silver devices with an open circuit voltage of 0.54, fill factor of 0.46, and current density of 3.83 mA/cm^2 as summarized in table 7.3. The silver paste used in this device is Dupont 5000, and JV graph is shown in figure 7.7. These results indicate the possibility of textile based ssDSSC device. However, the silver shows unstable in after heating at 450^{o}C for 30 minutes. It may be oxidized after heating, the conductive film may investigate in the future work.

Table 7.3. Results of screen printed silver glass devices.

Devices	Temperature	Open circuit voltage (V_{oc}), V	Fill factor (FF)	Current density (J_{sc}), mA/cm^2	Efficiency %	Cell Area, mm^2

Device 1	450°C	0.54	0.46	3.83	0.94±0.1%	3

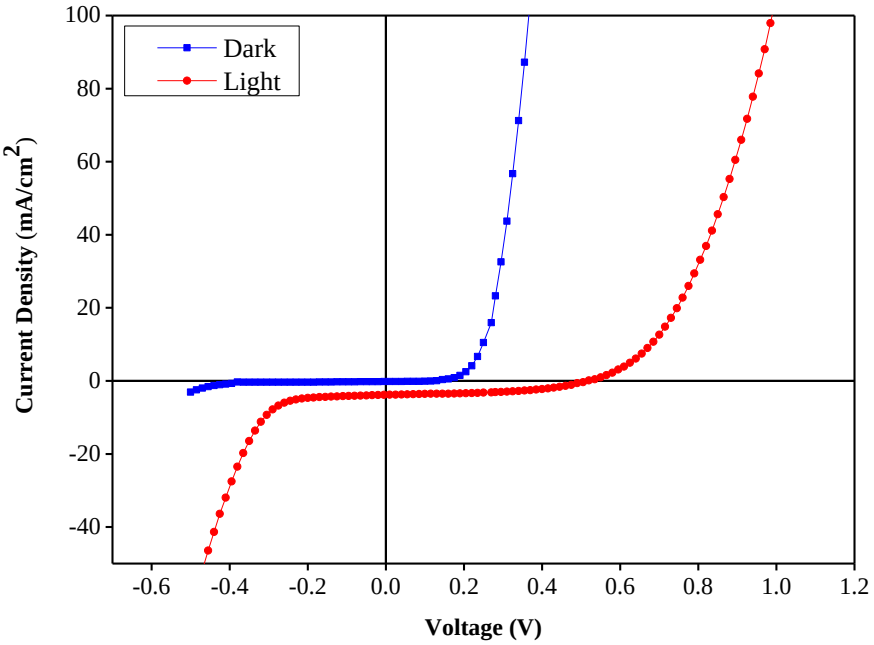

Figure 7.7. J/V graph of the screen printed silver glass substrates.

7.4.3 Results of spray coated silver glass based ssDSSC

The spray coated silver glass substrate is used to compare with the screen printed silver glass devices. The silver ink was used in this type of device, and a maximum PCE of 1.14 % was achieved by screen printed silver devices with an open circuit voltage of 0.54, fill factor of 0.49, and current density of 4.33 mA/cm^2 as summarized in table 7.4. The JV graph of spray coated silver glass device was shown in figure 7.8.

The PCE value of screen printed silver glass device is slightly lower than the spray coated silver glass substrates, this is because the viscosity of screen printed silver paste is higher than the spray coated silver ink, therefore the silver paste has more organic binders than spray coating silver ink. Once annealing at high temperature 450 °C, the organic binder in silver paste is not fully evaporated and reacts with the TiO_2 compact layer.

Table 7.4. Results of spray coated silver glass devices.

Devices	Temperature	Open circuit voltage (V_{oc}), V	Fill factor (FF)	Current density (J_{sc}), mA/cm^2	Efficiency %	Cell Area, mm^2
Device 1	450^{o}C	0.54	0.49	4.33	1.14±0.3%	3

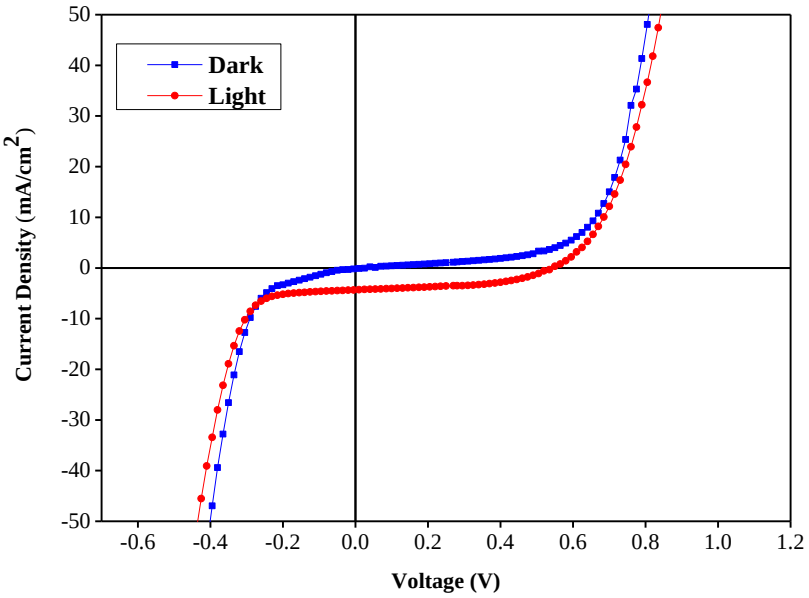

Figure 7.8. J/V graph of the spray coated silver glass substrates.

7.5 Conclusions

The device was fabricated and investigated based on the ssDSSC structure, the top electrode was replaced with the PEDOT:PSS layer with AgNW. An efficiency of 2.8% was achieved from this type of device which indicates that the top electrode of PEDOT:PSS layer can be used in the ssDSSCs. The conductive film FTO is replaced with Ag, the screen printed Ag and spray coated Ag is compared in this experiment with an efficiency of 0.94 % and 1.14 % respectively. The efficiency of spray coated and screen-printed silver based ssDSSC is incompatible with FTO glass substrate. The main reason is the organic binder inside the Ag paste and ink is reacted with the following layer. The conductive film needs to be optimized in

the future work. Therefore, the conductive film FTO is replaced with Ag, and the glass substrate will be replaced with fabric to achieve a fully flexible textile based ssDSSC in next stage.

This page intentionally left blank

Chapter 8

8 Investigation of printed ssDSSCs on glass fibre textile

8.1 Introduction

This chapter presents an investigation into the fabrication of solid-state dye sensitized solar cells directly on fabric substrates. The constraints of the fabric substrate mean that the existing processes and technologies cannot be simply applied directly onto the textile. Printing techniques are an established processing technique for realising e-textiles[159] and enable the functional film to be applied directly on the textile in the desired pattern. The ink formulations of the functional materials can be adjusted to meet the requirements of the different printing techniques and the specification of the application. The solution based processes presented in this work are all compatible with roll to roll processing for large area manufacturing.

To achieve a flexible and stable DSSC on textile, this chapter presents details of an investigation into the fabrication of a two-dimensional solid-state dye sensitized solar cell (ssDSSC) fabricated on different woven high temperature glass fibre textile substrates. Textile ssDSSCs were firstly printed on the glass fibre substrates with commercial conductive coatings, and subsequently onto the uncoated glass fibre substrates and on glass fibre textiles planarised using a liquid polyimide film. High temperature processed glass fibre textile is mainly investigated in this chapter is because high temperature processing of DSSC is particular creating a higher surface area of TiO_2 and increased inter-particle contact based on the study of previous chapters. Therefore, in this chapter all materials used can withstand the required 450 ^{o}C processing temperature and the performance in each case is compared with the reference structure fabricated on the glass substrate in Chapter 7.

8.2 Device design and structure

There are three types of textile based ssDSSC device structure is designed based on the glass substrate devices in chapter 7. The textile based ssDSSC is a flexible 2D planar structure that

is a variation of the version fabricated on the glass substrate as shown in figure 8.1 and figure 8.2. All functional layers on both FTO glass and textiles are same compare to chapter 7, except for the bottom electrode, which are the FTO on glass and a thick film silver layer on the textile substrates. The device was first designed on the commercial available aluminium laminated glass fibre textile substrates as shown in figure 8.1(a) to evaluate the characterization of textile structured ssDSSC, and subsequent moving onto the general non-coated glass fibre textile substrate as shown in figure 8.1(b), however, the commercial aluminium laminated layer was peeling off from the glass fibre substrate after 450 ^{o}C annealing, and the surface roughness was too high to achieve a homogenous functional film of the non-coated glass fibre textile. Therefore, liquid polyimide was deposited on the glass substrate to reduce the surface roughness improve the breathability, and chemical resistance of the glass fibre substrate. The structure of the polyimide coated glass fibre substrate device is shown in figure 8.2. The following functional layer was exactly the same with the glass substrate device in chapter 7. The screen printed Ag was used as the conductive film as the spray coated silver ink has a lower viscosity which is not suitable to deposit on the textile substrate.

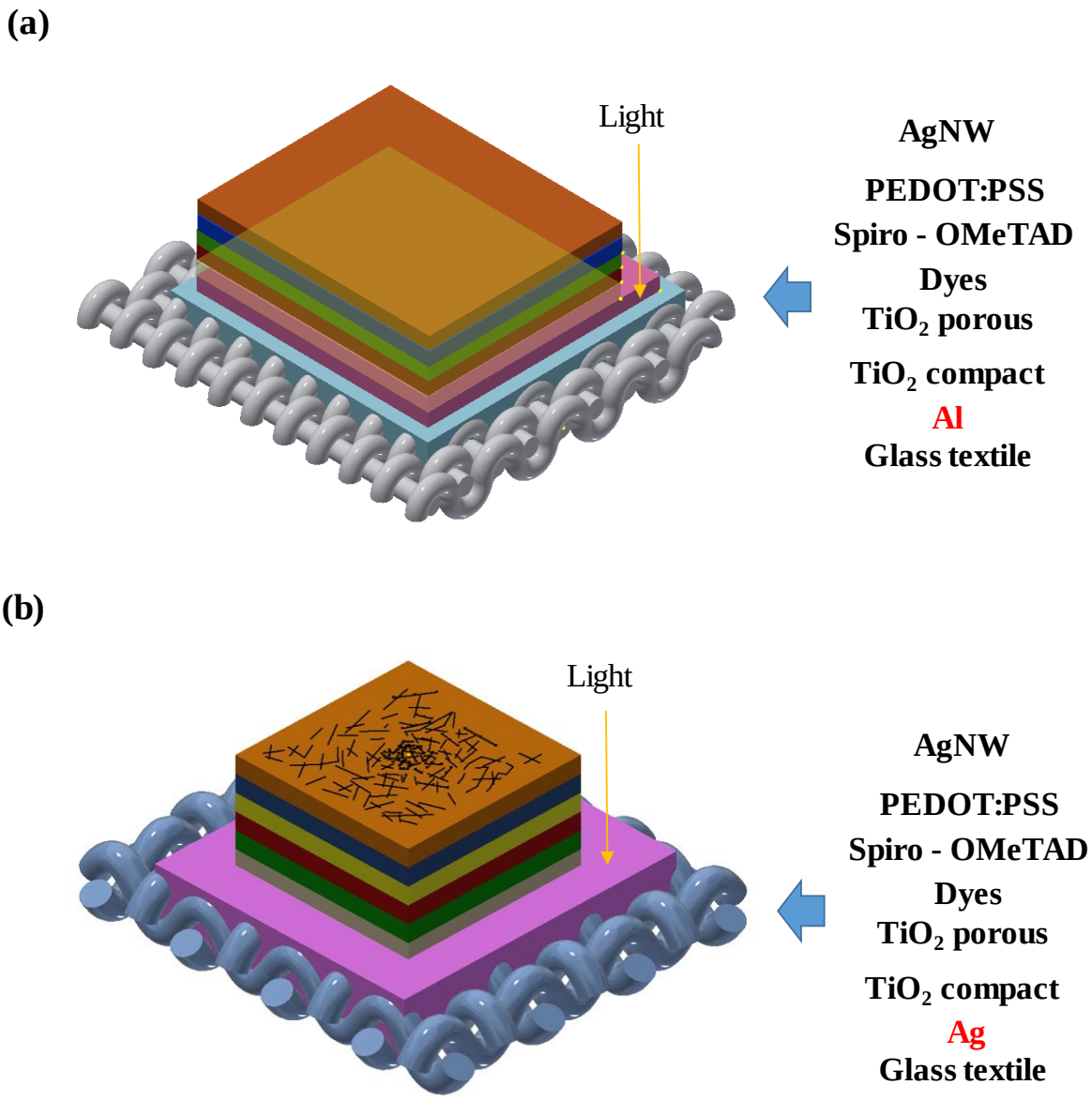

Figure 8.1. Device structure of (a) commercial available aluminium laminated glass fibre textile based ssDSSC, (b) non-coated glass fibre textile based ssDSSC.

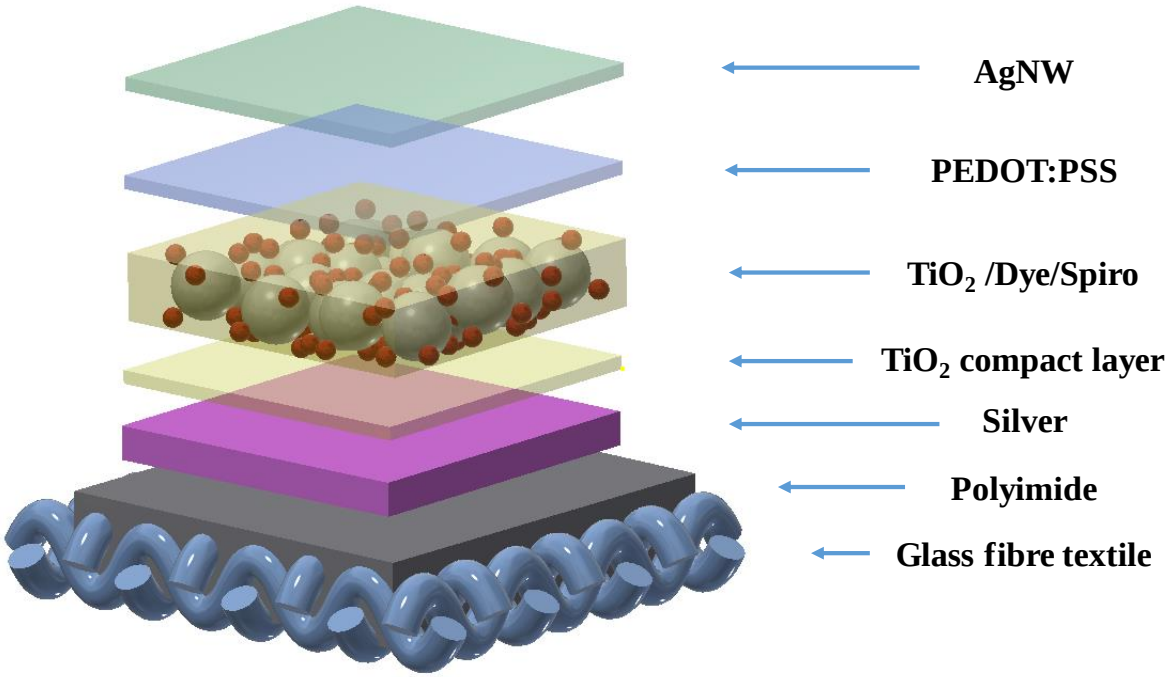

Figure 8.2. Isometric view of the schematic diagram of textile based ssDSSC device structure.

8.3 Experiment

8.3.1 Materials

The plain woven composite glass fibre textile, and the printed liquid polyimide was the same in chapter 6. The screen printable silver paste used in this chapter was the same with previous chapters. The compact layer solution of titanium di-isopropoxide bis(acetylacetonate 75% of isoproponal), the TiO_2 paste was the same in chapter 7. The ruthenizer 535-bisTBA dye sensitizer was the same with previous chapters. The ingredients for the solid-state electrolyte were: bis(trifluoromethane)sulfonimide lithium salt (544094), Cholorobenzene(284513), tert-butylpyridine (142379), acetonitrile (271004) and $N^2,N^2,N^{2'},N^{2'},N^7,N^7,N^{7'},N^{7'}$-octakis(4-methoxyphenyl)-9,9'-spirobi[fluorene]-2,2',7,7'-tetraamine (spiro-OMeTAD) (792071), all the same with chapter 7. Clevios™ PEDOT:PSS was supplied by Heraeus and the AgNW solution used in this experiment were also same with chapter 7.

8.3.2 Substrates

The textile substrates used in this experiment are commercial Aluminium laminated glass fibre textile (Valmiera glass Ltd, 440-2-Al), general resin reinforcement glass fibre textile (Valmiera glass Ltd, FK144). The liquid polyimide layer is screen printed onto the general resin reinforcement glass fibre textile substrates to reduce the surface roughness, and enhance the adhesion to the primary surface in order to improve the morphology of the following functional layers.

The polyimide is high temperature coating synthetic polymers which contains two acyl groups bonded to nitrogen in its chemical structure as shown in figure 8.3. It is a high chemical and solvent resistance. The liquid polyimide paste has a high viscosity and glass transition temperature (Tg) which is suitable for screen printing.

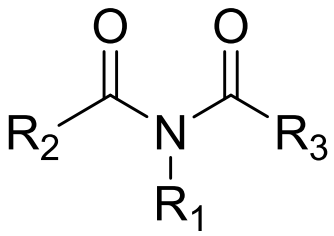

Figure 8.3. Chemical structure diagram of polyimide.

8.3.3 Fabrication process

The fabrication process for monolithic-structured ssDSSC on a single textile consists of five main steps as shown in figure 8.4 (a-e), where all functional layers were directly deposited onto the textile substrates using processes such as screen printing and spray coating. To fabricate the ssDSSC, after initial investigations on commercial aluminium laminated glass fibre textile and uncoated general glass fibre textiles, a flexible polyimide layer was required to reduce the surface roughness of fabric. Therefore, this section focuses on the fabrication process of liquid polyimide coated general glass fibre textile substrates. The usage of the liquid polyimide is to planarize the surface of the fabric is different to the polyurethane based material typically used due to the temperature limitation of the polyurethane film [160]. The printing rheological specifications are summarized in Table 8.1, the minimum required thickness of the liquid polyimide should be covered and filled the glass fibre textile surface texture. However, the higher thickness of the liquid polyimide layer results in the film crake and flake off. The

printing deposits were chosen at 2 times with the printing gap of 1.8 mm to achieve the lowest thickness of the film with no cracking after heating at 150°C for 15 minutes and 250°C for a further 20 minutes.

Table 8.1. Printing rheological specification summarization of liquid polyimide layer.

Printing deposits	Printing gap	Polyimide layer thickness	Surface texture status	Film status
1	1.6 mm	12 µm	High	Non-cracking
1	1.8 mm	22 µm	High	Non-cracking
1	2.0 mm	35 µm	Medium	Non-cracking
2	1.6 mm	30 µm	Medium	Non-cracking
2	1.8 mm	40 µm	Low	Non-cracking
2	2.0 mm	60 µm	Low	Cracking
3	1.6 mm	50 µm	Low	Cracking
3	1.8 mm	80 µm	Low	Cracking
3	2.0 mm	130 µm	Non	Cracking

Next, the silver bottom electrode was screen printed onto the dried polyimide and this serves to further reduce the surface roughness of the textile substrate, as shown in figure 8.4 (a). The screen design ensures that the functional layers are only printed where required, and the effect on the fabric properties, such as flexibility and breathability, is minimized.

Figure 8.4(b) shows the spray pyrolysis deposition of TiO_2 CL using a pre-designed shadow mask aligned with the silver bottom electrode on the fabric substrate. There are many parameters that influence the uniformity, roughness and coverage of the TiO_2 film on the substrates during spraying. This includes the flow rate of the functional ink concentration, the distance between the spray nozzle and the substrate and the gas flow pressure that carries the droplets to the substrates. A spray pressure of 0.3 bar was used for all the functional layers and the spray distance for the CL film was 12 cm. The TiO_2 CL was used to avoid direct contact of the solid electrolyte to the conductive bottom electrode that would otherwise short circuit the cell. The mesoporous TiO_2 layer was deposited on the TiO_2 CL and sintered to form photo anodes and this was followed by the dye staining process depicted in figure 8.4 (c). Figure 8.4 (d) shows the deposition of freshly prepared solid-state electrolyte solution, which was drop cast onto the dye stained devices and left for 16 hours to allow the solid-state electrolyte to fully infiltrate into the TiO_2 mesoporous film. To complete the fabrication, the devices are spray coated with PEDOT: PSS and AgNW top electrodes as shown in figure 8.4 (e).

A screen printer was used in all printing steps in this work using pre-designed polyester 75/55 mesh with a 45 µm diameter thread and an emulsion thickness of 5 µm. The glass fibre textile was cut into 15 cm × 15 cm, attached to an alumina tile by a Kapton tape, and placed on the substrate holder stage of the screen printer prior to printing. The screen printer was fully automatic and a squeegee speed 70 cm/min was used throughout. The printing gap for the liquid polyimide layer was set to 1.2 µm for the first two deposits, and increased to 1.4 µm for the last two deposits. The screen printed polyimide layer was subsequently annealed at 150 ^{o}C and 275 ^{o}C for 45 minutes in an oven respectively. For the silver bottom conductive layer, the printing gap was set to 1.6 µm for the first deposit and increased to 1.8 µm in the second deposit. The silver film was cured at 150 ^{o}C for 30 minutes.

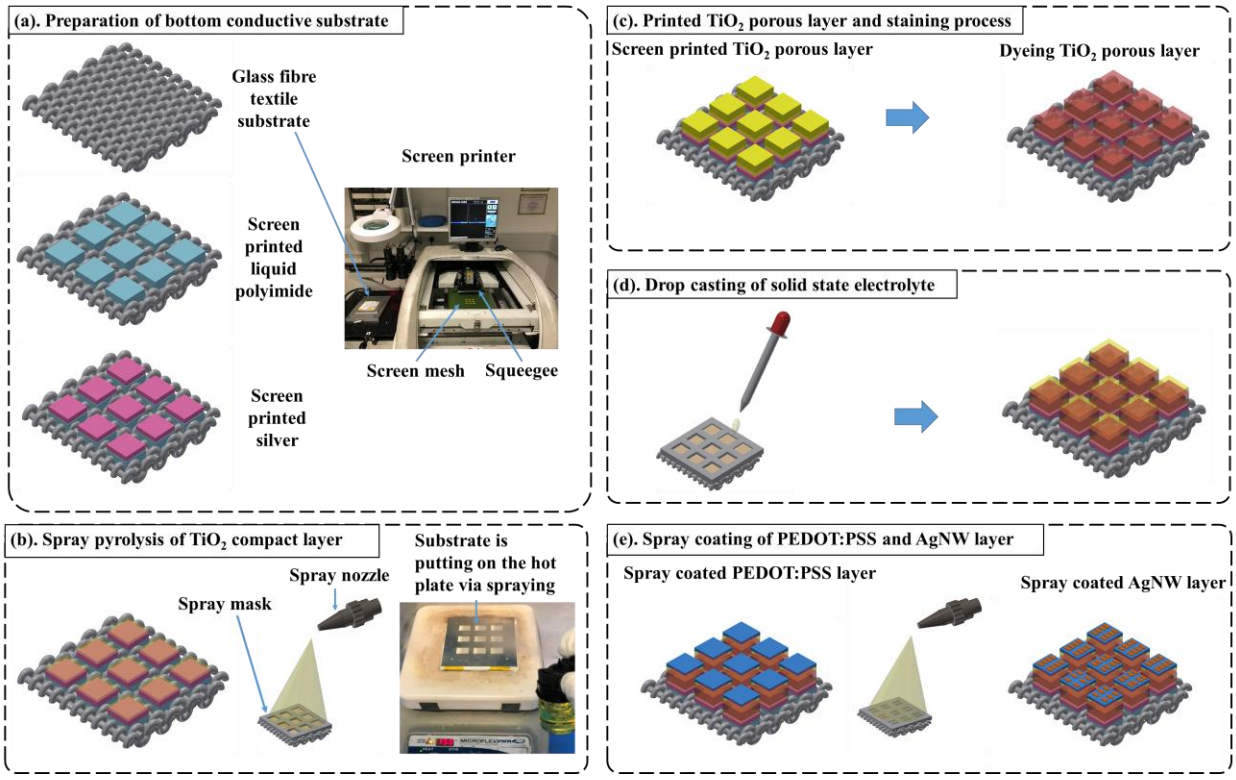

Figure 8.4. Fabrication process diagram of textile based ssDSSC, (a) screen printing polyimide and silver layer to form the bottom conductive substrate, (b) spray pyrolysis of TiO_2 compact layer, (c) screen printed TiO_2 porous layer and staining process, (d) drop casting of solid-state electrolyte, (3) spray coating of PEDO:PSS and AgNW layer.

A thin TiO_2 compact layer (CL) was deposited via spray pyrolysis using air as the carrier gas. A solution of titanium di-isopropoxide bis(acetylacetonate) was sprayed onto the silver coated glass fibre textile substrate which was pre-heated on a hot plate at 150 ^{o}C. The spray pyrolysis process of depositing TiO_2 compact layer (CL) was carried out with the same procedure and printing rheological specifications in Chapter 7. After printing the TiO_2 CL, the textiles

substrates were annealed at 500 °C for half an hour. The mesoporous TiO_2 films were screen printed using the commercially available paste and slowly heated to 500 °C for 30 min in an oven in an oxygen environment. The printing gap was set to 1.8 µm and the film was cured at 450 ^oC for 30 minutes, after which it was immersed into dye solution for 16 hours for staining. The dye solution was Ruthernizer 535-bisTBA in ethyl alcohol solution (100 mg dye powder added to 15 ml of ethyl alcohol). The dye-loaded devices were carefully washed with ethanol to remove loosely bound dye molecules and minimise the resistance of the films. Then the devices were transferred to a nitrogen filled glovebox for the drop casting 3 µl onto the surface of the dye loaded TiO_2 layer of the solid electrolyte. The organic hole conductor, or solid electrolyte solution, was made by dissolving 260 mg of spiro-OMeTAD in 1.2 ml of chlorobenzene and then adding 25 µl of tert-butylpyridine and 40 µl of bis(trifluoromethane)sulfonamide lithium salt solution. The lithium salt contains 170 mg lithium salt and 1ml of acetonitrile. The doped spiro-OMeTAD solution was allowed to infiltrate the TiO_2 for 12 hours in a nitrogen filled glove box. Then a thin layer of PEDOT:PSS was spray coated inside the glove box with a spray distance of 20 cm, and heated on a hot plate at 50 °C for half an hour. Finally, a thin transparent top AgNW electrode was spray deposited with a spray distance of 20 cm and dried on a hot plate at 50 °C for 30 minutes. Silver pads were applied to make a low resistance contact to the solar cells for probing. The cell area is 3 mm^2 which is controlled by the spray mask. After many iterations investigating thickness, curing temperature, stability of the functional layers 18 devices were tested with each containing 9 pixels (cells). Almost all devices functioned but some cells were short circuited at the edges of top and bottom electrodes. All textile devices were encapsulated using 1mm thick mask by doctor blading method.

The crystallinity of the TiO_2 compact layer was checked by X-ray diffraction (XRD, Rigaku SmartLab). The morphology and thickness of the TiO_2 mesoporous layer was observed in a scanning electron microscope (JEOL JSM 7500 FESEM). The surface roughness of the glass fibre textile was measured using surface profilometry (2-D Tencor P-11). The surface roughness of the TiO_2 compact layer on glass was examined by atomic force microscope (AFM) using a Veeco Innova 3100 instrument. All the devices are measured under dark and illuminated condition by using a digital source meter (Keithley, Model 2400), and a solar simulator (ABET Sun 300) to provide illumination of AM 1.5 conditions. Transmittance measurements were examined using Bentham PV instrumentation (PVE300).

8.4 Results and discussion

8.4.1 Results and discussion of commercial aluminium laminated glass fibre textile device

The textile structured ssDDSC device was firstly fabricated on the commercial Aluminium laminated glass fibre to study the characterization, device performance as well as the rheological specification required.

The structure of this type of device was similar to the FTO glass ssDSSC device, and the FTO glass was replaced with aluminium coated glass fibre textile. A maximum PCE value of 0.052 % was achieved with a V_{oc} of 0.13 V, FF 0.37, J_{sc} of 1.1 mA/cm^2 as shown in Figure 8.5. The JV curve was shown in Figure 8.5(a) along with the photograph of the device shown in Figure 8.5(b).

Table 8.2. The results of aluminium laminated glass fibre textile ssDSSC device.

Devices	**Temperature**	**Open circuit voltage (V_{oc}), V**	**Fill factor (FF)**	**Current density (J_{sc}), mA/cm^2**	**Efficiency %**	**Cell Area, mm^2**
Device 1	450^{o}C	0.13	0.37	1.1	0.052±0.023%	3

(a) **(b)**

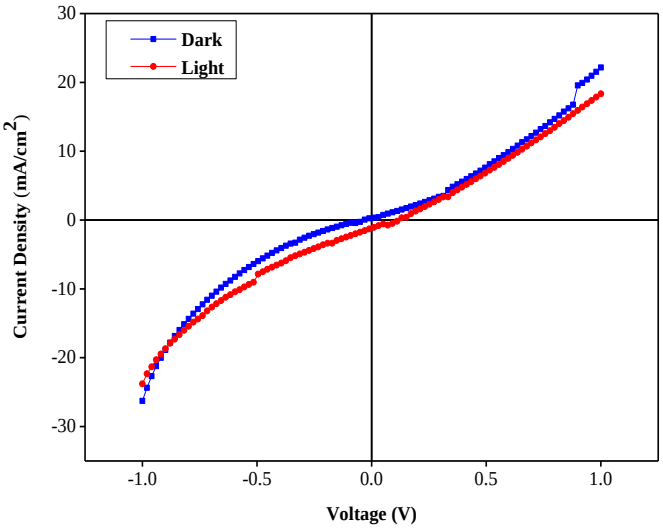

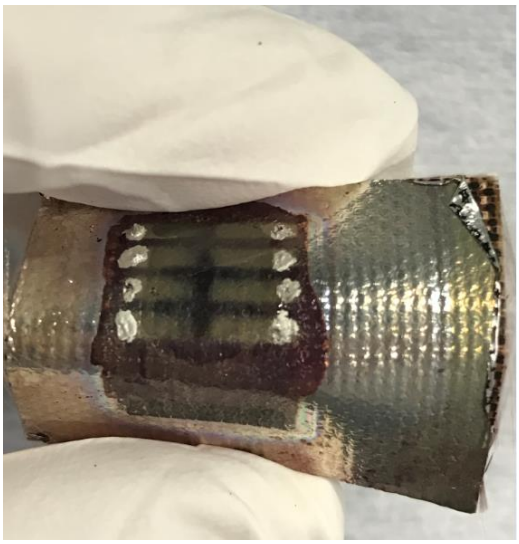

Figure 8.5. (a) JV graph of aluminium laminated glass fibre textile device, (b) photograph of aluminium laminated glass fibre textile device.

The PCE value of aluminium coated glass fibre textile was inefficient compared to the FTO glass based ssDSSC devices as the laminated Al coating was not reliable on the glass fibre textile after annealing at 450 ^{o}C. The FESEM photograph in Figure 8.6 shows in the Al coating is peeling off from the woven glass fibre textile. Figure 8.6 (a) clearly shows the Al layer is completely separating from the glass fibre textile, and the surface morphology and the breaking gap was shown in Figure 8.6 (b) and (c). The main problem of this device is the aluminium became oxidized after heating, Al_2O_3 is an electrical insulator, which blocks the current through the device. Furthermore, the surface of the laminated Al coating is not smooth enough for the nano-meter thin film layers which results in a large thickness of the TiO_2 layer. The thickness of TiO_2 was around 67 µm as shown in Figure 8.6 (d) which will affect the performance of the device.

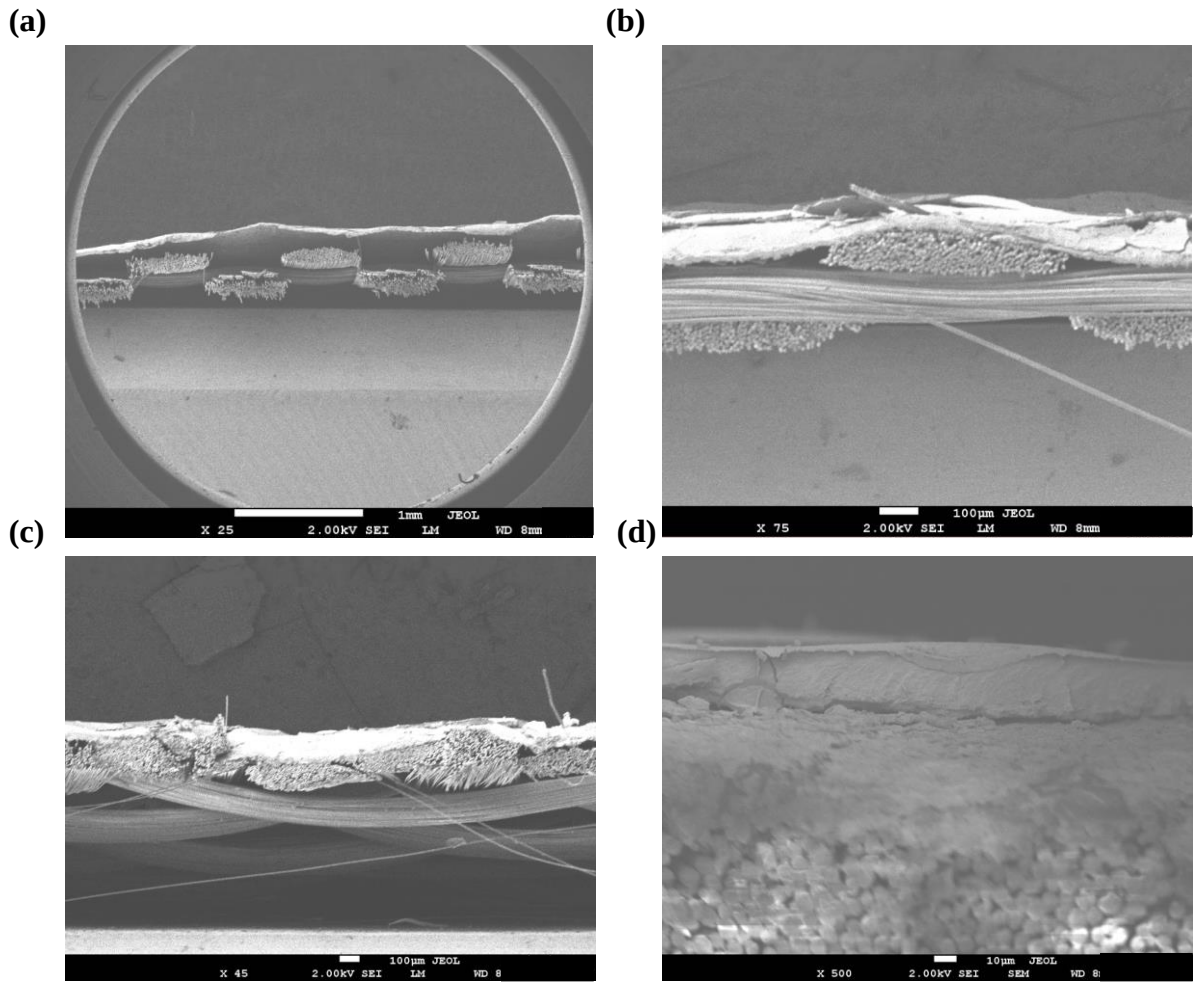

Figure 8.6. FESEM cross-sectional view of (a) the aluminium coated glass fibre textile device, (b) & (c) surface roughness and the peeling gap from the glass substrate, (d) morphology of the TiO_2 film of the aluminium laminated glass fibre textile device.

8.4.2 Results and discussion for non-coated and polyimide coated glass fibre textile device

With the optimisation of the fabrication conditions on rigid glass substrates, glass fibre textile ssDSSC devices were fabricated with the same steps. Figure 8.7 (a) shows the SEM micrograph of glass fibre textile used in this research. This was initially planarised and made conductive by screen printing a silver layer with a thickness of 30 µm. The surface roughness (R_a) values of glass fibre textile before and after printing the silver layer is 70.5 µm and 26.1 µm respectively. Whilst it shows the surface roughness of the textile was reduced by the silver, it is still far from ideal for the subsequent deposition of reliable functional layers which should all be sub-micron in thickness. The nanoporous TiO_2 paste was screen printed three times to achieve a smooth continuous layer with a final thickness of around 30 µm as shown in figure

8.7(b). The thickness of TiO_2 film is controlled by the screen-printing deposit times, the thickness achieved in this experiment is the minimum thickness of a non-cracking TiO_2 film to cover the texture of the textile surface. This is substantially greater than the previously identified target thickness of 7 µm but is unavoidable due to the rough textile surface.

The initial glass fibre ssDSSCs with the 30 µm thick TiO_2 layer demonstrated an efficiency of $4.14x10^{-6}$ with a V_{OC} of 0.22V, FF of 0.22 and J_{SC} of $3.1x10^{-5}$. The increased thickness of the TiO_2 means the glass fibre ssDSSC is much less efficient than the FTO glass version with 7 µm thick TiO_2 (

table 8.3) which is ultimately due to the surface roughness of the textiles. Figure 8.8(a) shows the J/V curves of the ssDSSC on textile that shows there is resistance to charge movement between the functional layers due to the excessive and uneven film thicknesses.

It was therefore necessary to further reduce the surface roughness of the glass fibre textile substrates using a screen printed liquid polyimide layer. The field emission scanning electron microscope (FESEM) image of the top surface of the liquid polyimide surface is shown in figure 8.7(c) and the measured surface roughness of the polyimide layer was 10 µm. As can be seen from figure 8.7(d), a 40 µm thick liquid polyimide layer was printed and the textile appears flat compared to the bare textile surface. The surface roughness was further reduced to 7 µm by the screen printed 20 µm conductive silver bottom electrode. This smoother surface enabled the thickness of the TiO_2 layer to be reduced to 20 µm, which reduced the resistance in the functional layer. Following the deposition of all functional layers, the device showed a maximum PCE of 0.4% with a V_{OC} of 0.31 V, while the FF and J_{SC} were 0.25 and 5.2 mA/cm^2 respectively, as shown in

table 8.3. The PCE of the textile devices improved significantly because of the smooth flat surface that enabled the even deposition of the subsequent functional layers. This is the first reported the fabrication of ssDSSCs on textiles with a PCE of 0.4%. The device also

demonstrated good stability with a negligible reduction in PCE after it was kept in air for a period of two weeks without encapsulation. In total, five cells obtained 0.4% with the remaining cells obtaining PCE values in the range of 0.1-0.4%. Devices failures were due to short circuits from either the top and bottom electrode contacting or peeling away from the functional layers around the edges.

Table 8.3. Results of textile based ssDSSC device.

Device	V_{oc} [V]	FF	J_{sc} [mA/cm^2]	PCE [%]
Bare Textile	0.22	0.23	$8.26x10^{-5}$	$4.14x10^{-6}$
Liquid polyimide coated glass	0.31	0.25	5.2	0.4±0.1%

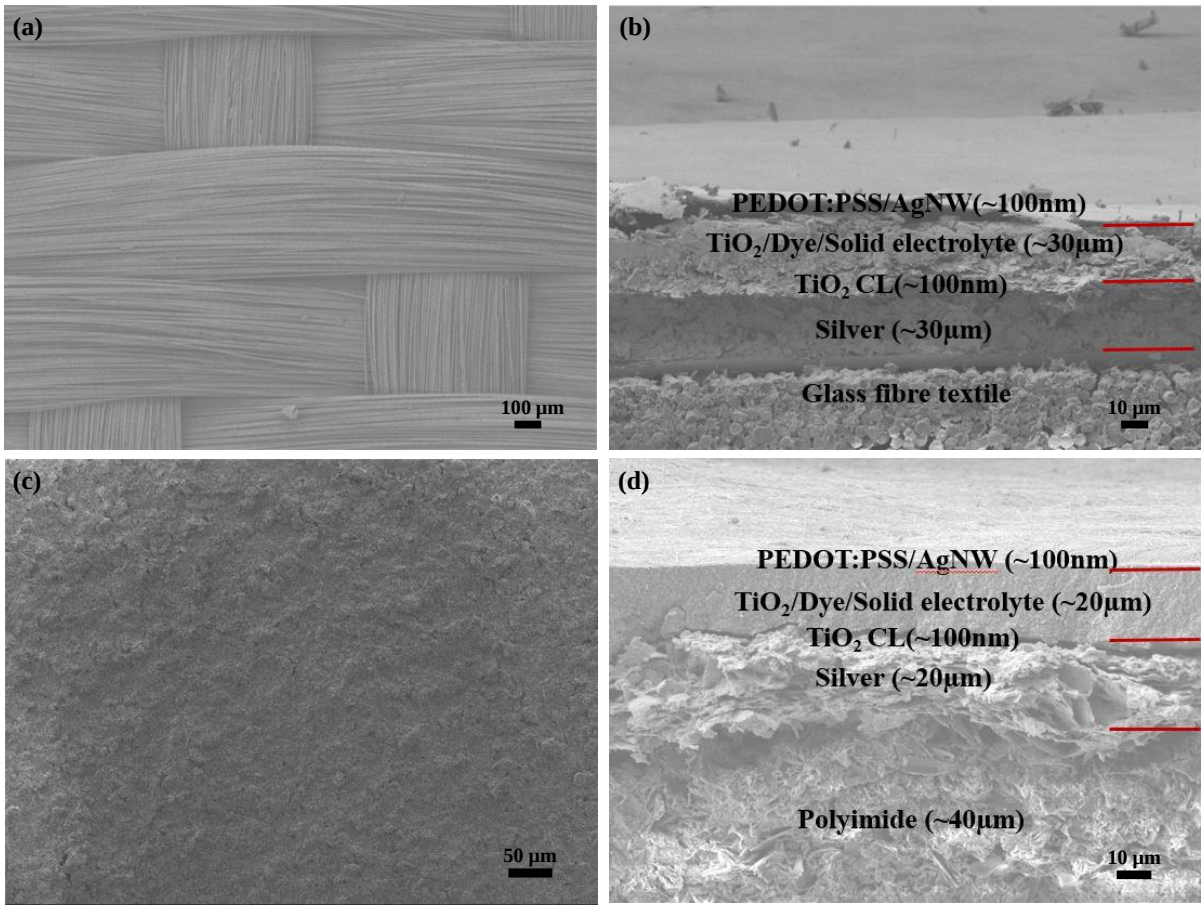

Figure 8.7. FESEM images of (a) Plan view of bare glass fibre fabric and (b) Cross sectional view of the printed bare textile ssDSSCs, (c) liquid polyimide surface on the glass fibre woven textiles, (d) Cross sectional view of the printed liquid polyimide coated textile ssDSSCs.

The flexibility of the monolithic structure was also investigated to determine how the textile device performs after deformation due to rolling and bending the cells. Figure 8.8 (b) shows the fabricated device under bending, and figure 8.8 (c) shows it wrapped around a pen with a radius of 0.5 cm. Further cyclical bending tests were performed using an automatic bending test rig around a radius of 2.5cm and it was important the devices were first encapsulated to prevent abrasive wear during the test. The encapsulated cells were tested with the top AgNW electrode side facing up. After 10 bending cycles there was a 60% reduction in efficiency, and after 30 cycles the devices failed. This was due to the strain induced in the cell during bending that caused the functional layers to mechanically fail. The amount of strain transferred to the device during bending is a function of the thickness and stiffness of the substrate and the polyimide coated glass fibre textile is quite stiff compared with a conventional textile. This strain can be alleviated by increasing the thickness of the encapsulation layer such that the cell is positioned closer to the neutral axis reducing the strain experienced during bending[161].

With regard to stability in air, the PCE versus time is shown in figure 8.8(d). The encapsulated cells showed no reduction in PCE after 15 days, and after a further 30 days storage the PCE had reduced by around 0.03%. However, after 100 days the PCE had reduced by 80%. This indicates that the encapsulation layer initially protects the devices against exposure to air but this protection fails over time.

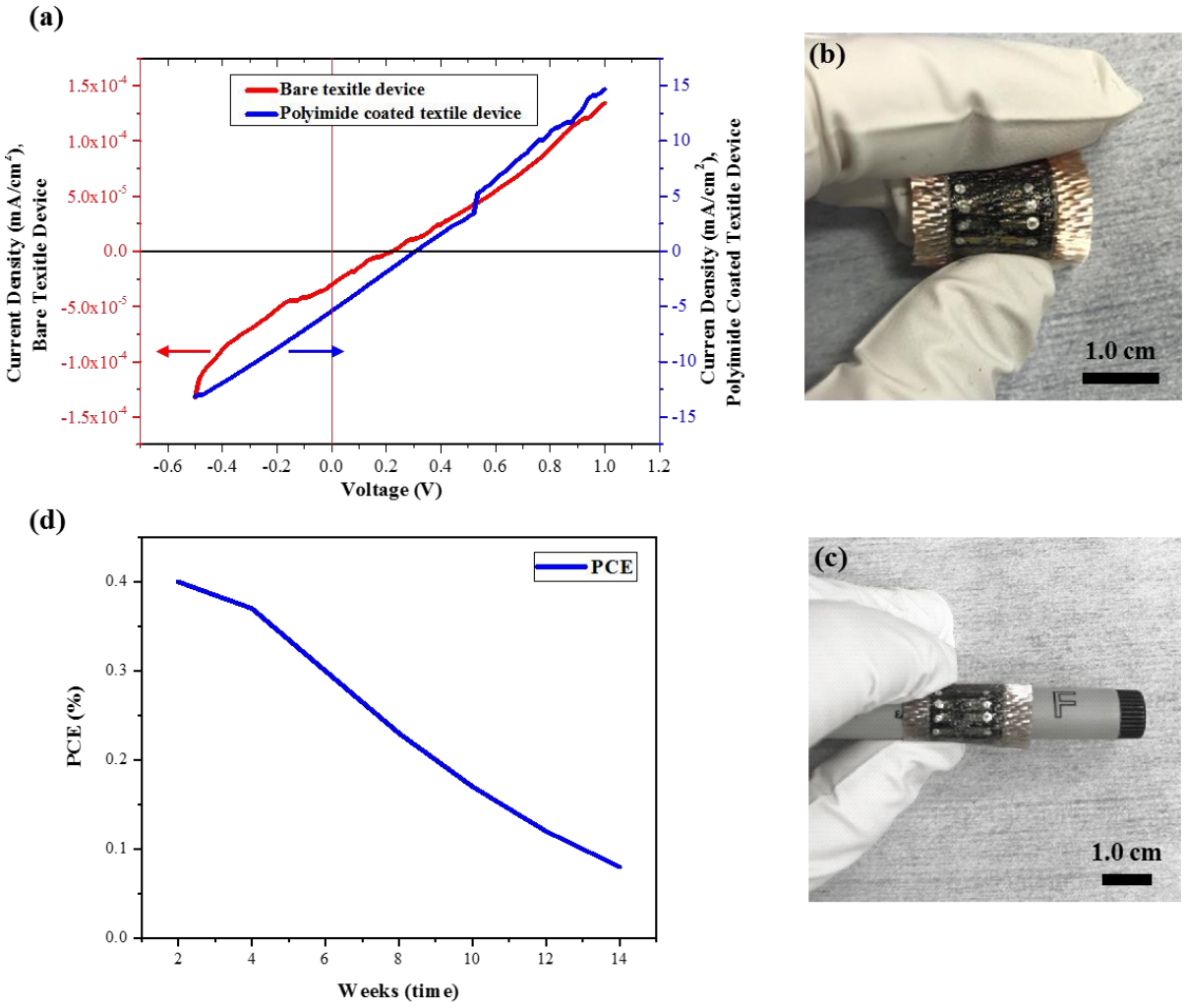

Figure 8.8. Photograph of (a) J/V curve of ssDSSCs fabricated on bare glass fibre textiles and polyimide coated glass, (b) Polyimide coated glass fibre textile device under bending, and (c) device rolling on a pen, (d) the PCE versus time with regard to stability in air for polyimide coated glass fibre textile.

An efficiency of 0.4% was achieved on glass fibre textile device, it is a high temperature textile which enable more reliable application of the device. However, the efficiency of the cells need to be improved to make a reliable portable energy source. One main problem is the flexibility

of the film of the cell, in order to achieve a smoother surface, the functional layer needs to be thick enough to fill the texture of the textile. That results in a cracking film which make the cell inefficient. In order to overcome this problem, a new woven method of glass fibre textile needs to investigate to a achieve a smoother surface. A more reliable TiO_2 paste needs to be further investigated to improve cell efficiency, and also perovskite could be used as the new photosensitizer to absorb more energy from the sunlight.

8.5 Conclusions

A fully printed textile functioning ssDSSC on a woven glass fibre textile has been demonstrated. Initial devices exhibited very low efficiency and this was due to the high surface roughness of the woven glass fibre textiles. A liquid polyimide was used to planarise the surface of the fabric. This is a flexible material that can withstand the processing temperature used throughout this work. Cells fabricated on the planarised textile obtained a maximum PCE of 0.4% for the fabricated cells on the textiles and this compared to 2.83% for the equivalent cells processed on the glass substrate. The cell encapsulation process initially protects the devices against oxidation and the flexibility of the cell and the ability to survive bending could be further improved by optimising the encapsulation thickness. This work demonstrates the potential for fabricating ssDSSCs directly onto fabric using processes suitable for continuous roll to roll manufacturing. This PV device configuration can also be fabricated on standard textiles such as cotton but the high temperature required by the TiO_2 CL is an issue. This highlights the importance of the materials for the compact layers to realise the ssDSSCs on standard textiles. Therefore, further research work is required to reduce the processing temperature required by the compact layers to less than 150°C. Future work will also be focused on improving the durability of the textile ssDSSCs and improving the PCE values of by using thinner silver and TiO_2 layers thereby reducing the resistance of the cells.

This page intentionally left blank

Chapter 9

9 Conclusions and future work

Working on textiles is extremely challenging due to the surface topology and structure which makes the fabrication of solution processed photovoltaic cells directly on the fabric surface very difficult. In this research, a fully printed and solution processed ssDSSC was fabricated on the surface of a textile with an efficiency of 0.4% and this is the first ever reported ssDSSC successfully realised on a flexible textile substrate. In addition, the results also include a comparison between the textile ssDSSC device and a FTO glass substrate reference device with an efficiency of 2.8% which shows the efficiency could be optimized in the future work. The formulation of low temperature processed TiO_2 paste and ink was also developed with an efficiency of 4.3 % achieved on FTO glass. This low temperature processed TiO_2 poste and ink can be applied on the textile polyester cotton fabric substrate. The rheological specification of screen printing and spray coating this low temperature processed TiO_2 paste and ink on kapton, and cotton fabric substrate was investigated with FTO glass as the top electrode, achieved a maximum PCE value of 7.03% and 2.78% respectively. A fully flexible liquid electrolyte based DSSC was also achieved on a glass fibre textile and cotton fabric interface substrate with ITO/PET as the top electrode, the maximum PCE value was 3.24% and 4.04%, this shows the cell performance of formulated low temperature processed TiO_2 paste is comparable with the commercial TiO_2 paste. The devices are encapsulated and tested over three months. The low temperature processed polyester cotton fabric devices are not working after three months due to the TiO_2 film was flacked off. Further research needs to improve the viscosity and stability of the TiO_2 film.

Although the ssDSSC has been successfully fabricated on the textile substrate, the processing temperature still remains problematics in fabricating the ssDSSC on the low temperature textile, since the TiO_2 compact needs to annealing at high temperature (450^oC) to form the crystalline. Besides this, the efficiency needs to be improved to produce sufficient power for the application device such as smart phone. The target efficiency needs to be at least around 10% to charge a smart phone with the cell area of 200cm^2. Therefore, future research needs to focus on investigating the approach on low temperature processed TiO_2 compact layer, and also improve

the performance of the cell. The details of the future work plan is shown in figure 9.1. The first 7 blocks in figure 9.1 was successfully achieved and demonstrated in this present research. The future work plan will be carried on the low temperature processed ssDSSC on the standard polyester cotton fabric as shown in Figure 9.1 8-10, with the similar research strategy, the standard low temperature processed ssDSSC was first fabricated on the FTO glass to investigate the printing rheological specifications of each particular layer in ssDSSC. Then Ag is replaced the FTO as the conductive layer as the intermediate stage towards the target cotton fabric textile. In order to improve the efficiency of the cell, the perovskite material such as $CH_3NH_3PbI_3$ can be used instead of dyes to increase the light absorption. The perovskite solar cell will be first fabricate on the FTO glass substrate, and subsequently move onto the fabric. The high temperature process of PSC in both creation of at higher surface area TiO_2 and also increased antiparticle contact is considered to enable the sufficient efficiency and power driving from the device. Therefore, high temperature processed perovskite solar cell will be fabricated as a comparison to study the characterization of the perovskite solar cell. Glass fibre will be used as the high temperature textile to improve the efficiency of the perovskite for more applications.

Figure 9.1. High efficiency textile based solar cell research plan.

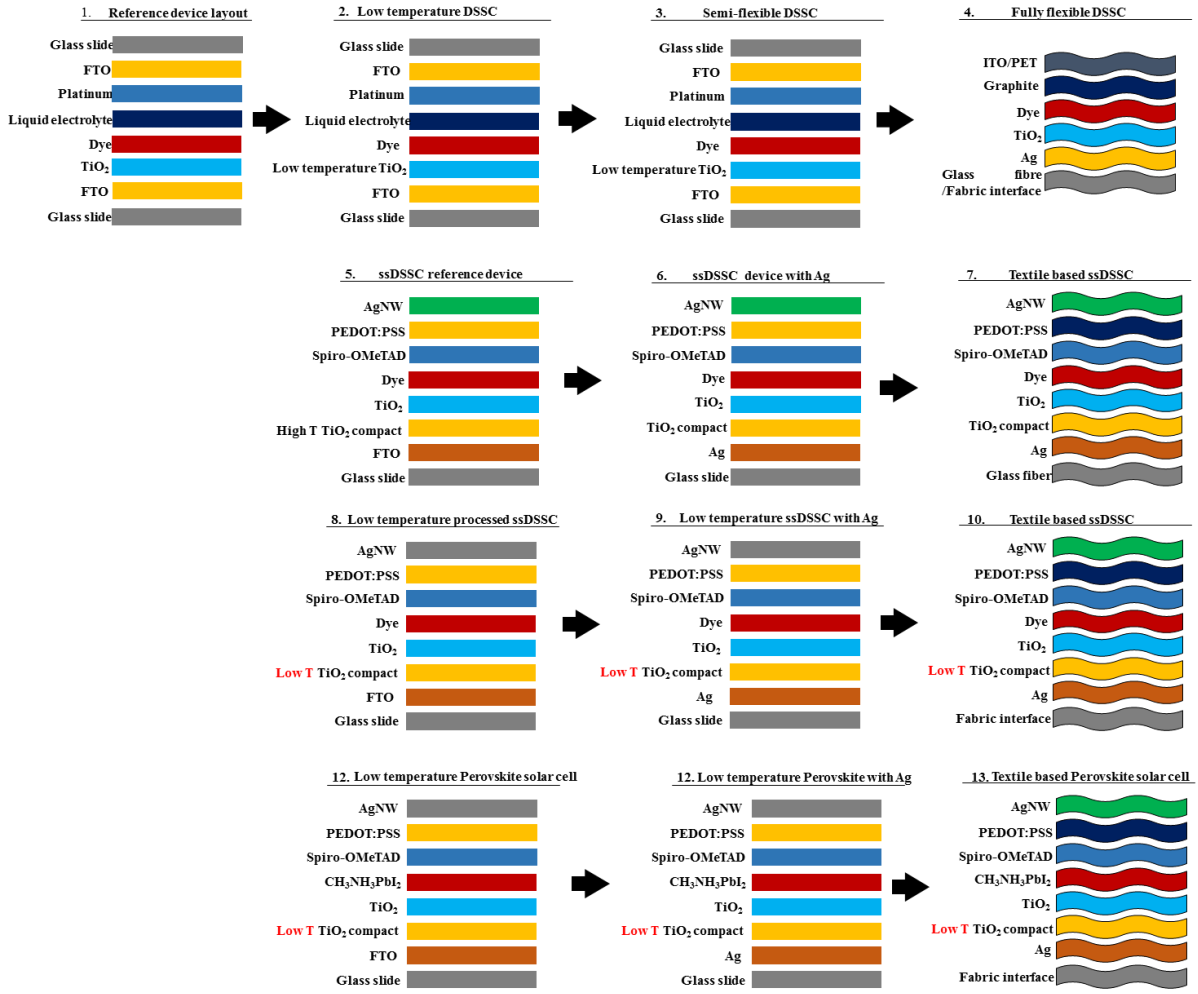

Reference:

1. Wang, J., et al., *A review on the application of photocatalytic materials on textiles.* Textile Research Journal, 2014. **85**(10): p. 1104-1118.
2. Cherenack, K. and L. van Pieterson, *Smart textiles: Challenges and opportunities.* Journal of Applied Physics, 2012. **112**(9): p. 091301.
3. Kaushik, V., et al., *Textile-Based Electronic Components for Energy Applications: Principles, Problems, and Perspective.* Nanomaterials (Basel), 2015. **5**(3): p. 1493-1531.
4. Coyle, S., et al., *BIOTEX--biosensing textiles for personalised healthcare management.* IEEE Trans Inf Technol Biomed, 2010: p. 364-70.
5. Cunha, J.P.S., et al., *A wearable wirless vital signs monitor for patients' monility in cardiology and sports.* Pervasive Computing Technologies for Healthcare 2010.
6. Shyamkumar, P., et al., *Wearable Wireless Cardiovascular Monitoring Using Textile-Based Nanosensor and Nanomaterial Systems.* Electronics, 2014. **3**(3): p. 504-520.
7. J. C. G. Matthews, G.P., *Development of Flexible, Wearable Antennas.* IEEE 2009.
8. Winterhalter, C.A., et al., *Development of Electronic Textiles to Support Networks, Communications, and Medical Applications in Future U.S. Military Protective Clothing Systems.* IEEE Transactions on Information Technology in Biomedicine, 2005. **9**(3): p. 402-406.
9. Opwis, K., et al., *Preparation of a Textile-Based Dye-Sensitized Solar Cell.* International Journal of Photoenergy, 2016. **2016**: p. 1-11.
10. Beeby, S. and N. White, *Energy Harvesting for Autonomous Systems*. 2010: Artech House.
11. Schubert, M.B. and J.H. Werner, *Flexible solar cells for clothing.* Materials Today, 2006. **9**(6): p. 42-50.
12. Xia, Z., *Characterization of the Dye-Sensitized Solar Cell.* Worcester polytechnic institute, 2012.
13. Bai, Y., et al., *Titanium dioxide nanomaterials for photovoltaic applications.* Chem Rev, 2014. **114**(19): p. 10095-130.
14. Ito, S., et al., *High-Efficiency Organic-Dye- Sensitized Solar Cells Controlled by Nanocrystalline-TiO2 Electrode Thickness.* Advanced Materials, 2006. **18**(9): p. 1202-1205.
15. Jasim, K.E., U.o.B. Department of Physics, and K.o. Bahrain, *Dye Sensitized Solar Cells Working Principles, challenges and opportunities.* 2011. **35**: p. 35.
16. Sun, H., et al., *Recent progress in solar cells based on one-dimensional nanomaterials.* Energy Environ. Sci., 2015. **8**(4): p. 1139-1159.
17. Wayne M. Campbell, K.W.J., Pawel Wagner, Klaudia Wagner, Penny J. Walsh,, et al., *Highly Efficient Porphyrin Sensitizers for Dye-Sensitized Solar Cells.* Physical Chemsitry.
18. Zulkifili, A.N.B., et al., *The Basic Research on the Dye-Sensitized Solar Cells (DSSC).* Journal of Clean Energy Technologies, 2015. **3**(5): p. 382-387.
19. Bignozzi, C.A., et al., *The role of transition metal complexes in dye sensitized solar devices.* Coordination Chemistry Reviews, 2013. **257**(9-10): p. 1472-1492.
20. Green, M.A., et al., *Solar cell efficiency tables (version 37).* Progress in Photovoltaics: Research and Applications, 2011. **19**(1): p. 84-92.
21. Bakke, J.R., et al., *Nanoengineering and interfacial engineering of photovoltaics by atomic layer deposition.* Nanoscale, 2011. **3**(9): p. 3482-508.
22. Chae, Y., et al., *Metal-free organic-dye-based flexible dye-sensitized solar textiles with panchromatic effect.* Dyes and Pigments, 2015. **113**: p. 378-389.

23. Kalaignan, G. and Y. Kang, *A review on mass transport in dye-sensitized nanocrystalline solar cells.* Journal of Photochemistry and Photobiology C: Photochemistry Reviews, 2006. **7**(1): p. 17-22.
24. Eslamian, M., *Spray-on Thin Film PV Solar Cells: Advances, Potentials and Challenges.* Coatings, 2014. **4**(1): p. 60-84.
25. Chen, L., et al., *Fabrication of high performance Pt counter electrodes on conductive plastic substrate for flexible dye-sensitized solar cells.* Electrochimica Acta, 2010. **55**(11): p. 3721-3726.
26. Ma, X., et al., *A high-efficiency cyanine dye for dye-sensitized solar cells.* Tetrahedron, 2008. **64**(2): p. 345-350.
27. Gagliardi, A., D. Gentilini, and A.D. Carlo, *Charge Transport in Solid-State Dye-Sensitized Solar Cells.* The Journal of Physical Chemistry C, 2012. **116**(45): p. 23882-23889.
28. Guo, K., et al., *Enhancement of properties of dye-sensitized solar cells by surface plasmon resonance of Ag nanowire core–shell structure in TiO2 films.* Journal of Materials Chemistry A, 2013. **1**(24): p. 7229.
29. Grätzel, M., *Dye-sensitized solar cells.* Journal of Photochemistry and Photobiology C: Photochemistry Reviews, 2003. **4**(2): p. 145-153.
30. Weerasinghe, H.C., F. Huang, and Y.-B. Cheng, *Fabrication of flexible dye sensitized solar cells on plastic substrates.* Nano Energy, 2013. **2**(2): p. 174-189.
31. Yang, Z., et al., *Stretchable, wearable dye-sensitized solar cells.* Adv Mater, 2014. **26**(17): p. 2643-7, 2613.
32. Avrutin, V., N. Izyumskaya, and H. Morkoç, *Semiconductor solar cells: Recent progress in terrestrial applications.* Superlattices and Microstructures, 2011. **49**(4): p. 337-364.
33. Mehmood, H., T. Tauqeer, and S. Hussain, *Recent progress in silicon-based solid-state solar cells.* International Journal of Electronics, 2018. **105**(9): p. 1568-1582.
34. Martin A. Green, J.Z., and A. Wang, *Recent progress in silicon solar cells.* IEEE, 1999: p. 6.
35. Jackson, P., et al., *Properties of Cu(In,Ga)Se2solar cells with new record efficiencies up to 21.7%.* physica status solidi (RRL) - Rapid Research Letters, 2015. **9**(1): p. 28-31.
36. N.Limam, A.B., *Analysis of CIGS andCdTe solar cell concentrators*

Journal of Ovonic Research, 2017. **13**: p. 5.
37. Gong, J., J. Liang, and K. Sumathy, *Review on dye-sensitized solar cells (DSSCs): Fundamental concepts and novel materials.* Renewable and Sustainable Energy Reviews, 2012. **16**(8): p. 5848-5860.
38. B.O'Regan, M.G., *A low-cost, high-efficiency solar cell based on dye-sensitized colloidal TiO_2 films.* nature. **353**.
39. Sharma, K., V. Sharma, and S.S. Sharma, *Dye-Sensitized Solar Cells: Fundamentals and Current Status.* Nanoscale Res Lett, 2018. **13**(1): p. 381.
40. A. Yella, H.L., H.Tsao, C.Yi, A.Chandiran, M. Nazeeruddin, E. Diau, C. Yeh, S. Zakeeruddin, M. Gratzel, *Porphyrin-Sensitized Solar cells with cobalt (II/III) based redox electrolyte exceed 12 percent efficiency.* Science, 2011. **334**: p. 6.
41. Mathew, S., et al., *Dye-sensitized solar cells with 13% efficiency achieved through the molecular engineering of porphyrin sensitizers.* Nat Chem, 2014. **6**(3): p. 242-7.
42. Kakiage, K., et al., *Highly-efficient dye-sensitized solar cells with collaborative sensitization by silyl-anchor and carboxy-anchor dyes.* Chem Commun (Camb), 2015. **51**(88): p. 15894-7.

43. Burschka, J., et al., *Sequential deposition as a route to high-performance perovskite-sensitized solar cells.* Nature, 2013. **499**(7458): p. 316-9.
44. J.Zhao, A.W., and M.Green, *24.5% Efficiency Silicon PERT Cells on MCZ Substrates and 24.7% Efficiency PERL Cells on FZ Substrates.* progress in Photovoltaics: Research and Applications, 1999. **7**: p. 5.
45. Bui, T.-T. and F. Goubard, *Recent advances in small molecular, non-polymeric organic hole transporting materials for solid-state DSSC.* EPJ Photovoltaics, 2013. **4**: p. 40402.
46. Boucharef, M., et al., *Solid-state dye-sensitized solar cells based on ZnO nanocrystals.* Nanotechnology, 2010. **21**(20): p. 205203.
47. A. Le Viet, R.J., *,†,‡ M. V. Reddy,† B. V. R. Chowdari,† and S. Ramakrishna†, *Nb2O5 Photoelectrodes for Dye Sensitized Solar Cells Choice of the Polymorph.* J. Phys. Chem, 2010.
48. Ning, Z., Y. Fu, and H. Tian, *Improvement of dye-sensitized solar cells: what we know and what we need to know.* Energy & Environmental Science, 2010. **3**(9): p. 1170.
49. Wang, B. and L.L. Kerr, *Dye sensitized solar cells on paper substrates.* Solar Energy Materials and Solar Cells, 2011. **95**(8): p. 2531-2535.
50. Anders Hagfeldt, †,‡,| Gerrit Boschloo,† Licheng Sun,‡,| Lars Kloo,‡ and Henrik Pettersson⊥, *Dye-Sensitized Solar Cells.* Chem. Rev., 2010.
51. Gemeiner, P. and M. Mikula, *Effi ciency of dye sensitized solar cells with various compositions of TiO2 based screen printed photoactive electrodes.* Acta Chimica Slovaca, 2013. **6**(1).
52. Hwang, D., et al., *Electrospray preparation of hierarchically-structured mesoporous TiO(2) spheres for use in highly efficient dye-sensitized solar cells.* ACS Appl Mater Interfaces, 2011. **3**(7): p. 2719-25.
53. Wei, D., *Dye sensitized solar cells.* Int J Mol Sci, 2010. **11**(3): p. 1103-13.
54. Wu, M. and T. Ma, *Recent Progress of Counter Electrode Catalysts in Dye-Sensitized Solar Cells.* The Journal of Physical Chemistry C, 2014. **118**(30): p. 16727-16742.
55. https://energyeducation.ca/encyclopedia/Conduction_band, Jan,2018.
56. M.G.Kana, *Introduction to organic solar cell devices and electrical characterization.* 2011.
57. https://chem.libretexts.org/Textbook_Maps/Inorganic_Chemistry/Book%3A_Inorganic_Chemistry_(Wikibook)/Chapter_10%3A_Electronic_Properties_of_Materials%3A_Superconductors_and_Semiconductors/10.6_Diodes%2C_LEDs_and_solar_cells, Aug, 2015.
58. *Electromagnetic Spectrum.*
59. Laboratory, A.I.C., *Power Conversion Efficiency of a Dye-Sensitized Solar Cell.* p. 6.
60. Nunzi, J.-M., *Organic photovoltaic materials and devices.* Comptes Rendus Physique, 2002. **3**(4): p. 523-542.
61. G. Lof, L.K., *Light intensity dependence of the open circuit voltage in organic bulk heterojunction solar cells.* University of Groningen Zernike Institute for Advanced Materials: p. 84.
62. C.Riordan, R.H., *WHAT IS AN AIR MASS 1.5 SPECTRUM.* Solar Energy Research Institute.
63. Ganapathy, V., B. Karunagaran, and S.-W. Rhee, *Improved performance of dye-sensitized solar cells with TiO2/alumina core–shell formation using atomic layer deposition.* Journal of Power Sources, 2010. **195**(15): p. 5138-5143.

64. Nazeeruddin, M.K., E. Baranoff, and M. Grätzel, *Dye-sensitized solar cells: A brief overview.* Solar Energy, 2011. **85**(6): p. 1172-1178.
65. Muniz, E.C., et al., *Synthesis and characterization of mesoporous TiO2 nanostructured films prepared by a modified sol–gel method for application in dye solar cells.* Ceramics International, 2011. **37**(3): p. 1017-1024.
66. Shao, F., et al., *Electrophoretic deposition of TiO2 nanorods for low-temperature dye-sensitized solar cells.* RSC Advances, 2014. **4**(15): p. 7805.
67. Ryan, M., *PGM Highlights: Ruthenium Complexes for Dye Sensitised Solar Cells.* Platinum Metals Review, 2009. **53**(4): p. 216-218.
68. Hagfeldt, A., *Brief overview of dye-sensitized solar cells.* Ambio, 2012. **41 Suppl 2**: p. 151-5.
69. Jena, A., et al., *Dye Sensitized Solar Cells: A Review.* Transactions of the Indian Ceramic Society, 2012. **71**(1): p. 1-16.
70. Zardetto, V., et al., *Formulations and processing of nanocrystalline TiO2 films for the different requirements of plastic, metal and glass dye solar cell applications.* Nanotechnology, 2013. **24**(25): p. 255401.
71. Li, B., et al., *Review of recent progress in solid-state dye-sensitized solar cells.* Solar Energy Materials and Solar Cells, 2006. **90**(5): p. 549-573.
72. Wu, J., et al., *Electrolytes in dye-sensitized solar cells.* Chem Rev, 2015. **115**(5): p. 2136-73.
73. P.Wang, S.Z., L.Exnar, and M.Grazel, *High-efficiency Dye-Sensitized Nanocrystailline Solar cell based on ionic liquid polymer gel electrolyte.* ChemComm Communication 2002. **2002**: p. 2.
74. S.Beaugre, J.D., and Mario.Leclerc, *Toward the Development of New Textile or Plastic Electrochromic Cells Using Triphenylamine-Based Copolymers.* 2006. **18**: p. 1.
75. Mehmood, U., et al., *Recent Advances in Dye Sensitized Solar Cells.* Advances in Materials Science and Engineering, 2014. **2014**: p. 12.
76. Han, H.-G., et al., *Ultrafast fabrication of flexible dye-sensitized solar cells by ultrasonic spray-coating technology.* Scientific reports, 2015. **5**: p. 14645.
77. M.K. Nazeeruddin, A.K., I. Rodicio, R. Humphry-Baker, E. Muller, P.Liska, N. Vlachopoulos, and M. Gratzel, *Conversion of Light to Electricity by cis-X2Bis(2,2'-bipyridyl-4, 4'-dicarboxylate)ruthenium(II) Charge-Transfer Sensitizer (X= Cl-, Br-, CN-, and SCN-) on Nanocrystalline TiO2 Electrodes.* Chemistry Society 1993. **115**: p. 9.
78. Ondersma, J.W. and T.W. Hamann, *Recombination and redox couples in dye-sensitized solar cells.* Coordination Chemistry Reviews, 2013. **257**(9-10): p. 1533-1543.
79. Chae, Y., et al., *All-solid, flexible solar textiles based on dye-sensitized solar cells with ZnO nanorod arrays on stainless steel wires.* Materials Science and Engineering: B, 2013. **178**(17): p. 1117-1123.
80. Chen, T., et al., *Intertwined aligned carbon nanotube fiber based dye-sensitized solar cells.* Nano Lett, 2012. **12**(5): p. 2568-72.
81. Chung, I., et al., *All-solid-state dye-sensitized solar cells with high efficiency.* Nature, 2012. **485**(7399): p. 486-9.
82. M.Karlsson, *Materials Development for Solid-State Dye-Sensitized Solar Cells.* 2012.
83. Bailie, C.D., et al., *Melt-infiltration of spiro-OMeTAD and thermal instability of solid-state dye-sensitized solar cells.* Phys Chem Chem Phys, 2014. **16**(10): p. 4864-70.

84. Yang, L., et al., *Comparing spiro-OMeTAD and P3HT hole conductors in efficient solid state dye-sensitized solar cells.* Phys. Chem. Chem. Phys., 2012. **14**(2): p. 779-789.
85. Hawash, Z., L.K. Ono, and Y. Qi, *Recent Advances in Spiro-MeOTAD Hole Transport Material and Its Applications in Organic-Inorganic Halide Perovskite Solar Cells.* Advanced Materials Interfaces, 2018. **5**(1): p. 1700623.
86. Hsu, C.Y., et al., *Solid-state dye-sensitized solar cells based on spirofluorene (spiro-OMeTAD) and arylamines as hole transporting materials.* Phys Chem Chem Phys, 2012. **14**(41): p. 14099-109.
87. T.Leijtens, I.D., T.Giovenzana, J. Bloking, M.McGehee, and A.Sellinger, *Hole transport materials with low glass transition temperatures and high solubility for application in solid-state dye-sensitized solar cells.* ACS Nano, 2012. **6**(2): p. 8.
88. Ding, I.K., et al., *Pore-Filling of Spiro-OMeTAD in Solid-State Dye Sensitized Solar Cells: Quantification, Mechanism, and Consequences for Device Performance.* Advanced Functional Materials, 2009. **19**(15): p. 2431-2436.
89. Roh, D.K., et al., *High Efficiency Solid-State Dye-Sensitized Solar Cells Assembled with Hierarchical Anatase Pine Tree-like TiO2Nanotubes.* Advanced Functional Materials, 2014. **24**(3): p. 379-386.
90. Rong, Y., et al., *Monolithic all-solid-state dye-sensitized solar cells.* Frontiers of Optoelectronics, 2013. **6**(4): p. 359-372.
91. Xu, C., et al., *High-efficiency solid-state dye-sensitized solar cells based on TiO(2)-coated ZnO nanowire arrays.* Nano Lett, 2012. **12**(5): p. 2420-4.
92. Yum, J.H., et al., *Recent developments in solid-state dye-sensitized solar cells.* ChemSusChem, 2008. **1**(8-9): p. 699-707.
93. Kavan, L., J.-H. Yum, and M. Graetzel, *Graphene-based cathodes for liquid-junction dye sensitized solar cells: Electrocatalytic and mass transport effects.* Electrochimica Acta, 2014. **128**: p. 349-359.
94. Velten, J., et al., *Weavable dye sensitized solar cells exploiting carbon nanotube yarns.* Applied Physics Letters, 2013. **102**(20): p. 203902.
95. Arbab, A.A., et al., *Multiwalled carbon nanotube coated polyester fabric as textile based flexible counter electrode for dye sensitized solar cell.* Phys Chem Chem Phys, 2015. **17**(19): p. 12957-69.
96. Zhang, Z., et al., *Integrated polymer solar cell and electrochemical supercapacitor in a flexible and stable fiber format.* Adv Mater, 2014. **26**(3): p. 466-70.
97. Bedeloglu, A., et al., *A Photovoltaic Fiber Design for Smart Textiles.* Textile Research Journal, 2009. **80**(11): p. 1065-1074.
98. Fang, X., et al., *Core-sheath carbon nanostructured fibers for efficient wire-shaped dye-sensitized solar cells.* Adv Mater, 2014. **26**(11): p. 1694-8.
99. Yang, Z., et al., *Photovoltaic wire derived from a graphene composite fiber achieving an 8.45 % energy conversion efficiency.* Angew Chem Int Ed Engl, 2013. **52**(29): p. 7545-8.
100. J.Yune, I.K., G.Triani, K.Wagner, D.Officer, *A study of TiO2 binder-free paste prepared for low temperature dye-sensitized solar cells.* Journal of Materials Research, 2013: p. 9.
101. Hastitha C. Weerasinghe, P.M.S., George P. Simon and Y. Cheng, *Cold isostatic pressing technique for producing highly efficient flexible dye-sensitised solar cells on plastic substrates.* Progress in Photovoltaics: Research and Applications, 2011. **20**: p. 11.

102. D.Zhang, T.Y., H.Minoura,, *Low-Temperature Fbarication of Efficient Porous Titania Photoelectrodes by Hydrothermal Crystallization at the Solid/Gas Interface.* Advanced Material, 2003. **15**.
103. Gutiérrez-Tauste, D., et al., *New low-temperature preparation method of the TiO2 porous photoelectrode for dye-sensitized solar cells using UV irradiation.* Journal of Photochemistry and Photobiology A: Chemistry, 2005. **175**(2-3): p. 165-171.
104. Murakami, T.N., et al., *Low temperature preparation of mesoporous TiO2 films for efficient dye-sensitized photoelectrode by chemical vapor deposition combined with UV light irradiation.* Journal of Photochemistry and Photobiology A: Chemistry, 2004. **164**(1-3): p. 187-191.
105. Garmaroudi, Z.A., et al., *A facile low temperature route to deposit a TiO2 scattering layer for efficient dye-sensitized solar cells.* RSC Advances, 2016. **6**(75): p. 70895-70901.
106. Mohammadi, M.R., et al., *Dye-sensitized solar cells based on a single layer deposition of TiO2 from a new formulation paste and their photovoltaic performance.* Solar Energy, 2012. **86**(9): p. 2654-2664.
107. Hsiao, P.-T. and H. Teng, *Coordination of Ti4+Sites in Nanocrystalline TiO2Films Used for Photoinduced Electron Conduction: Influence of Nanoparticle Synthesis and Thermal Necking.* Journal of the American Ceramic Society, 2009. **92**(4): p. 888-893.
108. B. Park, K.k., M. Kang, K. Ryu, S. Chang, and Y. Shin, *Chemical Sintering of Nanoparticles: A Methodology for Low-Temperature Fabrication of Dye-Sensitized TiO2 Films.* Advanced Material, 2005. **15**: p. 5.
109. J.Yune, I.K., G.Triani, K.Wagner, D.Officer, *A study of TiO2 binder -freepaste prepared for low temperature dye-sensitized solar cells.* Material of research, 2013. **28**: p. 9.
110. Miyasaka, T., M. Ikegami, and Y. Kijitori, *Photovoltaic Performance of Plastic Dye-Sensitized Electrodes Prepared by Low-Temperature Binder-Free Coating of Mesoscopic Titania.* Journal of The Electrochemical Society, 2007. **154**(5): p. A455.
111. Kim, K., et al., *Improvement of electron transport by low-temperature chemically assisted sintering in dye-sensitized solar cell.* Journal of Photochemistry and Photobiology A: Chemistry, 2009. **204**(2-3): p. 144-147.
112. Zhang, P., et al., *Low-Temperature Preparation of Hierarchical Structure TiO2 for Flexible Dye-Sensitized Solar Cell.* Journal of the American Ceramic Society, 2012. **95**(4): p. 1372-1377.
113. Weerasinghe, H.C., et al., *Low temperature chemically sintered nano-crystalline TiO2 electrodes for flexible dye-sensitized solar cells.* Journal of Photochemistry and Photobiology A: Chemistry, 2010. **213**(1): p. 30-36.
114. Weerasinghe, H.C., et al., *Anomalous rheological behavior in chemically modified TiO2 colloidal pastes prepared for flexible dye-sensitized solar cells.* Journal of Materials Chemistry, 2010. **20**(44): p. 9954.
115. T.Miyasaka, U.K., M.Ikegami, *Plastic Dye-sensitized Potovoltaic Cells and Modules Based on Low-temperature Preparation of Mesoscopic Titania Electrodes.* Electrochemistry, 2006: p. 12.
116. Jost, K., G. Dion, and Y. Gogotsi, *Textile energy storage in perspective.* Journal of Materials Chemistry A, 2014. **2**(28): p. 10776.
117. Wang, Z.L. and W. Wu, *Nanotechnology-enabled energy harvesting for self-powered micro-/nanosystems.* Angew Chem Int Ed Engl, 2012. **51**(47): p. 11700-21.
118. Karim, N., et al., *All inkjet-printed graphene-based conductive patterns for wearable e-textile applications.* Journal of Materials Chemistry C, 2017. **5**(44): p. 11640-11648.

119. Tang, S.L.P., *Recent developments in flexible wearable electronics for monitoring applications.* Transactions of the institue of measurement and control, 2007. **29**: p. 283-300.
120. Stoppa, M. and A. Chiolerio, *Wearable electronics and smart textiles: a critical review.* Sensors (Basel), 2014. **14**(7): p. 11957-92.
121. Sahito, I.A., et al., *Graphene coated cotton fabric as textile structured counter electrode for DSSC.* Electrochimica Acta, 2015. **173**: p. 164-171.
122. Arbab, A.A., et al., *Fabrication of textile fabric counter electrodes using activated charcoal doped multi walled carbon nanotube hybrids for dye sensitized solar cells.* Journal of Materials Chemistry A, 2016. **4**(4): p. 1495-1505.
123. Sun, H., et al., *Novel graphene/carbon nanotube composite fibers for efficient wire-shaped miniature energy devices.* Adv Mater, 2014. **26**(18): p. 2868-73.
124. Hu, L., et al., *Stretchable, porous, and conductive energy textiles.* Nano Lett, 2010. **10**(2): p. 708-14.
125. Velten, J., et al., *Weavable dye sensitized solar cells exploiting carbon nanotube yarns.* Applied Physics Letters, 2013. **102**(20): p. 203902.
126. Yun, M.J., et al., *Highly flexible dye-sensitized solar cells produced by sewing textile electrodes on cloth.* Sci Rep, 2014. **4**: p. 5322.
127. Yun, M.J., et al., *Insertion of Dye-Sensitized Solar Cells in Textiles using a Conventional Weaving Process.* Sci Rep, 2015. **5**: p. 11022.
128. Yun, M.J., et al., *Monolithic-Structured Single-Layered Textile-Based Dye-Sensitized Solar Cells.* Sci Rep, 2016. **6**: p. 34249.
129. Cao, Y., et al., *11% efficiency solid-state dye-sensitized solar cells with copper(II/I) hole transport materials.* Nat Commun, 2017. **8**: p. 15390.
130. Hardin, B.E., et al., *Laminating solution-processed silver nanowire mesh electrodes onto solid-state dye-sensitized solar cells.* Organic Electronics, 2011. **12**(6): p. 875-879.
131. HJ. Snaith, A.M., C. Klein, K. Meerholz, RH. Friend, and M.Gratzel, *Efficiency enhancements solid-state hybrid solar cells via reduced charge recombination and increased light capture.* Nano Letter, 2007. **7**(11): p. 5.
132. Street, R.A., et al., *Jet printing flexible displays.* Materials Today, 2006. **9**(4): p. 32-37.
133. Girotto, C., et al., *Nanoparticle-based, spray-coated silver top contacts for efficient polymer solar cells.* Organic Electronics, 2009. **10**(4): p. 735-740.
134. Hau, S.K., et al., *Spraycoating of silver nanoparticle electrodes for inverted polymer solar cells.* Organic Electronics, 2009. **10**(4): p. 719-723.
135. Margulis, G.Y., et al., *Spray Deposition of Silver Nanowire Electrodes for Semitransparent Solid-State Dye-Sensitized Solar Cells.* Advanced Energy Materials, 2013. **3**(12): p. 1657-1663.
136. Jiang, C.Y., et al., *Low temperature processing solid-state dye sensitized solar cells.* Applied Physics Letters, 2012. **100**(11): p. 113901.
137. Xue, Z., et al., *Fabrication of Flexible Plastic Solid-State Dye-Sensitized Solar Cells Using Low Temperature Techniques.* The Journal of Physical Chemistry C, 2013. **118**(30): p. 16352-16357.
138. Charbonneau, C., et al., *Solution processing of TiO 2 compact layers for 3rd generation photovoltaics.* Ceramics International, 2016. **42**(10): p. 11989-11997.
139. S.Ito, T.T., T.Katayama, M.Sugiyama, M.Matsuda, T.Kitamura, Y.Wada, S.Yanagida,, *Conductive and Transparent Multilayer Films for Low-Temperature-Sintered Mesoporous TiO2 Electrodes of Dye-Sensitized S.* 2003.

140. D.Zhang, T.Y., H.Minoura,, *Low-Temperature Fabrication of Efficient Porous Titania Photoelectrodes by Hydrothermal Crystallization at the SolidGas Interface.* 2003.
141. Hart, J.N., et al., *A comparison of microwave and conventional heat treatments of nanocrystalline TiO_2.* Solar Energy Materials and Solar Cells, 2007. **91**(1): p. 6-16.
142. H.Lindstrom, A.H., E.Magnusson, L.Malmqvist, A.Hagfeldt, , *A new method to make dye-snsitized nano crystalline solar cells at room temperature.* 2001.
143. Santa-Nokki, H., et al., *Dynamic preparation of TiO_2 films for fabrication of dye-sensitized solar cells.* Journal of Photochemistry and Photobiology A: Chemistry, 2006. **182**(2): p. 187-191.
144. Lee, H., et al., *Low-temperature fabrication of $TiO_{(2)}$ electrodes for flexible dye-sensitized solar cells using an electrospray process.* ACS Appl Mater Interfaces, 2012. **4**(6): p. 3308-15.
145. Miyasaka, T. and Y. Kijitori, *Low-Temperature Fabrication of Dye-Sensitized Plastic Electrodes by Electrophoretic Preparation of Mesoporous TiO_2 Layers.* Journal of The Electrochemical Society, 2004. **151**(11): p. A1767.
146. M.M. Byranvand, M.H.B., A.N. Kharat, , *Fabrication and investigation of flexible dye sensitized nanocrystalline solar cell utilizing natural sensitizer.* 2010.
147. Lin, L.-Y., et al., *Low-temperature flexible Ti/TiO_2photoanode for dye-sensitized solar cells with binder-free TiO2paste.* Progress in Photovoltaics: Research and Applications, 2012. **20**(2): p. 181-190.
148. Halme, J., J. Saarinen, and P. Lund, *Spray deposition and compression of TiO2 nanoparticle films for dye-sensitized solar cells on plastic substrates.* Solar Energy Materials and Solar Cells, 2006. **90**(7-8): p. 887-899.
149. Zen, S., Y. Ishibashi, and R. Ono, *Low-temperature sintering for plastic dye-sensitized solar cells using conventional TiO2 paste containing organic binders.* Applied Physics Letters, 2014. **104**(21): p. 213904.
150. Kim, S.-S., J.-H. Yum, and Y.-E. Sung, *Flexible dye-sensitized solar cells using ZnO coated TiO2 nanoparticles.* Journal of Photochemistry and Photobiology A: Chemistry, 2005. **171**(3): p. 269-273.
151. Baglio, V., et al., *Influence of TiO_2 Film Thickness on the Electrochemical Behaviour of Dye-Sensitized Solar Cells.* International Journal of Electrochemical Science, 2011. **6**: p. 3375 - 3384.
152. Kumari, J.M.K.W., et al., *The effect of TiO2 photoanode film thickness on photovoltaic properties of dye-sensitized solar cells.* Ceylon Journal of Science, 2016. **45** (1): p. 33-41.
153. Arumugam, S., et al., *Fully spray-coated organic solar cells on woven polyester cotton fabrics for wearable energy harvesting applications.* Journal of Materials Chemistry A, 2016. **4**(15): p. 5561-5568.
154. Liu, J., et al., *Screen Printed Dye-Sensitized Solar Cells (DSSCs) on Woven Polyester Cotton Fabric for Wearable Energy Harvesting Applications.* Materials Today: Proceedings, 2018. **5**(5, Part 3): p. 13753-13758.
155. Peng, B., et al., *Systematic investigation of the role of compact TiO_2 layer in solid state dye-sensitized TiO_2 solar cells.* Coordination Chemistry Reviews, 2004. **248**(13-14): p. 1479-1489.
156. Nguyen, W.H., et al., *Enhancing the hole-conductivity of spiro-OMeTAD without oxygen or lithium salts by using spiro(TFSI)(2) in perovskite and dye-sensitized solar cells.* J Am Chem Soc, 2014. **136**(31): p. 10996-1001.
157. WH.Nguyen, C.N., E. Unger, and MD. McGehee, *Enhancing the Hole-Conductivity of Spito-OMeTAD without Oxygen or Lithium Salts by Using Spiro (TFSI)2 in*

perovskite and Dye-Sensitized Solar Cells Supporing Information. Journal of the American Ceramic Society, 2014. **136**: p. 6.
158. Charbonneau, C., et al., *Solution processing of TiO_2 compact layers for 3rd generation photovoltaics.* Ceramics International, 2016. **42**(10): p. 11989-11997.
159. Locher, I., et al., *Design and Characterization of Purely Textile Patch Antennas.* IEEE Transactions on Advanced Packaging, 2006. **29**(4): p. 777-788.
160. Yang, K., et al., *Waterproof and durable screen printed silver conductive tracks on textiles.* Textile Research Journal, 2013. **83**(19): p. 2023-2031.
161. Komolafe, A.O., et al., *Modelling and experimental validation of the effect of the elastic properties of fabrics on the durability of screen printed e-textiles.* Smart Materials and Structures, 2018. **27**(7): p. 075046.